

ORE MINERALOGY OF MATTABI MINE, NORTHWESTERN ONTARIO, CANADA.

By

Geoffrey Khalil Abdallah

Submitted in Partial Fulfillment of the  
Requirements for the Degree of  
MASTER of SCIENCE

Department of Geology  
Faculty of Science and Arts  
LAKEHEAD UNIVERSITY  
Thunder Bay, Ontario, Canada

May, 1990.

To my parents whose love I cherish and on whose blessings I thrive.

# LAKEHEAD UNIVERSITY

The undersigned hereby recommend to the Faculty of Graduate Studies acceptance of this thesis, submitted by Geoffrey Kholil Abdallah, in partial fulfillment of the requirements for the degree of Master of Science.

\_\_\_\_\_

\_\_\_\_\_

\_\_\_\_\_

May, 1990

## Abstract

The Mattabi Mine, a volcanogenic massive sulfide deposit located 60 km north of Ignace, Ontario, in the Archean Superior Province, produced 13.5 mt of ore with an average grade 7.5% Zn, 0.88% Cu, 0.77% Pb and 3.10 oz/t Ag in the period 1970-1983. Preliminary studies indicated the presence of an especially varied mineral assemblage, which was studied in detail. As well as chalcopyrite and sphalerite, the deposit contains abundant galena accounting for its unusual lead production. Argentian tetrahedrite, or freibergite, is also abundant, and in the absence of native silver and acanthite, is clearly a major carrier of silver. Other sulfide minerals include pyrite, pyrrhotite, arsenopyrite, bornite, mackinawite, pyrargyrite, boulangerite, freieslebenite, stephanite and veenite. Oxide minerals include magnetite, hematite, ilmenite, rutile, jacobite, cassiterite and gahnite.

The mineral zoning in the orebody is pronounced. Sphalerite, tetrahedrite, galena and the sulfosalts all occur in the upper portion of the orebody, whereas pyrrhotite and chalcopyrite are concentrated in the lower portion. The oxide minerals, except for jacobite, occur in the ore zone as well as in the footwall alteration zone.

A Brillouin zone model for tetrahedrite in which 204 to 208 electrons are accommodated in the 51st Brillouin zone is verified in analytical data from 60 grains. However, when three or more Ag atoms per unit formula are present, the number of valence electrons increases from 204 to 208 as Ag atoms increase from three to six. The presence of (Fe+Zn) in excess of two atoms per unit formula appears to stabilize the 52nd Brillouin zone, with >208 valence electrons per unit cell.

Analyses of sphalerite yielded a mean mole % FeS =  $12.11 \pm 0.70$ , indicating a pressure of metamorphism of 7.53 kbar, using the sphalerite geobarometer. This pressure is approximately 2 to 3.77 kbar too high in comparison with pressures suggested by silicate systems. A possible explanation is that sphalerite-pyrite-pyrrhotite equilibrated at peak pressure, whereas silicate assemblages indicate conditions of peak temperature in the P-T-t history of metamorphism of the deposit. Retrograde alteration variably affected sphalerite composition, producing some scatter in data, as well, as evidenced by variable occurrence of late-stage monoclinic pyrrhotite.

The low gold content, high lead content, diversity of sulfosalt species and abundance of silver in tetrahedrite are features more similar to those of kuroko-type deposits of the Phanerozoic than to Noranda or primitive-type massive sulfide deposits characteristic of the Archean.

## TABLE OF CONTENTS

	PAGE
Abstract.....	i
Table of Contents.....	ii
List of Figures.....	iv
List of Tables.....	vi
Acknowledgements.....	vii
CHAPTER I INTRODUCTION.....	1
1.1 General statement.....	1
1.2 Previous geological work.....	3
1.3 Regional geologic setting.....	4
1.4 Geology of south Sturgeon Lake area.....	8
1.5 Geology of Mattabi orebody.....	11
1.5.1 Alteration in the Mattabi deposit.....	12
1.5.2 Nature of the alteration zone.....	15
1.5.3 Ore zonation.....	18
1.6 Aims and objectives.....	22
1.7 Abbreviations.....	22
CHAPTER II METHODOLOGY.....	25
2.1 Optical methods.....	25
2.2 Electron microprobe methods.....	27
CHAPTER III TEXTURE AND MINERALIZATION.....	29
3.1 Introductory statement.....	29
3.2 Ore textures.....	29
3.3 Aspects of mineralization.....	35
3.4 Descriptive mineralogy.....	40

	PAGE
3.4.1 Sulfides.....	40
3.4.2 Sulfosalts.....	49
3.4.3 Oxides.....	52
3.5 Element and mineral zoning.....	55
CHAPTER IV MINERAL CHEMISTRY OF TETRAHEDRITE.....	56
4.1 Introduction.....	56
4.2 Analytical results.....	57
4.3 The Brillouin zone model.....	62
CHAPTER V SPHALERITE GEOBAROMETRY.....	66
5.1 Introduction.....	66
5.2 Equilibrium model.....	67
5.3 Pressure and metamorphism.....	75
CHAPTER VI COMPARATIVE STUDY, SUMMARY, CONCLUSIONS AND RECOMMENDATIONS.....	79
6.1 Comparison to related Canadian ore deposits.....	80
6.2 Summary.....	83
6.3 Conclusions.....	86
6.4 Recommendations.....	87
REFERENCES.....	88
APPENDIX I Tetrahedrite analyses based on 29 atoms.....	97
II Tetrahedrite analyses based on 13 atoms of sulfur.....	113
III Reflectivities of tetrahedrite.....	121
IV Sphalerite analyses.....	133
V Frequency distribution of minerals.....	139
VI Sample preparation.....	144

## LIST OF FIGURES

	PAGE
CHAPTER I.....	
1.1 Location map of Mattabi Mine.....	2
1.2 Stratigraphy and structural map of Sturgeon Lake area.....	5
1.3 Geologic map of Sturgeon Lake area.....	9
1.4 Mattabi stratigraphic section.....	10
1.5 Geologic map of Mattabi orebody.....	13
1.6 Generalized distribution of alteration types of Mattabi.....	16
1.7 Plan of Mattabi deposit-bench 5.....	19
CHAPTER II.....	
2.1 A section of the sample locations at Mattabi Mine.....	26
CHAPTER III.....	
3.1 Idiomorphic annealed grains of pyrite.....	31
3.2 Chalcopyrite blebs in sphalerite.....	31
3.3 Irregular fractures in pyrite.....	34
3.4 Recrystallization pyrite.....	34
3.5 Mineral and element zoning.....	36
3.6 a) Photomicrograph of interstitial tetrahedrite.....	38
b) Photomicrograph of cassiterite in sphalerite.....	38
c) Photomicrograph of subhedral ilmenite.....	38
d) Photomicrograph of stephanite.....	38
e) Photomicrograph of boulangerite.....	38
f) Photomicrograph of magnetite.....	38
g) Photomicrograph of rutile.....	38
h) Photomicrograph of gahnite and hematite.....	38

	PAGE
3.7 Colloform banding in pyrite.....	42
3.8 Earlier framboids of recrystallized pyrite.....	42
3.9 Irregular intergrowths of chalcopyrite.....	45
3.10 Concave boundaries in tetrahedrite.....	50
CHAPTER IV.....	
4.1 Graph of copper atoms versus silver atoms.....	58
4.2 Structure of tetrahedrite.....	59
4.3 Graph of antimony atoms versus arsenic atoms.....	61
4.4 Graph of silver atoms versus arsenic atoms.....	63
4.5 Graph of valency electrons versus silver atoms.....	64
CHAPTER V.....	
5.1 FeS contents of sphalerite differing assemblages.....	69
5.2 A schematic P-T-t path during regional metamorphism.....	71
5.3 Alteration of secondary monoclinic pyrrhotite.....	72
5.4 An etched pyrrhotite grain.....	72
5.5 Remnant of hexagonal pyrrhotite.....	73
5.6 Stability relations of pure iron end members.....	77



## LIST OF TABLES

	PAGE
CHAPTER I.....	
1.1 Preliminary study of Mattabi Ore Mineralogy.....	23
CHAPTER II.....	
2.1 List of standards for tetrahedrite analyses.....	27
CHAPTER III.....	
3.1 Minerals identified in the study area.....	41

## ACKNOWLEDGEMENTS

This investigation has been carried out within a research program sponsored by the NSERC grant (No. OGP0003814) of **Dr.S.A. Kissin**. Additional funding came from the graduate scholarship awarded to the author by the Centre for Northern Studies. The graduate school deserves mention for awarding a Lakehead University Entrance Scholarship. Thanks to **Dr. J. M. Franklin** of the Geological Survey of Canada for supplying the drill core samples for this project. The author is indebted to **Dr. S. A. Kissin** for his patience and persistent guidance in initiating and developing this thesis project. His valuable advice and suggestions are highly appreciated. **Anne Hammond** and **Reino Viitala** assisted in the sample preparation. **Sam Spivak** drafted some of the diagrams. **Al Mackenzie** was instrumental in developing the operating skills of the author on the scanning electron microscope (SEM), X-ray microanalysis (EDS) and the shooting of the microphotographs. I would like also to thank the faculty, the department and dear fellow graduate students for their input in various aspects of the project.

## CHAPTER 1

### Introduction

#### 1.1 General statement

The Mattabi massive sulfide deposit is located near the southern end of Lake Sturgeon area, approximately 60 km north of Ignace (Fig.1.1), in northwestern Ontario and falls within the eastern part of the Wabigoon Greenstone Belt in the Superior Province of the Canadian Shield (Stockwell, 1972). Highway 599 extends through the western part of the area and provides access to Sturgeon Lake.

The discovery of the orebody by Mattagami Lake Mines Ltd. in 1969, sparked an exploration rush in the region. The ground geophysical follow-up correlated the Mattabi deposit to an anomaly indicated on an airborne survey. Subsequent diamond drilling outlined a massive sulfide deposit with a length of 550 meters and a maximum width of 92 meters. This type of deposit is common to the Canadian Shield but is known to occur throughout Canada. This deposit is polymetallic and generally considered as Cu-Zn type (Hutchinson, 1973) on the basis of major chemical constituents. But more recent literature classify the deposit as the Noranda or primitive-type deposit (Franklin et al.1981).

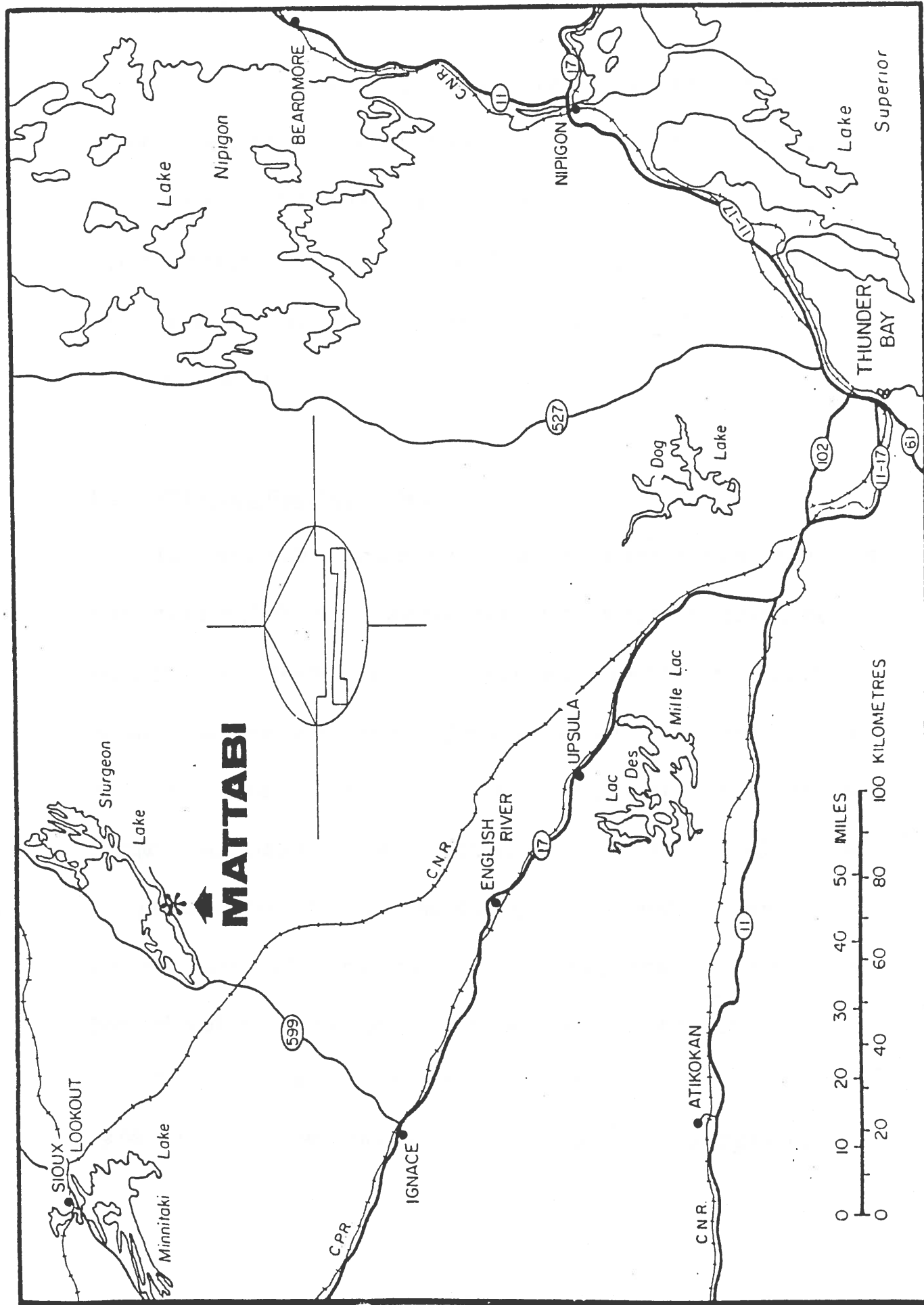


FIG. 1.1 Location map of the Mattabi massive sulfide deposit.

Mattabi Mines Ltd. was incorporated in 1970 to develop and mine this orebody. Pre-production reserves were estimated at 13.5 million tons with an average grade of 7.5% Zn, 0.8% Cu, 0.77% Pb, and 3.10 Oz/ton. of Ag. Production began in 1974 (Franklin et al., 1977) and continued until the ore was exhausted in 1983 at an average rate of 0.95 million tons per year (Canadian Mining Perspective., 1983).

## **1.2 Previous Geological Work**

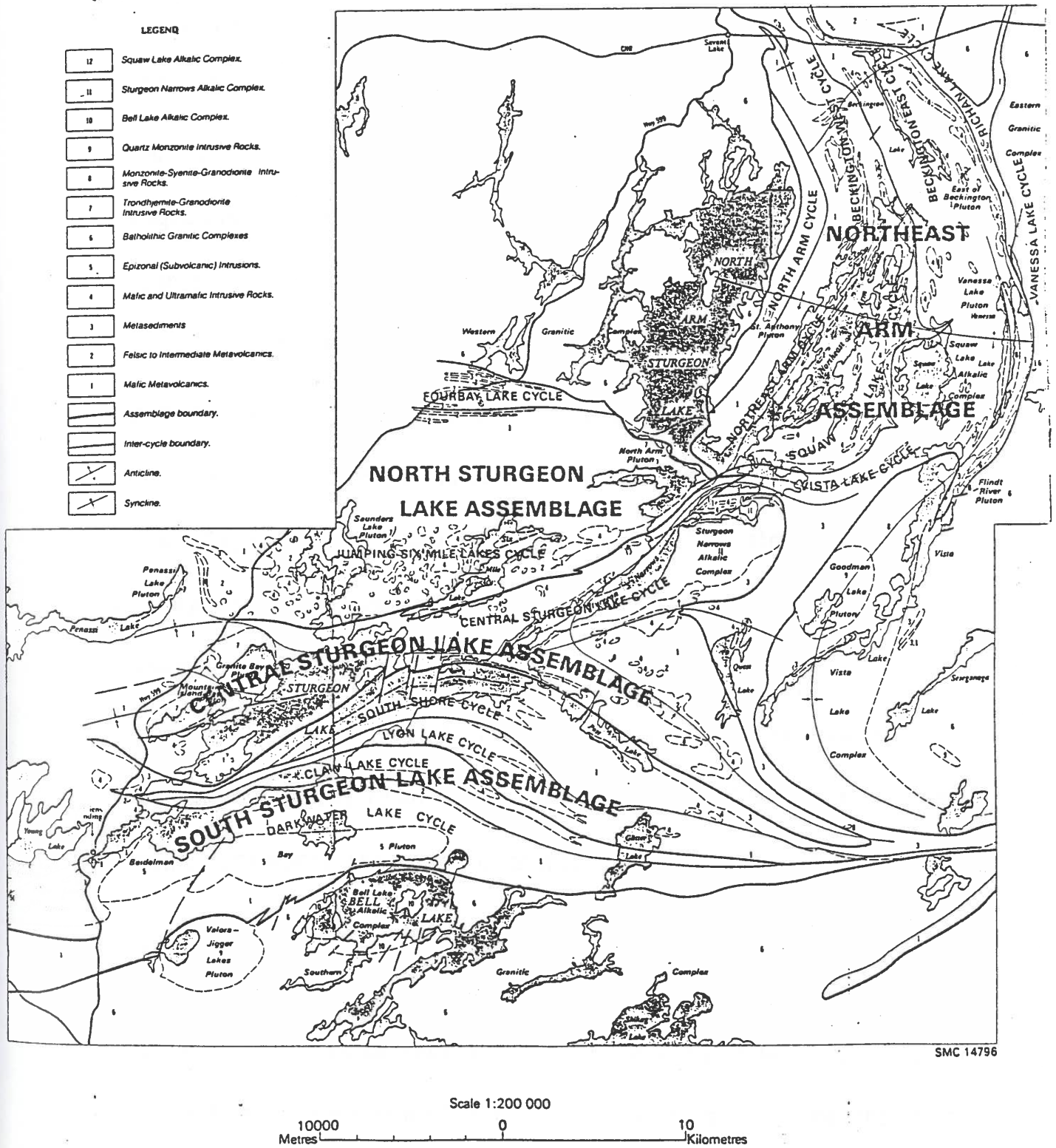
McInnes (1900) was presumably the first to map in the Sturgeon Lake area. Davidson (1901) described the area in the report of the survey and exploration of northern Ontario. Coleman (1902), in his report on the iron ranges of northwestern Ontario, reported on some of the gold prospects on the Sturgeon Lake. Collins (1907) mapped the area between Lake Nipigon and Sturgeon Lake. Gledhill (1924), Graham (1930), and Horwood (1937a) gave fairly detailed descriptions of the geology of the general Sturgeon Lake area. Pettijohn (1937) made brief mention of the Sturgeon Lake area in his discussion of the northern province of the Lake Superior region.

The most recent mapping is by Trowell (1970, 1972, 1974a, 1974b, 1974c, 1976, 1978) who has comprehensively studied the Sturgeon Lake

area. Unpublished theses completed in the area include those of Beggs (1975), Covello (1971), Friske (1974), Gordanier (1975), Hiscott (1974), Karsada (1973), Nielsen (1974) and Scott (1976). In addition, Shegelski (1975, 1976) has undertaken a study of the sedimentary rocks, including iron formation of the Sturgeon-Savant Lakes region. Published papers about the area include Franklin, Karsada and Poulsen (1975) and Grove, Morton and Franklin (1987).

### **1.3 Regional Geologic Setting**

The Sturgeon-Savant Lakes region is composed of Archean volcanic and minor sedimentary strata, which are deformed about two sets of fold axes and cut by numerous granitoid and amphibolitic intrusive bodies ( Fig. 1.2). In the Sturgeon Lake area, the supracrustal rocks may be divided into two domains. The northern domain of predominantly basaltic rocks contains less than 5% felsic strata and is approximately 13,720 meters thick. The southern domain includes approximately 9,150 meters of approximately equal amounts of felsic and mafic volcanic strata and approximately 15% of sedimentary rocks. The strata are cut by two major granitoid bodies. The Bell Lake complex (Fig.1.2) underlies the pile and is composed of monzonite (Trowell, 1970). The Dark-Water complex is a sill-like quartz



**FIG. 1.2** Stratigraphy and structure of the Sturgeon Lake volcano-sedimentary belt (After Trowell, 1983).

diorite-granodiorite mass 2140 meters thick, which was emplaced approximately 460 meters above the base of the volcanic pile (Trowell, 1983). Two major synclinal structures dominate the map area (Fig.1.2). The South and the North Sturgeon Lake Assemblages form the opposing limbs of a synclinal structure. The axial trace of this structure extends from west of Mountain Island along the north side of the Sturgeon Lake and eastwards through the Princess Quest Lake area. In the west part of the area, the axial trace has been deflected around and has been bifurcated into subsidiary synclinal and anticlinal structures by the emplacement of the Mountain Island Bay and Granite Bay plutons. A second synclinal structure trends approximately northwest from north of Post Lake to Sturgeon Narrows where it swings to the northeast through the Vanessa Lake.

In addition, amphibolitic intrusive stocks of irregular shape are abundant in the area 13 km east of the Mattabi Mine. The strata dip steeply, facing northwards, and form the southern limb of the synform centred through Sturgeon Lake. Trowell et al. (1980), however, indicated that the volcanic units of the northern synformal limb are not correlative with the South Sturgeon Lake succession. The strata on either side of the synform are displaced along a major N 60° E fault zone that cuts the entire stratigraphic sequence.



The synclines are relatively tight, whereas the anticlines are broad.

The two fold sets were probably developed during the Kenoran Orogeny due to the emplacement of large granitoid diapirs or domes, which bound the supracrustal rocks.

Numerous faults and lineaments transect the map area (Fig. 1.2).




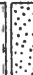





Pervasive shearing associated with movement along the Sturgeon Narrows cataclastic zone extends from the top of the northeast arm of Sturgeon Lake south east through Sturgeon Narrows. The rocks here are metamorphosed to middle and upper greenschist facies, and almandine-amphibolite assemblages are locally present adjacent to large synorogenic intrusions (Trowell, 1974, 1983; Groves, 1984). The late movement along this zone is indicated by brecciation of the Sturgeon Narrows alkalic complex and the development of the kink folds in intermediate to felsic schists and phyllites along the Northeast Arm. In the Northeast Arm area, shear zones reflect movement along this zone.

The shear zones trend both parallel and discordant to primary bedding (Trowell, 1978). The Mountain Island Bay fault is indicated both by shear and carbonatized zones in mafic metavolcanics and by ground magnetic data.

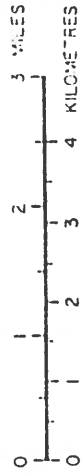
#### 1.4 Geology of South Sturgeon Lake Area

The South Sturgeon Lake area is an Archean volcanic edifice in a north-facing sequence with a generally steep northerly dip, which forms the southern limb of a syncline with a shallow easterly plunge (Fig.1.3). The strata are not tightly folded locally and major faulting is absent. The strata are divided into three cycles (Fig.1.4). Each cycle represents a major period of volcanism, normally with a mafic base and a felsic top.

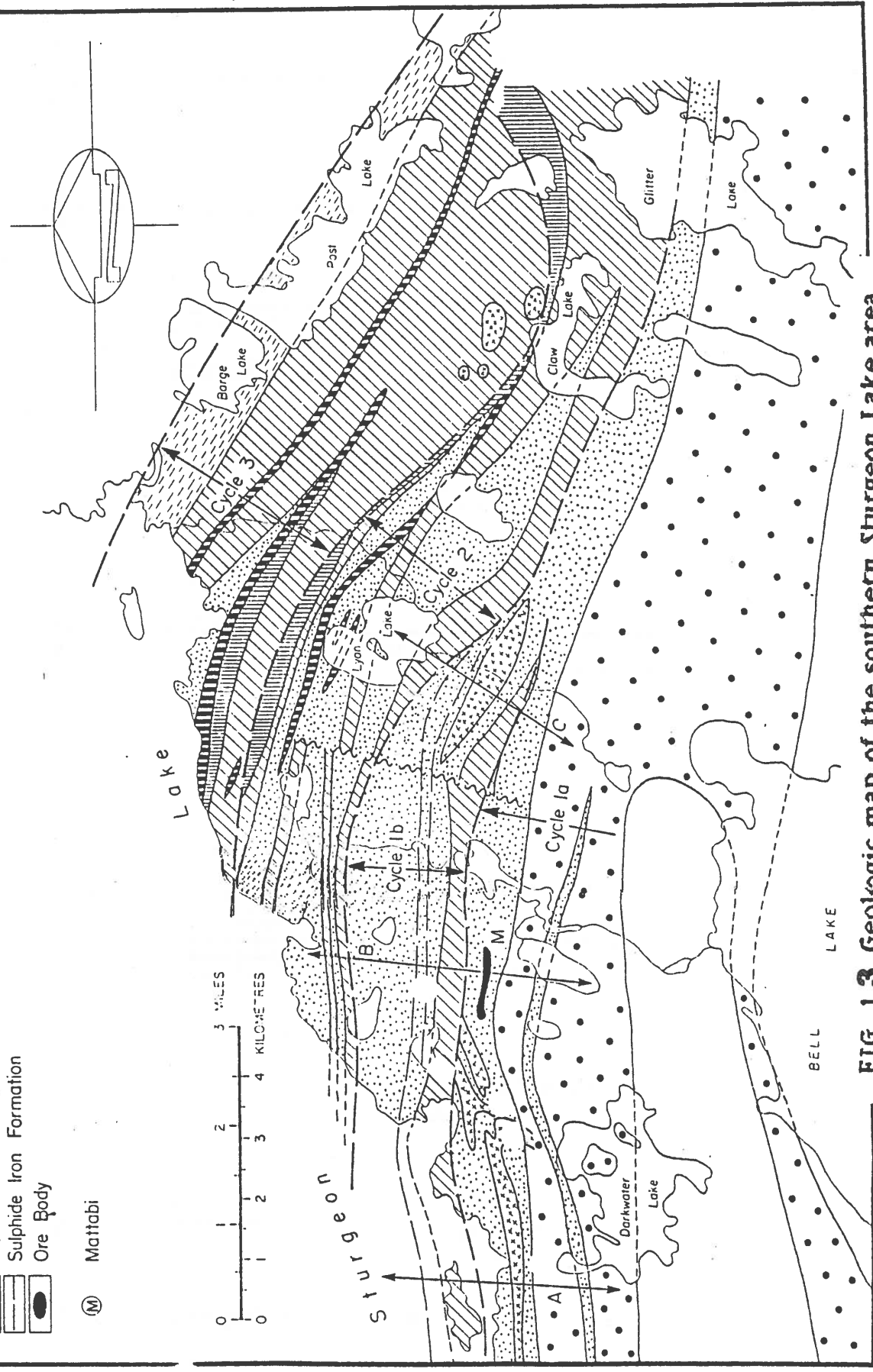
The chemical data (Franklin, Kasarda and Poulsen, 1975) show a preponderance of basalt with minor andesite representing the mafic division, rhyolite and dacite representing the felsic to intermediate division. Mafic to intermediate metavolcanics compose the dominant lithology in the map area (Fig.1.3). These rocks occur at several stratigraphic levels (Fig.1.4) and generally compose the lower part of individual volcanic cycles. Mafic to intermediate pyroclastics and redeposited fragmental rocks are noticeably abundant towards the base of the South Sturgeon Lake assemblage (Fig.1.2). Autoclastic and hyaloclastic breccias locally comprise the top and more rarely the bottom zones of flow. Felsic to intermediate metavolcanics occur at several stratigraphic intervals within the assemblages. The metavolcanics are variably massive, foliated and schistose. Banding is fairly common in metavolcanics and is

-  Basic Intrusive
-  Granitoids
-  Greywacke
-  Rhyolite Pyroclastic
-  Andesite
-  Tuff - wacke / Graphitic Shale
-  Lapilli Tuff
-  Sulphide Iron Formation
-  Ore Body

(M) Mattabi



GEOLOGY OF THE  
**SOUTHERN STURGEON LAKE**  
VOLCANIC BELT



**FIG. 1.3** Geologic map of the southern Sturgeon Lake area, Ontario (After Franklin et al 1977)

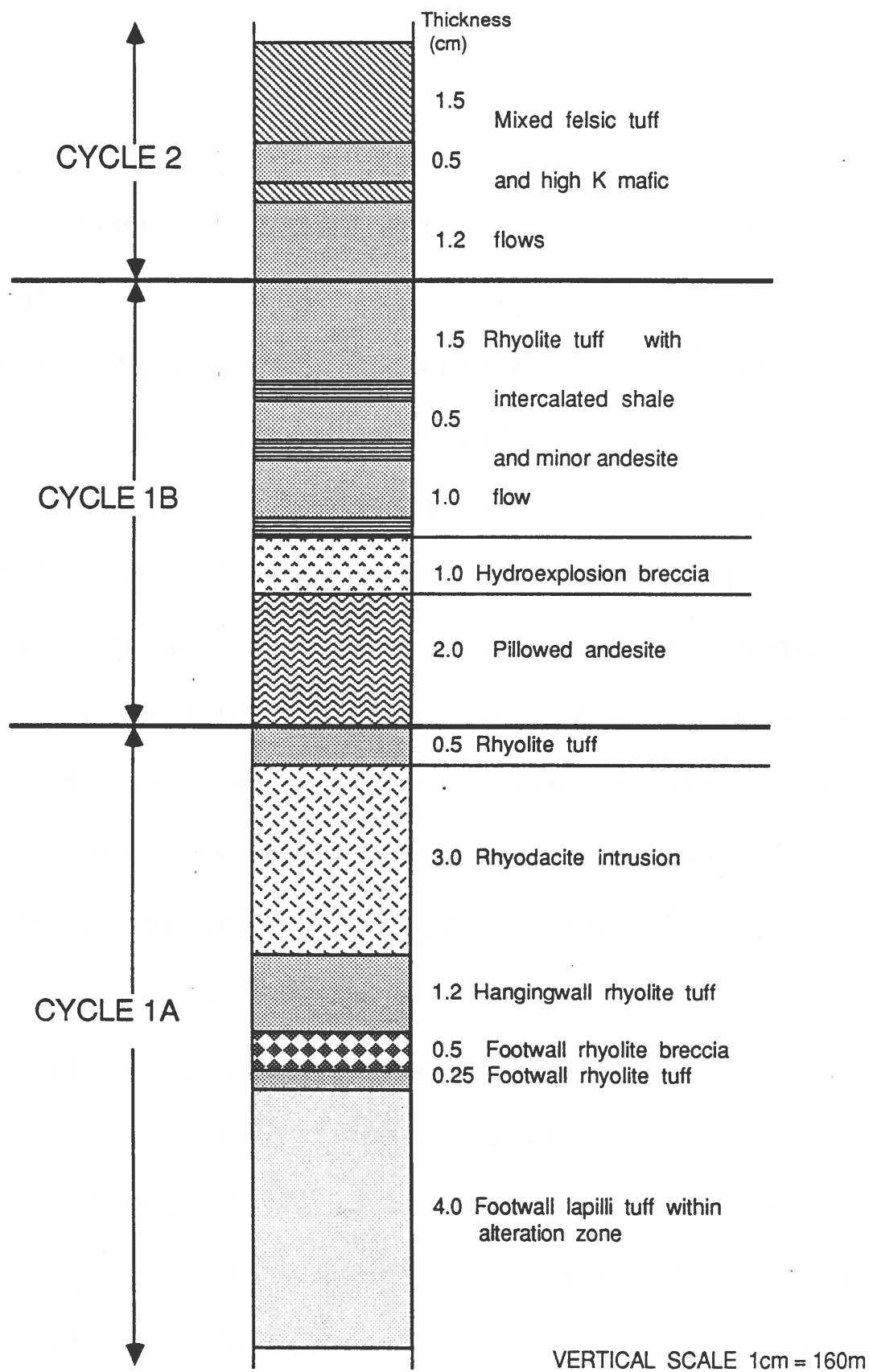


Fig. 1.4 Mattabi stratigraphic section (After Franklin et al.1977)

probably due to accentuation of primary bedding features of tuffaceous members or to metamorphic differentiation accompanying deformation.

The granitoid pebbles and cobbles in the conglomerate units are exposed in the southern part of the Sturgeon Lake. Synvolcanic intrusions are emplaced within mafic to intermediate metavolcanic sequences. Sills predominate, but dikes that occasionally acted as feeders to sills and flows are also present. These cycles are separated by either a disconformity or a sedimentary unit, indicating a distinct break in volcanism (Fig.1.3). These cycles are typified by pillowed and massive andesite flow units ranging to several thousand meters in thickness, intercalated with and overlain by approximately equal amounts of dacitic to rhyolitic ash flow tuffs. The lower cycle may conveniently be divided into lower and upper members (A and B). The lower member contains the Mattabi deposit (Fig.1.3).

### **1.5 Geology of Mattabi Orebody**

The Mattabi deposit occurs at a major mafic-felsic break within the volcanic sequence of the south Sturgeon Lake region and is underlain by a complex succession of altered, largely fragmental mafic and felsic rocks. This 5 km thick succession of volcanic rocks beneath the Mattabi deposit is intruded and displaced by the Beidelman Bay intrusion ( Fig.1.2) and a

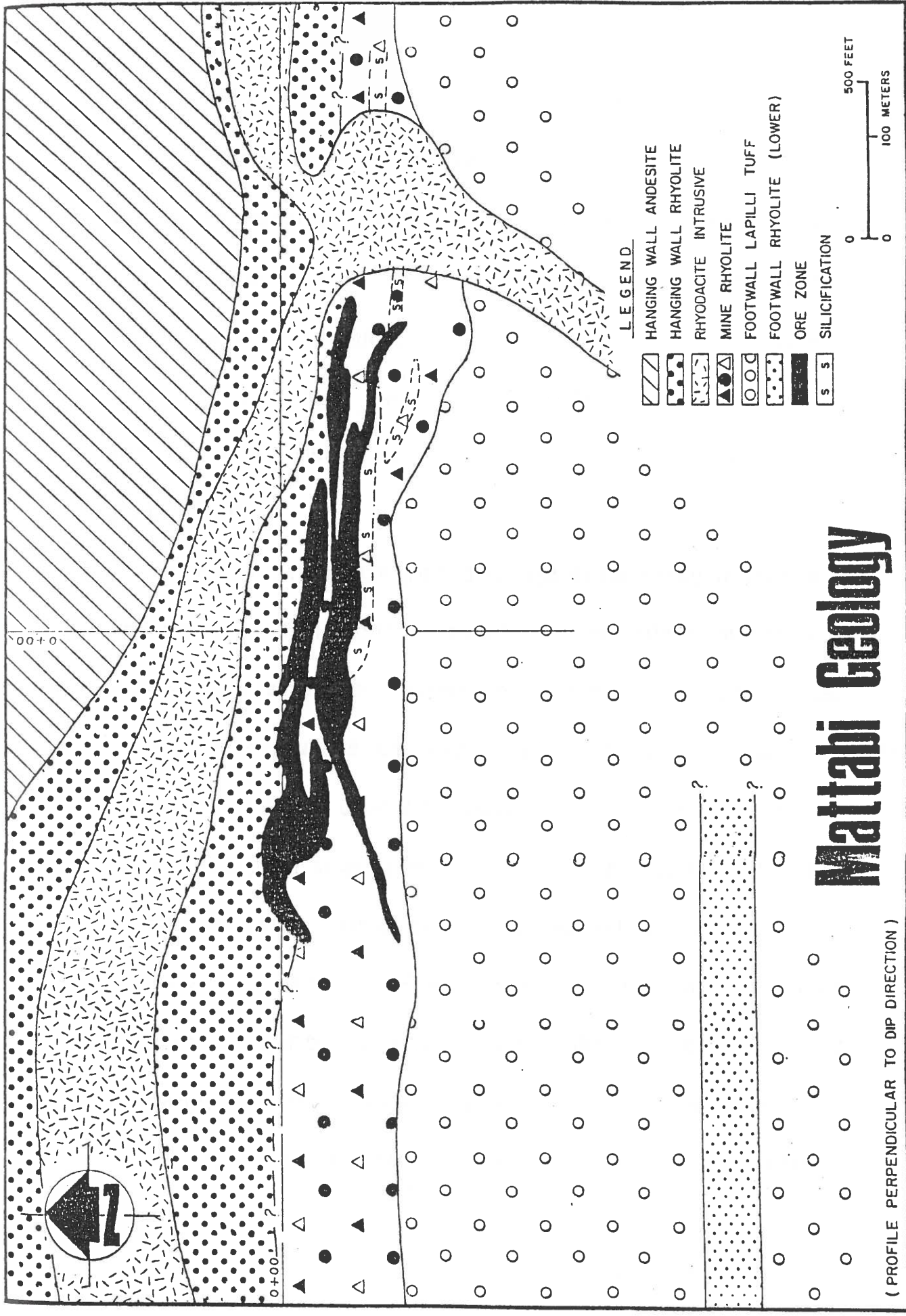
dioritic to trondhjemitic sill-like body of synvolcanic origin.

The Mattabi orebody is grossly similar to the typical body described by Roscoe (1965) and Sangster (1972) in that it is a conformable stratabound zoned accumulation of massive to semi-massive sulfide in a volcanic or volcano-clastic terrain (Fig.1.5). It is a proximal-type deposit as defined by Sangster (1972). It consists in part of stratiform accumulations of at least 60% sulfide minerals (Sangster and Scott, 1976).

Approximately 1070 meters west of the Mattabi ore zone, the volcanic section is cut by a thick, north-trending, fine-to medium-grained ophitic textured rock of basalt to andesite composition (Franklin et al.1975). A 1.5 meter thick feldspathic rhyodacite sill cuts subconcordantly through the top of the massive sulfide zone. The Mattabi deposit is characterized by a great concentration of ore in one place as opposed to a disseminated or vein-like deposit, (Fig.1.5). The massive ore zone has undergone extensive precontemporaneous brecciation and slumping.

### **1.5.1 Alteration in the Mattabi deposit**

Franklin et al. (1975) documented the alteration in the Mattabi orebody in detail and noted characteristic mineralogical and geochemical



# Mattabi Geology

FIG. 1.5 Geologic map of the Mattabi orebody. (After Franklin et al. 1977)

changes in the alteration zone. The alteration mineralogy includes all minerals that have been formed due to metamorphism of the original alteration assemblage. The main alteration minerals are quartz, kyanite and biotite. Alteration in the Mattabi deposit occurs as crosscutting veins and as massive, pervasive replacement. Quartz is the most ubiquitous mineral comprising up to 95% of the rocks. It occurs as dense, serrated, medium-grained, unstrained grains, as banded chert and as relatively coarse grains in veins.

Sericite occurs as fine grained aggregates commonly in rhyolite agglomerate and lapilli tuff. It is confined principally to the matrix. In veins sericite is medium-to coarse-grained and forms as vein fillings.

Carbonate occurs as coarse spherical aggregates of siderite or dolomite resembling lapilli and often surrounded by chlorite. In areas of less concentration, both siderite and dolomite occur as moderately to evenly distributed masses in either pyroclastic fragments or matrix.

Chloritoid is a common alteration mineral found in all rock types as well as in stringer ore veins. It occurs as bladed single metacrysts and coarse-grained fibrous irregular aggregates. Distal to the ore as well as in the hanging wall rocks, it forms altered poikiloblastic medium-grained aggregates.



Chlorite occurs as medium-to coarse-grained felted aggregates. It is generally less abundant than chloritoid although commonly forms local massive zones. The predominance of chloritoid over chlorite is not typical of Archean massive sulfide deposits.

Andalusite occurs as equant, ragged porphyroblasts or as coarse, bladed euhedral grains in all rock types. Kyanite occurs only within massive ore and in veins in the immediate footwall. It forms coarse-grained massive bladed aggregates. Almandine garnet occurs as very coarse aggregates in chlorite-rich zones. Although very prominent within the ore, no garnets have been observed in veins or at a distance of more than three meters from the ore. Biotite grains are rare but are present in veins and coarse-grained anhedral aggregates.

### **1.5.2 Nature of the Alteration zone**

The nature of the alteration zone is defined as indicated in Fig.1.6. The mineralogical and chemical changes are diagnostic of alteration zones (Sangster, 1972). Petrologic (Franklin, 1975) and chemical data (Kasarda, 1973) indicate that, a zoned, pipe-like alteration assemblage extends for at least 305 meters directly below the deposit.

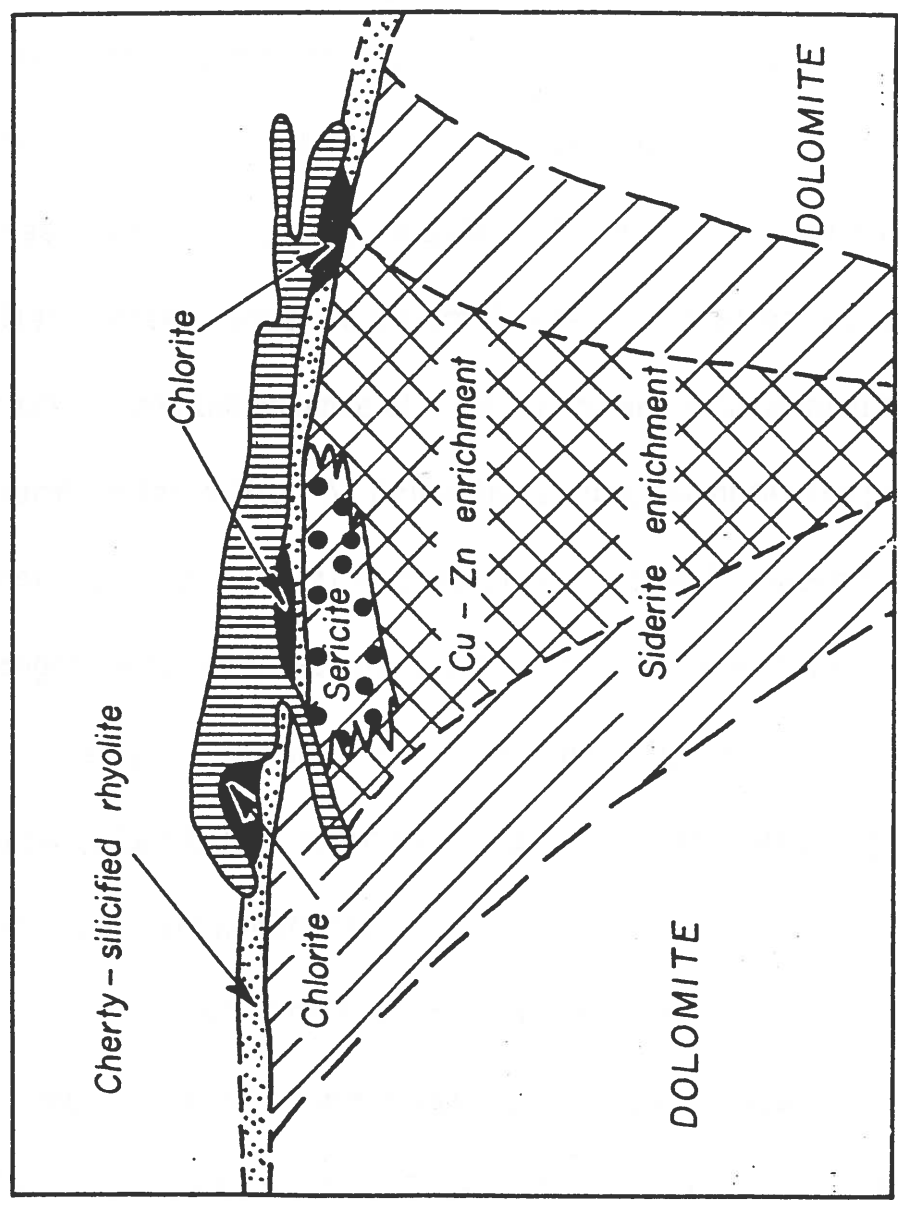


Fig. 1.6 Generalized distribution of alteration types in the footwall rocks of Mattabi deposit (After Franklin et al.1975)

Within the basal portion of the massive ore and the intermediate base of the ore, local massive chlorite pods are formed (Fig.1.6); however, chlorite is not a major alteration mineral. A silicified rhyolite and chert-bearing tuff zone forms a stratigraphic unit, which underlies much of the orebody; this quartz- andalusite zone probably was a quartz-kaolin alteration product. Silicification is highly pronounced in this zone. Local nodes of sericitized rhyolite underlie the silicified zone and where the latter is absent, underlie the ore. These are characterized by the presence of chloritoid and the absence of chlorite and are accompanied by siderite alteration spots (Fig.1.6). Below the sericitized nodes the pervasive and most significant alteration product is siderite. The siderite is manganiferous and, near the top of this zone in the footwall rhyolite agglomerate, forms spherical spots commonly surrounded by chlorite. In the footwall lapilli tuff, siderite partially replaces lapilli fragments as well as forming a matrix material.

From 3 to 5 % disseminated pyrite is pervasive throughout the footwall rocks for several thousand meters each side of the deposit and does not define a pipe zone. Copper and zinc are concentrated in anomalous proportions in the central portion of the pipe and are not clearly zoned

relative to each other. Their formation appears independent of the formation of siderite. Vein deposits cut all footwall rocks and generally confined to the zone directly below the ore. Sphalerite occurs only in the uppermost veins, chalcopyrite in a zone 16 to 25 meters below; pyrite and magnetite occur in all vein environments and are formed in veins that extend for several hundred meters below the economic copper zone. Sericite, quartz, andalusite and siderite are in decreasing order, the most common gangue minerals. Other geochemical trends include Na, Ca, K depletion and Fe, Mn, Si, enrichment in the vicinity of the deposit (Franklin, Kasarda and Poulsen, 1975).

### **1.5.3 Ore Zonation**

The orebody is made up of two conformable portions, the upper and the lower zones (Franklin et al. 1977, 1981). The zones are separated by a layer of cherty rhyolite tuff, which thins rapidly to the east. Each zone has been subdivided on mineralogical and textural bases into five facies. These are massive sphalerite ore, high pyrite-low sphalerite ore, massive chalcopyrite ore, high galena ore and stringer ore and alteration pipe (Franklin et al., 1977). The distribution of the ore zones in plan view is shown in Fig.1.7.

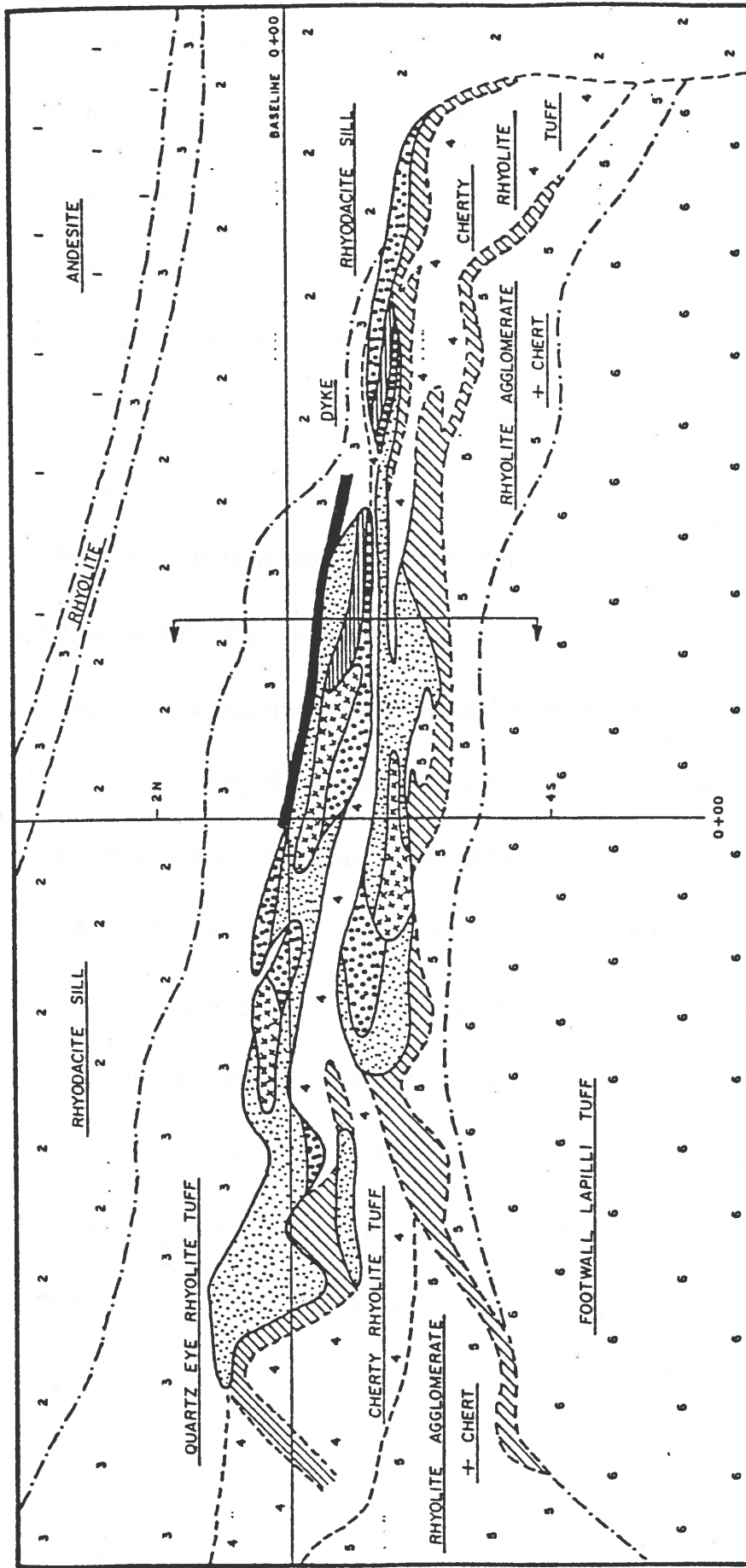
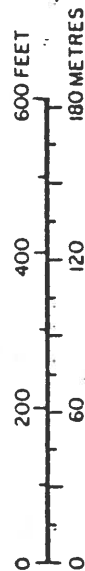


Fig. 1.7 PLAN OF THE MATTABI DEPOSIT - BENCH 5 (After Franklin et al. 1977)

STURGEON LAKE AREA

- MINERALOGICAL ZONING**
- 1 HIGH SPHALERITE
  - 2 LOW SPHALERITE - HIGH PYRITE
  - 3 HIGH CHALCOPYRITE
  - 4 HIGH GALENA CONTENT ZINC ORE
  - 5 STRINGER ORE



**ROCK TYPES**

- 1 ANDESITE
- 2 RHYODACITE DYKE -- SILL
- 3 QUARTZ EYE RHYOLITE TUFF
- 4 CHERTY RHYOLITE TUFF
- 5 RHYOLITE AGGLOMERATE + CHERT
- 6 FOOTWALL LAPILLI TUFF
- 7 DYKE

High sphalerite ore typically consists of 50-75 % sphalerite, 20-45 % pyrite, 5 % chalcopyrite and 2-5 % gangue. The pyrite bands are discontinuous and generally conformable to the ore body but are locally contorted, slumped or brecciated. Massive sphalerite in this zone often contains inclusions of galena and chalcopyrite.

High pyrite ore consists of fine to coarse, massive pyrite with up to 10 % sphalerite forming a matrix. This ore is low in copper and contains up to 50 % pyrrhotite close to the bottom of the zone. Coarse pyrite is commonly euhedral, whereas fine pyrite occurs as reticulate and dendritic, felted masses enclosing sphalerite. Massive chalcopyrite ore is generally 75-90 % chalcopyrite with streaks of sphalerite. The ore is coarse-grained and contains accessory, euhedral arsenopyrite. In addition, members of the tetrahedrite-tennantite series and pyrite occur as minor constituents.

High galena ore typically contains 50 % sphalerite, 25 % galena, 10 % pyrite, 2-3 % arsenopyrite and 1-2 % tetrahedrite-tennantite. On the edges of this facies, galena occurs as inclusions in sphalerite and outlines sphalerite grain boundaries and twin planes. In the central part of a galena-rich area, galena completely surrounds sphalerite blebs. Tetrahedrite is

commonly associated with galena. Arsenopyrite occurs as fine-grained, dusty aggregates intermixed with pyrite. The above facies make up the massive ore, and all grade into each other.

The chalcopyrite stringer zone is essentially conformable with the structure of the orebody and appears more extensive laterally than the massive sulfide zone. They form the top of the alteration pipe and appear to have formed in the zone immediately below the surface on which the massive sulfide were precipitated. This ore is formed of veins and blebs of sulfide which crosscut both the footwall rhyolite and the cherty rhyolite. The ore is composed of coarse grained chalcopyrite with minor pyrite, pyrrhotite and accessory arsenopyrite. Pyrrhotite is more abundant than pyrite in the footwall stringer zone.

The bottom of each of the two ore zones is chalcopyrite-rich grading into massive sphalerite ore. The massive sphalerite ore is generally galena-rich. The top of each zone is pyrite -rich ore. Massive ore is underlain by stringer ore, which is chalcopyrite- rich and is located at the top of the alteration pipe. The massive ore crosscuts the footwall rhyolite agglomerate and the cherty rhyolite.

## 1.6 Aims and Objectives

The preliminary studies in the area have indicated that there is a fairly diverse association of minerals (Table 1.1) present that are not commonly reported in the Archean. The objectives of the project are:

- 1) To study the composition, textures, distribution and interrelationships of the minerals;
- 2) To examine the presence and distribution of minor elements, whether as discrete minerals or as substitutions within one of the major minerals;
- 3) To study element and mineral zonation of the assemblages in the ore body.

It is hoped that the study will provide basic data to be used in comparative examination of Canadian ore deposits.



Table 1.1

Preliminary study of ore Mineralogy of Mattabi deposit (Franklin et al.1977).

Mineral	Analysis		Formula
Pyrite			FeS <sub>2</sub>
Pyrrhotite			Fe <sub>(1-x)</sub> S
Chalcopyrite			CuFeS <sub>2</sub>
Sphalerite	Zn=58.11 Mn=0.19 Hg=0.41	Fe=7.37 Cd=0.09 S =32.89	(Cu <sub>.001</sub> Hg <sub>.002</sub> Mn <sub>.003</sub> Fe <sub>.129</sub> Zn <sub>.866</sub> ) <sub>1.001</sub> S <sub>1.00</sub>
Galena	Pb=81.99 Bi=1.52 Se=4.48	Ag=0.67 S=11.75	(Pb <sub>.936</sub> Bi <sub>.017</sub> Ag <sub>.014</sub> ) <sub>.967</sub> (Se <sub>.135</sub> S <sub>.865</sub> ) <sub>1.00</sub>
Tetrahedrite	Cu=15.08 Ag=32.42 Sb=26.42 S =20.85	Fe=4.86 Zn=1.02 As=0.13	(Ag <sub>1.445</sub> Cu <sub>1.138</sub> ) <sub>2.583</sub> (Fe <sub>.418</sub> Zn <sub>.077</sub> ) <sub>.495</sub> (Sb <sub>1.042</sub> As <sub>.010</sub> ) <sub>1.052</sub> S <sub>3.121</sub>
Bournonite	Pb=42.17 Cu=12.60	Sb=29.24 S=19.11	Cu <sub>.984</sub> Pb <sub>1.02</sub> Sb <sub>.995</sub> S <sub>3.00</sub>
Cubanite	Cu=23.41 S=35.26	Fe=40.72	Cu <sub>1.01</sub> Fe <sub>1.99</sub> S <sub>3.00</sub>
Gudmundite	Fe=27.00 S=14.58	Sb=56.91	Fe <sub>1.03</sub> Sb <sub>1.00</sub> S <sub>0.97</sub>
Pyrrargyrite	Cu=0.11 Zn=0.12 As=0.38 S=16.16	Fe=0.36 Ag=61.82 Sb=20.81	Ag <sub>3.21</sub> Sb <sub>.96</sub> S <sub>2.83</sub>
Dyscrasite	Sb=25.21 As=5.67	Ag=70.95	Ag <sub>3.03</sub> (As <sub>.25</sub> Sb <sub>.75</sub> ) <sub>1.00</sub>
Amalgam	Ag=58.15	Hg=37.2	Approx. Ag <sub>3</sub> Hg
Electrum	Ag=56.16 Hg=5.57	Au=36.88 Sb=0.55	

## 1.7 Abbreviations

The following abbreviations have been used where appropriate

in the text:

py	Pyrite
po	Pyrrhotite
sp	Sphalerite
cp	Chalcopyrite
gn	Galena
tetr	Tetrahedrite
il	Ilmenite
ht	Hematite
mt	Magnetite
ct	Cassiterite
ru	Rutile
gh	Gahnite

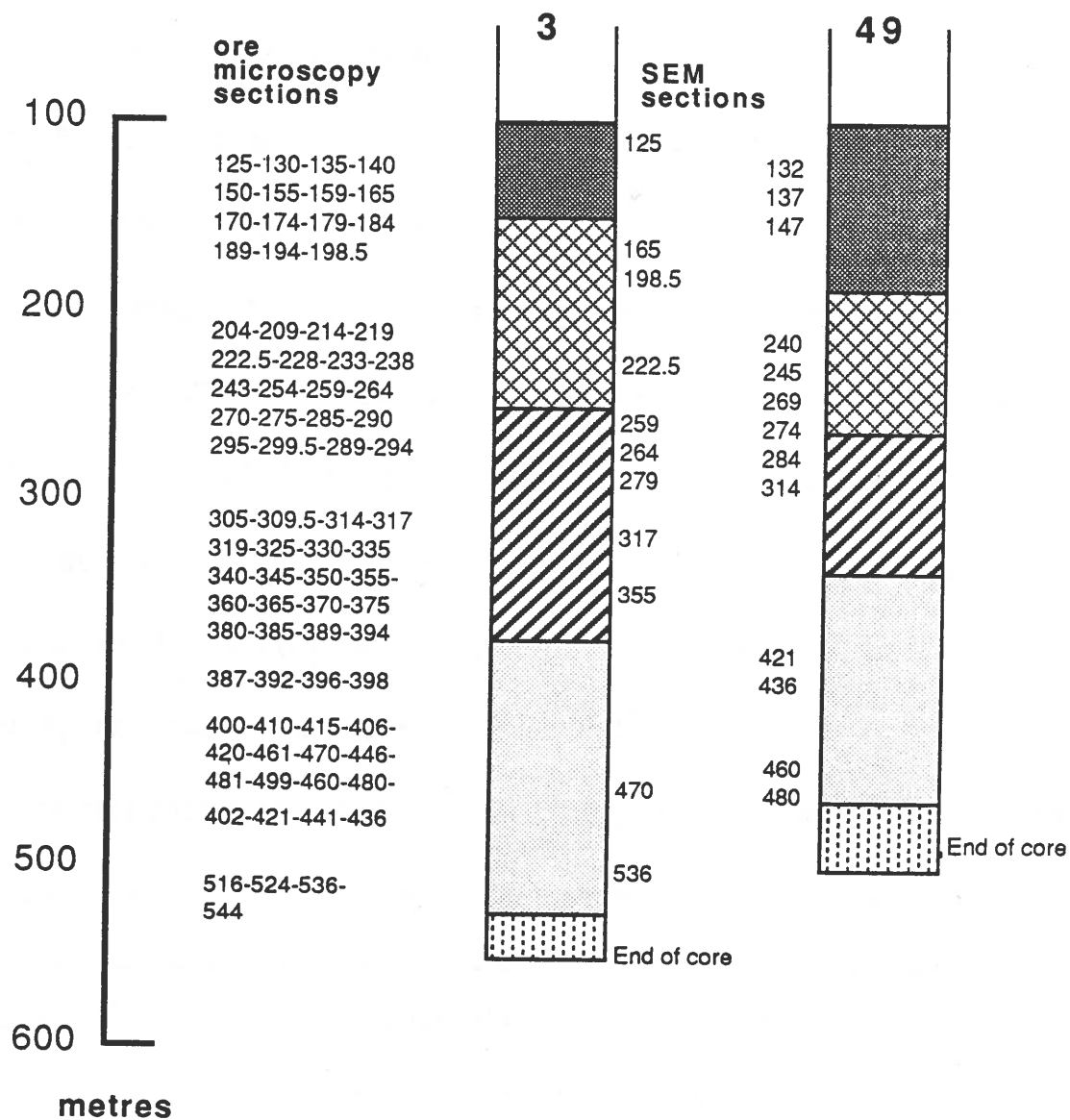
## CHAPTER II

### Methodology

207 polished sections of core samples from diamond drill holes 3 and 49 were examined. Sample locations are shown in Fig. 2.1. The various methods that have been employed in the collection of the mineralogical data, are described below.

#### 2.1 Optical methods

A reflecting light microscope was used to study 151 polished thin sections for the examination of opaque mineral assemblages and ultimately determine textural relationships of these mineral associations. Photomicrography was used to obtain the photographs. Etching was used to distinguish between monoclinic and hexagonal polymorphic phases of pyrrhotite. This was achieved by placing a drop of HI and H<sub>2</sub>O (ratio 1:1) on a pyrrhotite grain. A gradual chemical reaction was observed revealing a dark portion of the grain to be hexagonal pyrrhotite and the light or white portion to be monoclinic pyrrhotite (fig. 5.4, 5.5, 5.6). Reflectances of the selected tetrahedrite samples were determined using a Zeiss MPC 64 microscope photometer system. A WTIC reflectance standard was employed. The results are given in Appendix III.



#### Legend

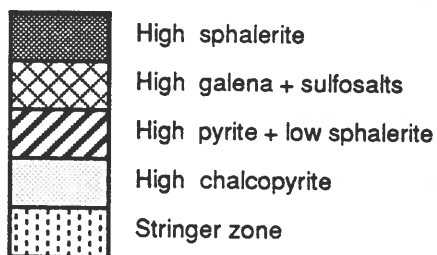


Fig. 2.1 A section of the sample locations of Mattabi mine. The numbers represent the depth of the core samples in metres from the diamond drill holes 3 and 49.

## 2.2 Electron microprobe methods

56 polished sections were studied using scanning electron microscopy (SEM) and energy dispersive spectrometry (EDS). Point mineral analyses were performed on a Hitachi 570 scanning electron microscope (SEM) with 5502 Trecor Northern MICROQ program operated at 20kv and 18° take-off angle with on-line ZAF corrections assuming target homogeneity.

Backscattered scanning electron (BSE) microscopy and x-ray energy dispersive spectrometry (EDS) were utilized concurrently to select and identify individual mineral grains for analysis.

The data base consists of 300 point analyses on the tetrahedrite and the standards used in this quantitative analysis are listed in Table 2.1

Table 2.1	elements	standards
	Cu	Chalcopyrite
	Fe	Chalcopyrite
	S	Chalcopyrite
	Ag	Pure metal
	Zn	Pure metal
	Sb	Pure metal
	As	Pure metal

A synthetic sphalerite containing 25 mole % FeS was used as the standard for 120 point analyses. The standards were acquired at 0.380 nA beam current, 20 kv operating voltage, 18° take-off angle, working distance of 28 mm, 100 seconds count times on peaks, data were processed with full matrix ZAF corrections, (FeK-alpha, CuK-alpha, ZnK-alpha, SK-alpha, AgL-alpha, SbL-alpha, AsL-alpha) lines were examined for the tetrahedrite and (FeK-alpha, ZnK-alpha, SK-alpha) for sphalerite. The analytical totals ranged between 98 and 101 wt %. The values for the tetrahedrite are quoted in numbers relative to 13 atoms of sulfur (Appendix II) and those for sphalerite are quoted in mole percentages of FeS (Appendix IV).

## CHAPTER III

### Texture and Mineralization

#### 3.1 Introductory statement

The Mattabi deposit contains a variety of sulfides, sulfosalts and oxide minerals. The ensuing pages describe the occurrence, texture, composition and the nature of ore mineralization of the mineral assemblages. Some of the minerals were identified using BSE imagery and EDS, since this method is more definitive than optical microscopy. The textures observed are secondary and tertiary in nature and may have been developed during diagenetic reconstitution of the ores after deposition on the sea-floor followed by metamorphic overprinting to the lower amphibolite facies. The primary textures may have been obliterated, and hence, the general paragenetic sequence is indeterminate due to lack of evidence.

#### 3.2 Ore Textures

The most prevalent textures present in the Mattabi deposit include medium -to coarse -grained, granular aggregates of pyrite ranging in shape

from idiomorphic annealed grains to rounded (Fig. 3.1, sample 3-222.5). Commonly, massive-textured galena can be observed in association with chalcopyrite and sphalerite. Occasional grains of rounded to subrounded magnetite are invariably associated with pyrite and pyrrhotite. This is in agreement with the textural assessment of the Sturgeon Lake deposits (Severin, 1982).

Chalcopyrite was encountered as anhedral interlocking grains interstitial to sphalerite and gangue but was also found as minute blebs and streaks in sphalerite ( Fig. 3.2, sample 49-436 ), often described as chalcopyrite disease, (Barton, 1978). This was at first thought of as being due to crystallographic intergrowth as is evident from orientation of the guest into one, two or three crystallographic directions of the host mineral (Nielsen et al. 1972). Coarse, crystallographically oriented inclusions of chalcopyrite in sphalerite have been interpreted by Hutchison and Scott (1981) as a metamorphic product of an originally fine-grained, two-phase assemblage. Comparison of the fine grain-size of chalcopyrite in the metamorphosed kuroko ores with coarser texture in Noranda ores supports this interpretation (Kalogeropoulos and Scott, 1987).



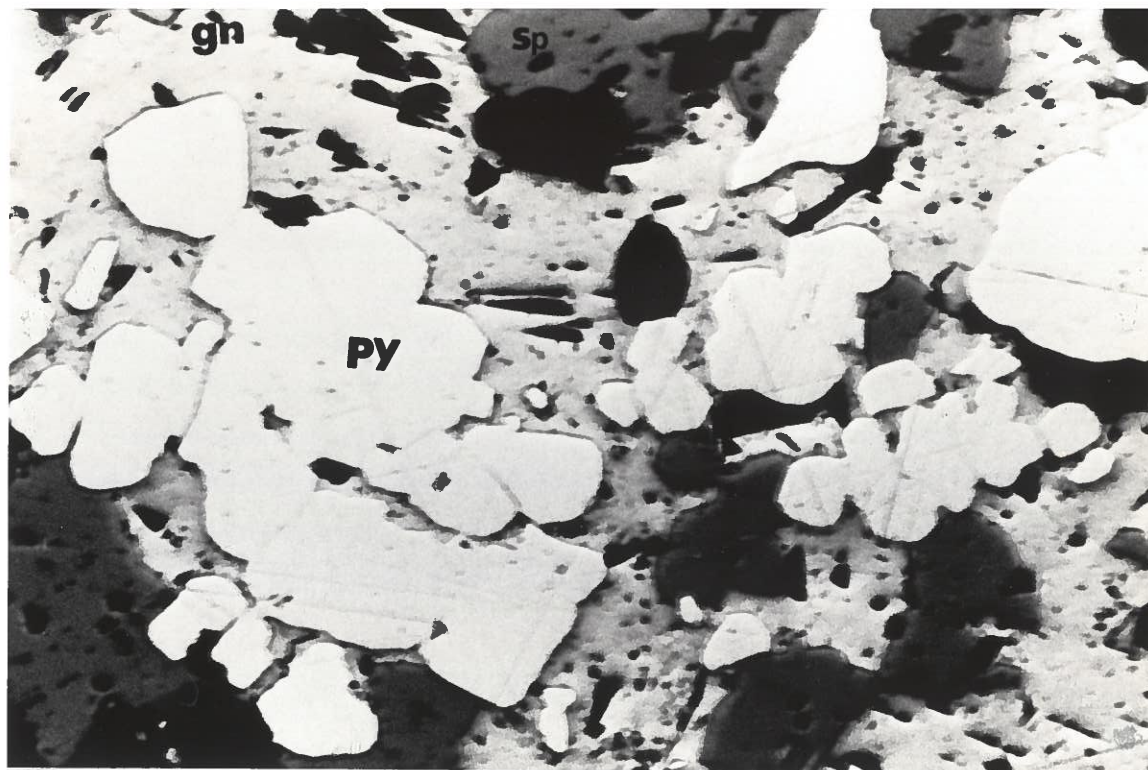


Fig. 3.1 Idiomorphic annealed grains of pyrite in association with galena and sphalerite. Sample 3-222.5

0.4mm

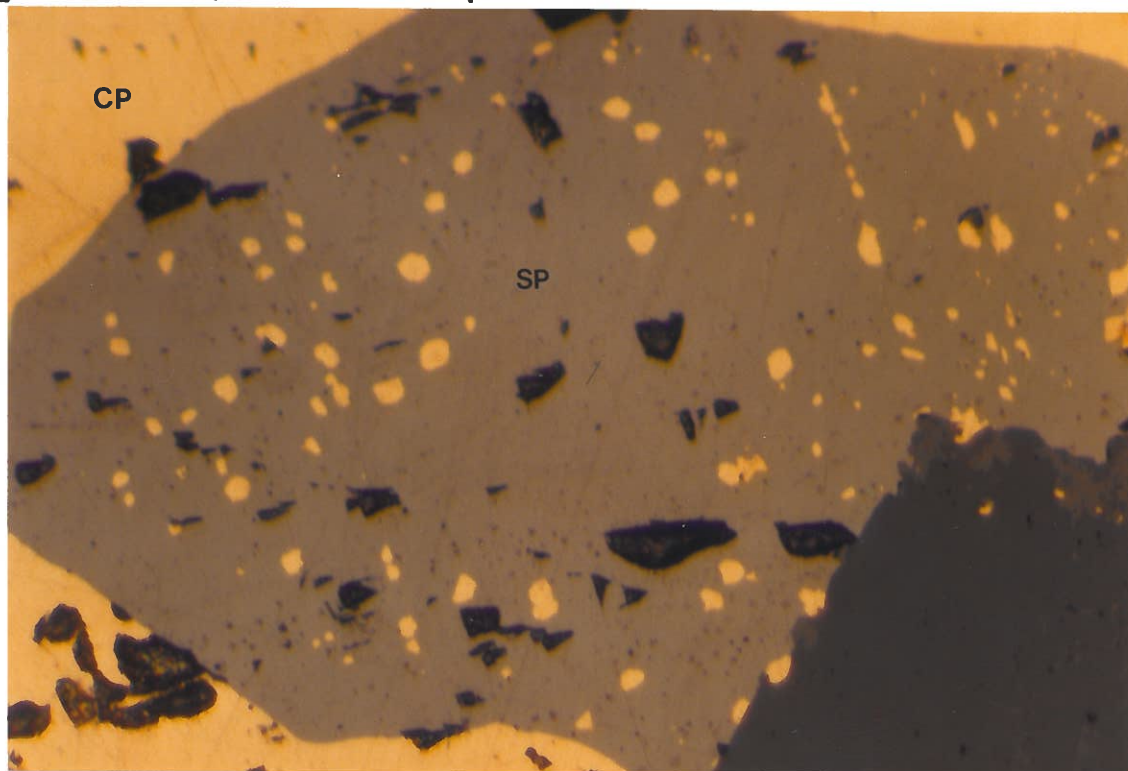


Fig. 3.2 Mottled, spotty texture of chalcopyrite blebs in sphalerite (chalcopyrite disease). The dark spots are silicate gangue. Sample 49-436

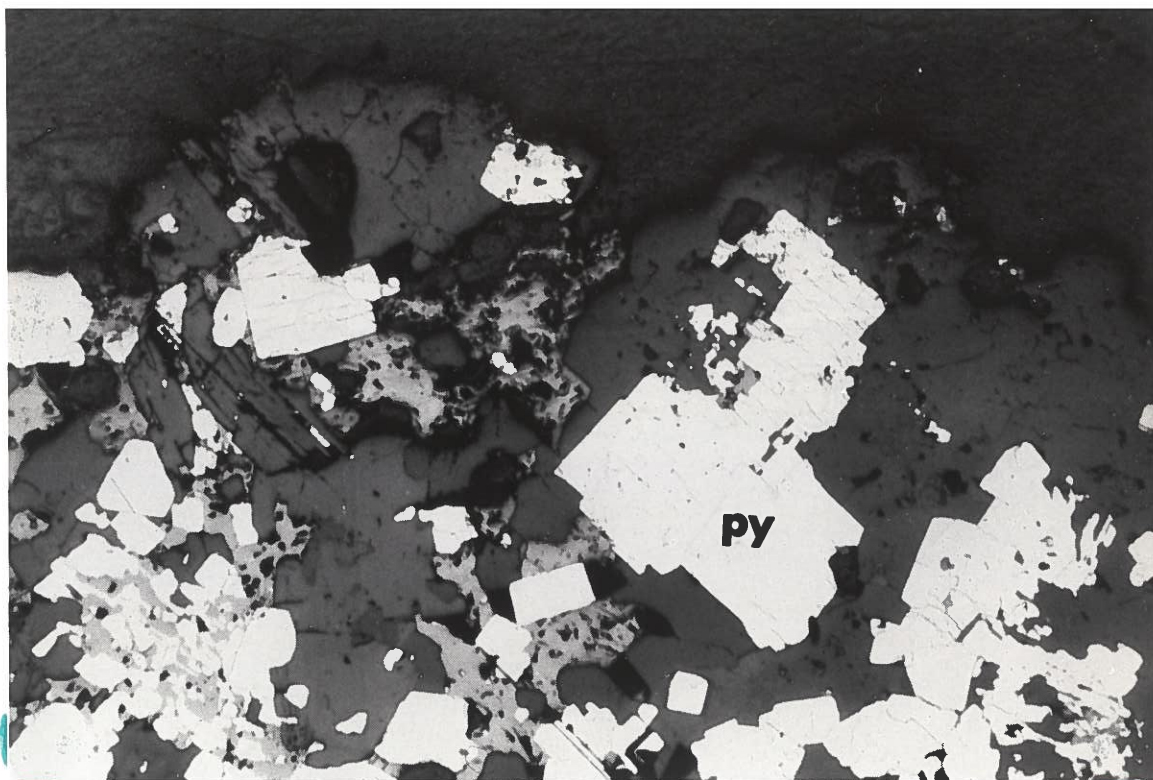
0.2mm

Barton (1970) believed that chalcopyrite disease could be produced by copper in aqueous solution reacting with FeS in sphalerite during the late stages of ore formation. However, Hutchinson (1978) proved in two experimental studies that exsolution is not a viable mechanism. Yui and Shitoya, (1983) attributed chalcopyrite disease to physical segregation of remnants of a primitive stage of formation of chalcopyrite and sphalerite. Sphalerite and chalcopyrite may have formed contemporaneously as small blebs and sphalerite grew to its present grain size (up to 3mm), while pushing and squeezing the small chalcopyrite blebs to grain boundaries. This process, however, does not explain the majority of textures. Johnson (1981) attempted to explain the chalcopyrite disease in terms of supergene phenomena, but the supergene processes only relabel the environment. Clark (1970) proposed that the breakdown of a metastable Cu-Zn-S is related to the chalcopyrite disease texture formation, but this suggestion was found to entail the removal of copper originally dissolved in sphalerite during an interaction with fluids of higher sulfur fugacity (Ohmoto et al. 1983). The problem with this mechanism is that the initial sphalerite is unlikely to have contained sufficient copper to form chalcopyrite by simple sulfidation. However, it was experimentally demonstrated that the chalcopyrite disease in natural samples may have formed by interaction of a

hot copper-bearing fluid and an iron-bearing sphalerite with the most likely mechanism being the replacement of FeS in sphalerite by chalcopyrite (Eldridge et al. 1988).

Deformational features are the only microstructures observed in the ore minerals. The presence of predominant subregular to irregular networks of fractures in pyrite ( Fig. 3.3 ), is suggestive of cataclastic texture. The pyrite grain boundaries appear to be occupied by matrix sulfides and most commonly by chalcopyrite, sphalerite, galena and pyrrhotite ( Fig. 3.4, 49-358 ). Unlike pyrite, the matrix sulfides do not show any effects of cataclasis owing to their ductile nature. But the effects of deformation are obvious from the elongated nature of pyrrhotite grains and the presence of translation lamellae showing microfolding and microfaulting in them.

It was found that the ore minerals, particularly pyrite and arsenopyrite, tend to become coarser grained at depth. Tanimura et al. (1974) noted a similar trend in their textural description of the kuroko orebody in the Hokuroku district in Japan. In addition, pyrite tends to be less euhedral at depth and occurs as compact aggregates. Chalcopyrite blebs in sphalerite appear to become more abundant at depth. Pyrrhotite and



0.4mm  
 Fig. 3.3 Irregular network of fractures in pyrite, suggestive of cataclasis and is pervasive throughout the deposit. Sample 3-360



0.4mm  
 Fig. 3.4 Annealing texture characterized by triple junctions due to recrystallization of pyrite during the slow cooling process of the deposit. Sample 49-358

magnetite content were observed to increase at depth, which suggest a decrease in sulfur content. The bulk of the tetrahedrite occurs in the upper portion of the orebody. Galena was found associated commonly with tetrahedrite and to exhibit mutual grain boundaries indicating no distinct age relationships.

### 3.3 Aspects of Mineralization

Copper sulfide mineralization in the Mattabi deposit is characterized by both massive and disseminated chalcopyrite and, to a lesser extent, by tetrahedrite. The disseminated chalcopyrite is about 1.5 mm in diameter and is scattered throughout the deposit. Massive chalcopyrite makes up the high copper ores and becomes more apparent in the basal section of the deposit (Fig. 3.5). Visual estimation of the abundance of massive chalcopyrite ranges from 60-80 % with sphalerite forming streaks through it. Massive chalcopyrite is coarse-grained and grades into 1-4 cm thick aggregates.

Zinc sulfide mineralization is characterized by massive sphalerite and rarely, by disseminated sphalerite. The visual estimate ranges from 60-90 % in abundance. Massive sphalerite is coarse-grained and is prevalent in the upper portion of the deposit, whereas the disseminated

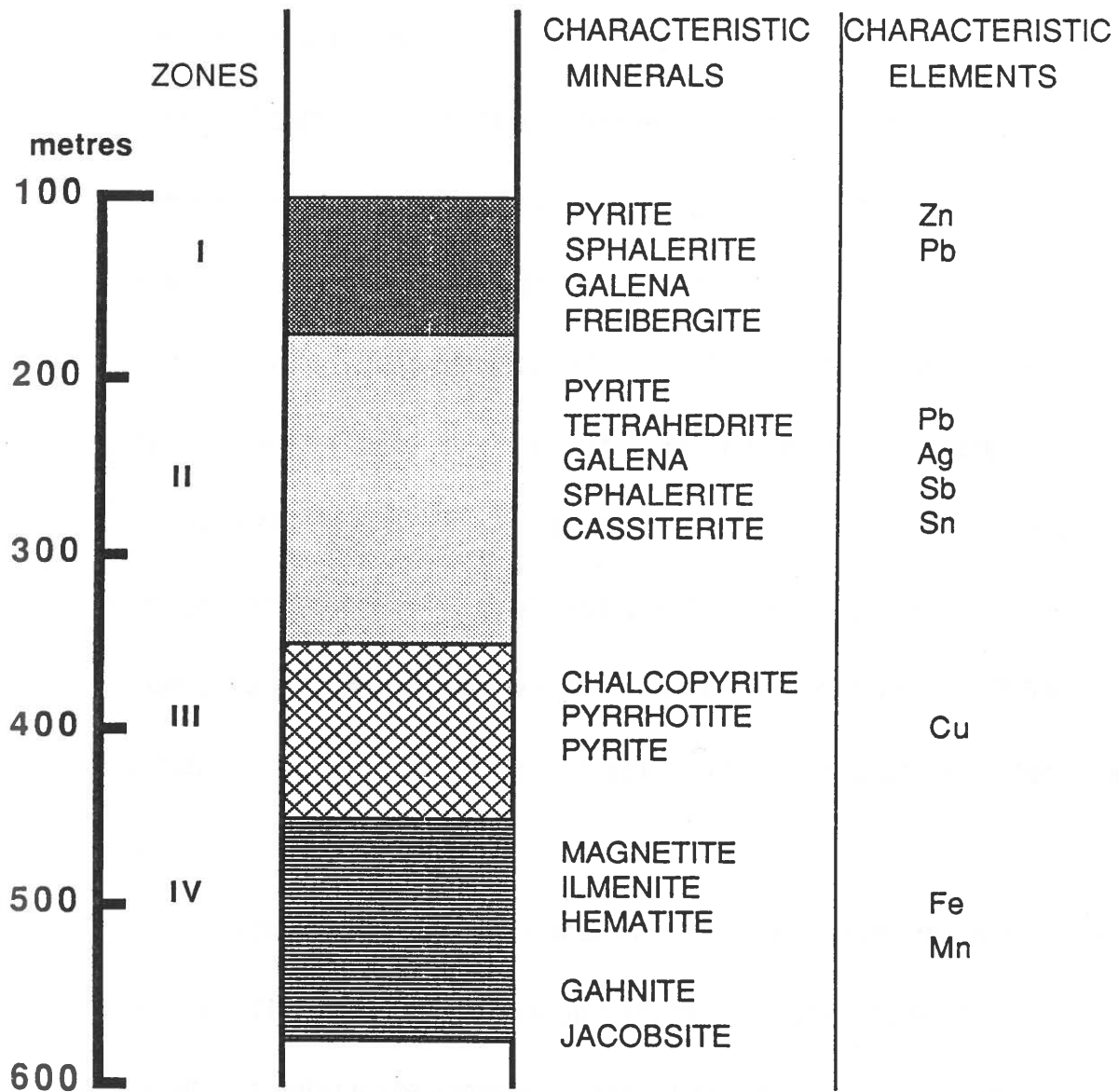


Fig. 3.5 Mineral and element zoning of Mattabi deposit.

sphalerite is sporadic with depth and associated with contorted, composite grains of pyrite. The massive sphalerite encloses minor blebs of galena and chalcopyrite. Cassiterite is observed as euhedral porphyroblasts largely scattered in massive sphalerite aggregation.

Lead sulfide mineralization is restricted to the upper portion of the deposit, where galena is commonly associated with tetrahedrite and occasionally intergrown with sphalerite and arsenopyrite. Visual estimates range from 50 to 80 % massive to coarse-grained galena. The galena grains contain elongated, blade-like inclusions of sulfosalts ( Fig. 3.6 e ).

Arsenopyrite occurs as fine-to medium-grained aggregates intermixed with pyrite.

Oxide mineralization is predominant at the basal contact of the deposit. The most common oxide minerals include magnetite, gahnite and jacobite, which are commonly interstitial to sulfides in this oxidized zone. Ilmenite and hematite occur mainly as fine, exsolved lamellae within magnetite. These oxides are mainly associated with silicates and occasionally disseminated within the sulfides.

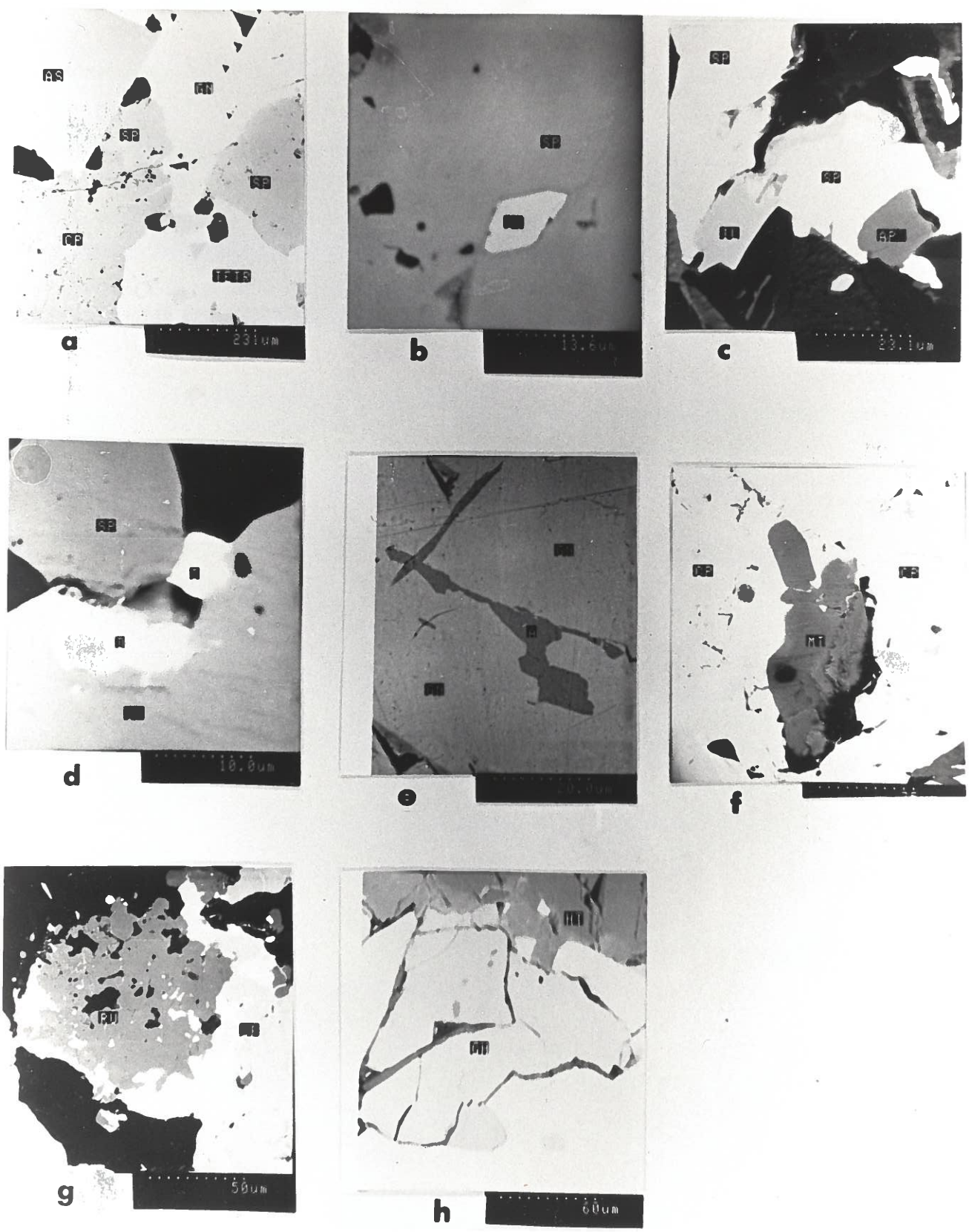


Fig. 3.6



## Captions for photomicrographs of Figure 3.6

- a) Interstitial tetrahedrite sharing grain boundaries with sphalerite, galena and chalcopyrite (sample 49-269).
- b) Porphyroblastic cassiterite grain in massive sphalerite (sample 3-228).
- c) Subhedral ilmenite at grain boundaries with sphalerite (sample 49-455).
- d) Mineral D is stephanite identified in sample 49-289 and occurs in sphalerite veins particularly at grain borders.
- e) Mineral A is boulangerite identified in sample 3-198.5 and occurs as idiomorphic platy blades projecting into galena.
- f) Elongate magnetite grain invariably associated with chalcopyrite (sample 49-455).
- g) Disseminated subhedral to anhedral aggregated rutile grains intergrown with chalcopyrite (sample 49-166).
- h) Euhedral coarse granular gahnite in association with hematite (sample 3-400).

### 3.4 Descriptive Mineralogy

This section describes the metallic minerals of the Mattabi deposit. Most of these minerals are present as veins, masses and disseminations. The order of description is sulfides, sulfosalts and oxides (Table 3.1). Paragenetic relationships between the minerals are described where appropriate.

#### 3.4.1 Sulfides

**Pyrite (  $\text{FeS}_2$  )** is the most ubiquitous of the sulfides present. It was identified as creamy white to yellowish white. It is homogeneously distributed throughout the deposit and occasionally disseminated. Pyrite occurs as equigranular, small to medium, euhedral cubic and pyritohedral crystals ranging in size from 0.1-3mm in diameter and the euhedral nature of the crystals may be as a result of recrystallization during prolonged annealing, which give rise to triple junctions (fig. 3.4). In sample 49-269, pyrite aggregates form colloform banding ( Fig. 3.7 ). Idiomorphic annealed pyrite grains (Sample 3-222.5, Fig. 3.1) form aggregates of mutually curving, annealed grain boundaries with negligible interpenetration. Earlier formed aggregates of framboids (Sample 3-150, Fig. 3.8) may be overgrown

**Table 3.1** The study area has revealed the presence of the following minerals:

**Sulfides**

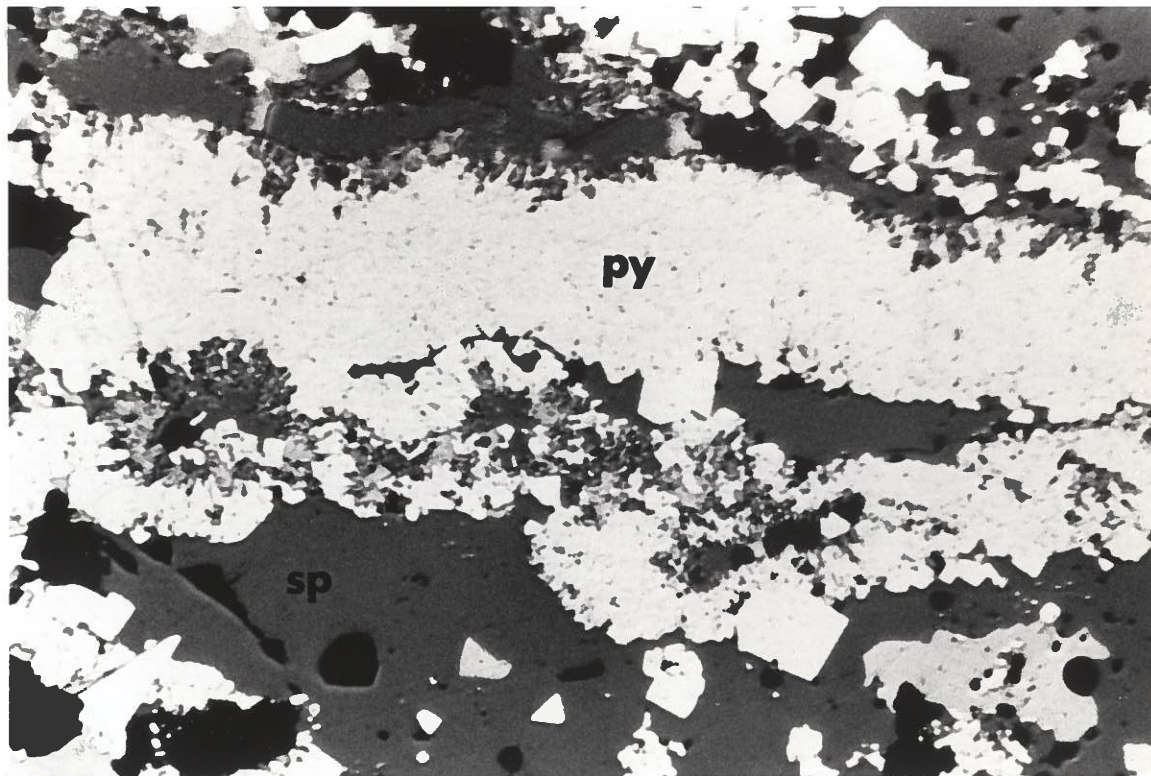
Pyrite	$\text{FeS}_2$
Sphalerite	$\text{ZnS}$
Chalcopyrite	$\text{CuFeS}_2$
Pyrrhotite	$\text{Fe}_{1-x}\text{S}$
Galena	$\text{PbS}$
Arsenopyrite	$\text{FeAsS}$
Bornite	$\text{Cu}_5\text{FeS}_4$
Mackinawite	$(\text{Fe,Ni})_9\text{S}_8$

**Sulfosalts**

Tetrahedrite	$(\text{Cu,Ag})_{10}(\text{Fe,Zn})_2\text{Sb}_4\text{S}_{13}$
Freibergite	$(\text{Ag,Cu})_{10}(\text{Fe,Zn})_2\text{Sb}_4\text{S}_{13}$
Pyrargyrite	$\text{Ag}_3\text{SbS}_3$
Boulangerite	$\text{Pb}_5\text{Sb}_4\text{S}_{11}$
Freieslebenite	$\text{PbAgSbS}_3$
Veenite	$\text{Pb}_2(\text{Sb,As})_2\text{S}_5$
Stephanite	$\text{Ag}_5\text{SbS}_4$

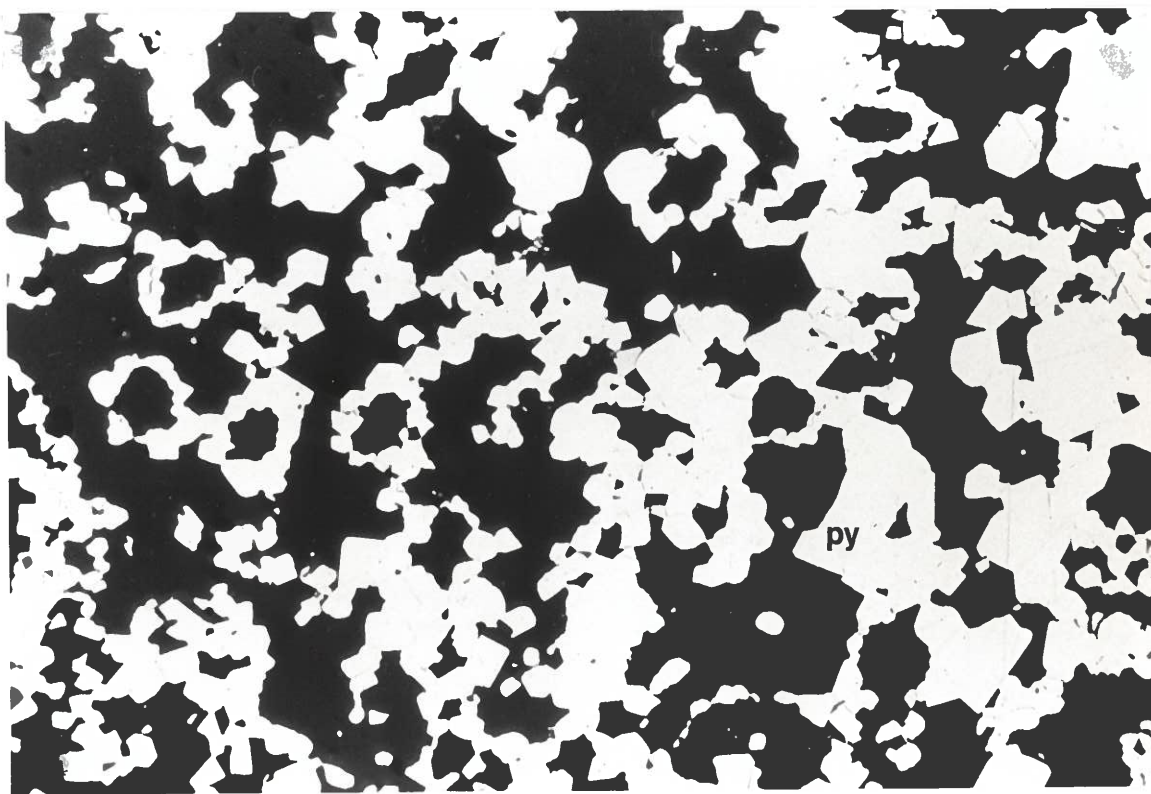
**Oxides**

Magnetite	$\text{Fe}_3\text{O}_4$
Hematite	$\text{Fe}_2\text{O}_3$
Ilmenite	$\text{FeTiO}_3$
Rutile	$\text{TiO}_2$
Jacobsite	$\text{Fe}^{+3}(\text{Mn,Fe}^{+3})_2\text{O}_4$
Cassiterite	$\text{SnO}_2$
Gahnite	$\text{ZnAl}_2\text{O}_4$



0.4mm

**Fig. 3.7 Colloform banding in pyrite associated with alteration mineralization around the main sphalerite. Sample 49-269**



0.4mm

**Fig. 3.8 Earlier formed aggregates of framboids overgrown by recrystallized subhedral coarser pyrite at depth. Sample 3-150**

by subhedral coarser pyrite at depth. Throughout the massive ores, pyrite retains morphological diversity.

Where the groundmass is homogenous, pyrite tends to be more idiomorphic. Sometimes grains are elongate in appearance, commonly pitted and highly fractured along grain boundaries and intensely crushed exhibiting cataclasis. Pyrite also occurs as finely disseminated grains within gangue (Sample 3-204). Locally, pyrite grains enclose silicate minerals or are skeletal in nature. The paragenetic sequence of pyrite is rather obscure, since subhedral to euhedral pyrite are distinct at every stage of deposition.

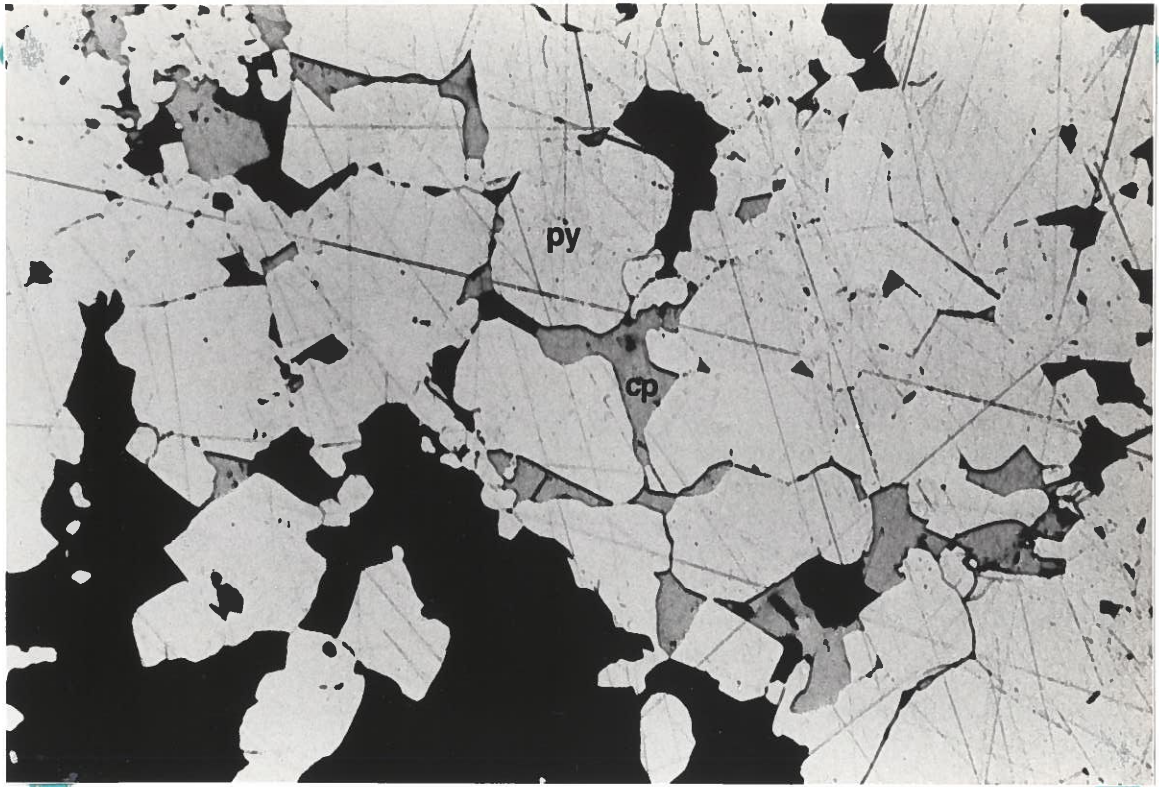
**Sphalerite (  $ZnS$  )** forms an important ore constituent of the Mattabi deposit. It is invariably associated with chalcopyrite, pyrrhotite, pyrite, galena and occurs as groundmass and commonly as euhedral to anhedral aggregates. The grains are typically pale grey in reflected light and unzoned. Frequently, sphalerite is observed as massive. Occasionally, sphalerite fills the interstices between pyrite cubes. The grain boundaries are sharp and undulose. Partial replacement of sphalerite by chalcopyrite masked the initial character of much of the sphalerite suggesting that most of the sphalerite crystals formed before the chalcopyrite. Lamellae twinning is apparent when sphalerite is etched with HI.

The observed textures of sphalerite are suggestive of the following relative order of deposition:

- 1) Precipitation of early sphalerite;
- 2) Recrystallization to massive, coarse-grained sphalerite. Homogeneous aggregates of crystals were cemented by later sulfides or gangue minerals.
- 3) Hydrothermal dissolution may have removed part of the growth history creating a microkarst texture (Barton, 1978) similar to those described in sphalerite from Mississippi Valley-type deposits (McLimans et al. 1980).
- 4) Minor precipitation of sphalerite terminated the sphalerite mineralization.

**Chalcopyrite (  $\text{CuFeS}_2$  )** occurs as euhedral to anhedral aggregates.

It is ubiquitous, and its abundance increases with depth. It occurs also as coarse, elongate grains, occasionally finely disseminated throughout the deposit. Chalcopyrite commonly appears as a major component of composite grains with sphalerite. The size ranges from  $< 0.1\text{mm}$  to  $6\text{mm}$  in diameter. Elongate grains are approximately  $2.5\text{cm}$  in length and  $5\text{mm}$  in width. Commonly, chalcopyrite fills the voids between pyrite grain boundaries (Fig. 3.9, sample 3-125) and encloses silicate grains exhibiting skeletal habit. It occurs also as small inclusions within pyrite and often penetrates to the



0.4mm  
Fig. 3.9 Irregular intergrowths of chalcopyrite between annealed grains of pyrite. Sample 3-125.

interior of cubes to form atoll texture. Chalcopyrite forms cusped and curvilinear margins as common boundary relationship with other sulfides but frequently forms chalcopyrite-disease with sphalerite ( Fig. 3.2). Chalcopyrite appears in some cases to have co-precipitated in minor amounts with the other sulfides. Commonly, it is found as matrix sulfide together with sphalerite and pyrrhotite. It forms irregular intergrowths of chalcopyrite between annealed grains of pyrite ( Fig. 3.9 ).

**Pyrrhotite (  $Fe_{1-x}S$  )** is a major constituent of the Mattabi deposit and occurs as anhedral to subhedral grains, composite in nature or as allotriomorphic patches . Pyrrhotite is pinkish grey and exhibits weak to moderate pleochroism and anisotropism. Pyrrhotite forms interstitial irregular aggregates with pyrite and occasionally may appear columnar, fibrous and prismatic in gangue. The grain size is highly variable. Single grains range from < 0.1mm to 2.5mm in length to 2mm in diameter. It is commonly associated with pyrite, chalcopyrite, sphalerite and magnetite. Occasionally, pyrrhotite exhibits radiating and atoll textures and is partially skeletal. Individual grains are locally elongated parallel to the schistosity exhibited by the ores. It also shows mutual boundary relationship with other sulfides. The boundaries are sharp and undulose and



sometimes fused. The abundance of pyrrhotite increases with depth within the deposit.

**Galena ( PbS )** is concentrated in the upper half of the deposit. It is commonly subidiomorphic to xenomorphic in coarse-to medium-grained net-textured aggregates. Galena occurs as veins, large masses, and irregular inclusions in sphalerite and pyrite. The size ranges from 0.1mm to 6mm in length to 5mm in diameter. It is frequently intergrown with tetrahedrite and occasionally contains bladed, fibrous, elongate, flame-like inclusions of boulangerite, veenite and freieslebenite ( Fig. 3.6 e ). Galena is often cross-cut by and enclosed in chalcopyrite.

**Arsenopyrite ( FeAsS )** occurs as euhedral to subhedral, coarse grains, frequently porphyroblastic in sphalerite, chalcopyrite and galena. It is observed as inclusions in tetrahedrite and is often intergrown with pyrite and contains inclusions of galena, sphalerite and chalcopyrite. Arsenopyrite displays rectilinear boundary relationships with other sulfides. It is commonly rhomb-shaped, occasionally rectangular and lath-like with sharp borders. Most grains are 1mm to 3mm in length and 2.5 mm in diameter.

**Meckinawite (  $(\text{Fe,Ni})_9\text{S}_8$  )** occurs sporadically in siliceous veins as anhedral, isolated, coarse to medium grains. It is strongly pleochroic, from grey to dark grey, and anisotropism is distinct.

**Bornite (  $\text{Cu}_5\text{FeS}_4$  )** occurs as rims and irregular polycrystalline aggregates between chalcopyrite and pyrrhotite. It is a rare mineral in the deposit. It was identified optically as pinkish-grey, tarnishing to purple along grain boundaries, and is isotropic.

### 3.4.2 Sulfosalts

**Tetrahedrite**  $(\text{Cu,Ag})_{10}(\text{Fe,Zn})_2(\text{Sb,As})_4\text{S}_{13}$  occurs as coarse, subhedral to anhedral grains, commonly interstitial (sample 49-269, Fig. 3.10 and Fig. 3.6 a), and shares grain boundaries with sphalerite, chalcopyrite and galena. The size ranges from  $10\ \mu\text{m}$ - $200\ \mu\text{m}$  in diameter but averages  $70\ \mu\text{m}$ - $150\ \mu\text{m}$ . In reflected light, its colour varies from olive-green-gray to bronze-gray. It is the most common sulfosalt at Mattabi. It is present as irregular veinlets, masses and remnants in sulfides. It also occurs as minute, disseminated grains commonly associated with chalcopyrite in zone III (Fig. 3.5). The mineral chemistry of tetrahedrite is discussed in chapter IV.

**Freibergite**  $(\text{Ag,Cu})_{10}(\text{Fe,Zn})_2\text{Sb}_4\text{S}_{13}$ , or argentian tetrahedrite, occurs as small subhedral, often prismatic grains ranging in size from  $40\ \mu\text{m}$ - $150\ \mu\text{m}$  in diameter but averaging  $60\ \mu\text{m}$ - $100\ \mu\text{m}$ . It invariably appears as inclusions within galena and is commonly interstitial to sphalerite, pyrite, chalcopyrite and gangue. In reflected light, it appears as dark olive-gray (sample 49-279), and no anomalous anisotropy or

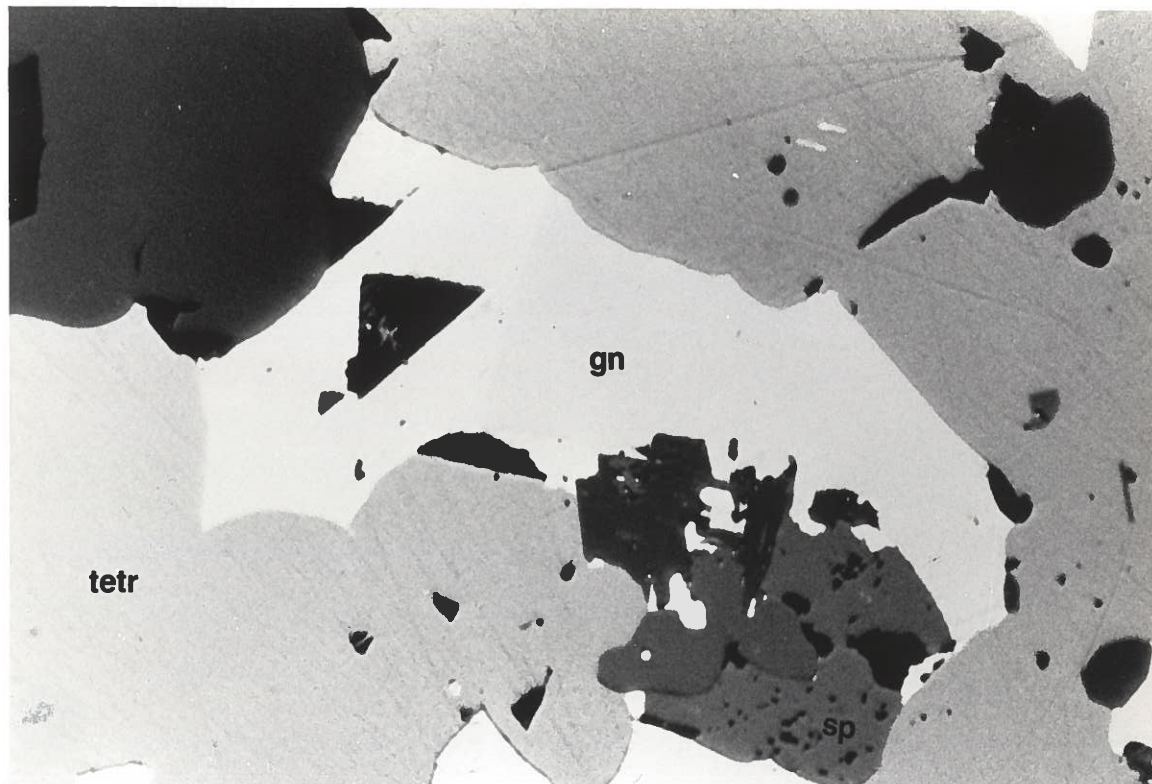


Fig. 3.10 Tetrahedrite in association with galena, exhibiting the concave grain boundary relationship. Sample 49-269

internal reflection was observed. The compositional range of freibergite is given in Appendix I, grains 9, 13, and 49.

**Pyrrargyrite (  $\text{Ag}_3\text{SbS}_3$  )** was identified in sample 49-284 only as a tiny grain interstitial to tetrahedrite and galena. It is the least common sulfosalt at Mattabi. Its grain size was  $10\mu\text{m}$  in diameter. The composition of pyrrargyrite was confirmed by scanning electron microprobe and X-ray energy dispersive spectrometry.

**Boulangerite (  $\text{Pb}_5\text{Sb}_4\text{S}_{11}$  )** occurs as elongated, iso-oriented aggregates, platy-like blades commonly projecting in galena (sample 3-198.5, Fig. 3.6 e). Isolated crystals and terminations are rare. It is locally observed also as thin, hair-like crystals in vugs. It is strongly pleochroic, from light green to dark green. Anisotropy is distinct. Its composition was confirmed by X-ray energy dispersive spectrometry.

**Freieslebenite (  $\text{PbAgSbS}_3$  )** was identified in sample 49-226 as dark, elongate, bladed inclusions in galena. Its composition was confirmed by X-ray energy dispersive spectrometry.

**Stephanite** ( $\text{Ag}_5\text{SbS}_4$ ) occurs in veins mineralized with sphalerite particularly at grain borders ( Fig. 3.6 d ). It was identified in sample 49-289. It is whitish pink with apparent lamellar twinning. It is strongly anisotropic. The grain boundaries are sharp and rectilinear with relatively simple locking. Its observed as short prismatic to tabular, locally with oblique striations on prism faces and often disseminated. X-ray energy dispersive spectrometry confirmed the composition of stephanite.

**Veenite** ( $\text{Pb}_2(\text{Sb,As})_2\text{S}_5$ ) occurs as minute grains associated with boulangerite and galena in sample 3-222.5.

### 3.4.3 Oxides

**Magnetite** ( $\text{Fe}_3\text{O}_4$ ) is the most common oxide mineral in the Mattabi deposit. It occurs as massive, coarse to medium, subhedral to subrounded grains having an average size from  $40\mu\text{m}$  to  $120\mu\text{m}$  in diameter. Occasionally, magnetite grains are found to be elongate in nature ( sample 49-455, Fig. 3.6 f ). It is commonly associated with gangue silicates and chalcopyrite. Magnetite occurring within gangue minerals is observed to be intimately intergrown with them suggesting their simultaneous formation.

**Hematite (  $\text{Fe}_2\text{O}_3$  )** was identified optically by its strong anisotropy, deep red internal reflections and apparent lamellar twinning. Its presence was confirmed by the scanning electron microprobe analysis. Hematite is found commonly associated with ilmenite and magnetite.

**Rutile (  $\text{TiO}_2$  )** is commonly concentrated in the gangue minerals and invariably associated with magnetite and ilmenite and intergrown with chalcopyrite ( sample 49-166, Fig. 3.6 g ) averaging in size between 20  $\mu\text{m}$ -25  $\mu\text{m}$  in diameter. It occurs as irregular needles but most commonly as disseminated subhedral to anhedral aggregated grains forming lensoidal layers and locally, as prismatic grains in zone IV ( Fig. 3.5 ). It occasionally consists of intimate intergrowths with hematite. Anisotropy and pleochroism are both weak.

**Cassiterite (  $\text{SnO}_2$  )** is the only tin-bearing mineral in the ore. It was identified by the scanning electron microprobe analysis. It appeared as whitish yellow to yellowish brown ( sample 3-228, Fig. 3.6 b ), distinctly idiomorphic and occurs as isolated, scattered, short prismatic to subrounded grains in sphalerite. It is restricted to zone II within the deposit

( Fig. 3.5 ) A spectrographic analysis showed that cassiterite contains no other metallic elements.

**Ilmenite (  $\text{FeTiO}_3$  )** occurs mainly as finely exsolved lamellae within magnetite and rarely as prismatic grains within gangue. Sometimes, it is observed as subhedral grains at grainboundaries with sphalerite.

( sample 49-455, Fig. 3.6 c ).

**Jacobsite (  $\text{Fe}^{+3}(\text{Mn},\text{Fe}^{+3})_2\text{O}_4$  )** occurs as subhedral to anhedral grains, usually massive and coarse. This is the only manganese-bearing mineral in the deposit and is commonly found in zone IV ( Fig. 3.5 ).

**Gahnite (  $\text{ZnAl}_2\text{O}_4$  )** occurs as euhedral coarse granular ( Fig. 3.6 h ) to compact or rounded grains. The average size of gahnite is 2 mm in diameter. These grains are octahedral, dark green and contain zones of inclusions. It is pervasive throughout the deposit but concentrated in zone IV ( Fig. 3.5 ).



### 3.5 Element and mineral zoning

The Matabi massive sulfide deposit is characterized by Cu+Fe+Mn-rich ores at the base and Zn+Pb-rich ores at the top( Fig. 3.5 ).

The boundaries are transitional in nature and were not necessarily stationary during the different periods of mineralization.

Zone I is characterized by pyrite, sphalerite, galena and freibergite.

Zone II is characterized by sphalerite, pyrite, galena, Ag-rich tetrahedrite and other sulfosalts. Cassiterite is restricted to the stratigraphic upper portion of the section.

Zone III is characterized by chalcopyrite,pyrrhotite and pyrite. The presence of pyrite here is probably due to the oxidation of pyrrhotite during which there is loss of iron and ultimately leading to the formation of magnetite and hematite in zone IV, fig. 3.5. Chalcopyrite accounts for a relatively high copper ore.

Zone IV is not part of the deposit and is characterized by oxide minerals .Magnetite, gahnite and jacobsite are the pervasive minerals in this oxidized zone. With exception of jacobsite, the rest of the oxide minerals occur in the deposit.

## CHAPTER IV

### Mineral Chemistry of Tetrahedrite

#### 4.1 Introduction

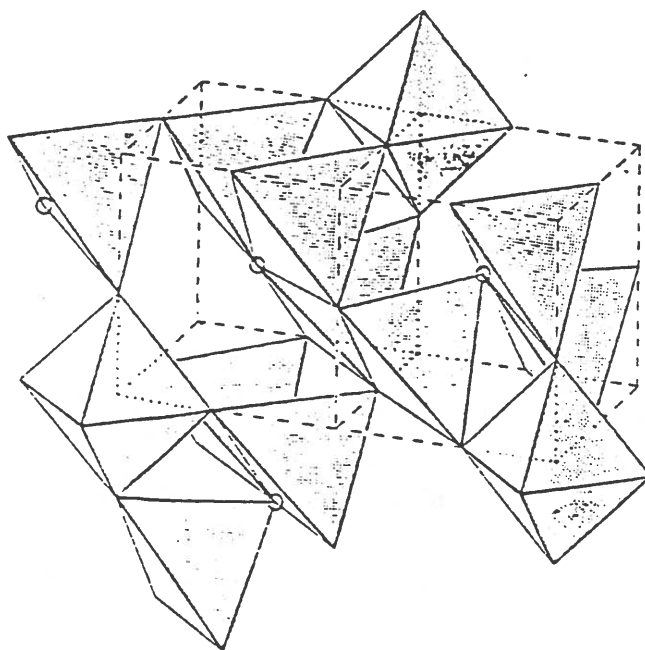
The tetrahedrite-freibergite series of minerals are widespread and carry significant amount of Ag, Cu, Sb in the Mattabi deposit. The tetrahedrite, in particular, is a common member of the fahlore group of minerals and approximates the formula  $(\text{Cu, Ag})_{10}(\text{Fe, Zn})_2(\text{Sb, As})_4\text{S}_{13}$  (Springer, 1969; Johan and Kvacek, 1971; Skinner et al. 1972; Tatsuka and Morimoto, 1973; Charlat and Levy, 1974; Wu and Petersen, 1977; Pattrick, 1978; Čvech and Hak, 1979; Amcoff, 1981; Basu et al. 1981; Craig et al. 1986, 1988; Johnson, 1987; Sack et al. 1987;). This formula, while complicated, is stoichiometric (Appendix I and II). To establish element zoning, compositional ranges and well defined positive and negative correlations in terms of metal contents, a 5-point analyses per grain for 60 grains of tetrahedrite were made. For the purpose of explaining the complex compositional variations in the tetrahedrite, the simple Brillouin zone model (Johnson and Jeanloz, 1983) was employed.

## 4.2 Analytical results

The composition of tetrahedrite was determined by calculating the mean of a 5-point analyses per grain in 60 grains (Appendix I) from Mattabi deposit. The approximate mean chemical composition was  $(\text{Cu}_{6.76} \text{Ag}_{3.34}) (\text{Fe}_{1.60} \text{Zn}_{0.62}) (\text{Sb}_{3.75} \text{As}_{0.28}) \text{S}_{13}$ . The sulfur content was found to be low and varied from 21 to 25 wt % (Appendix I). Similar low sulfur contents have been reported from other deposits by Petruk et al. (1971), Riley (1974), Pattrick (1978) and Sandeck and Amcoff (1981), among others. The greatest elemental variations in the analysed samples occur with Cu, Ag; Sb, As; but Zn is found to decrease whereas Fe remains between 1/2 and 2 as Ag increases beyond the value of 3 per 29 atoms. This effect has also been noted by Pattrick and Hall (1983). No distinct pattern of compositional zonation was observed, implying that cation exchange was pervasive and complete. This probably suggests that tetrahedrite was homogenized during the metamorphic event.

A plot of Ag versus Cu atoms displays a negative linear correlation (Fig. 4.1) indicating that the structure accepts a solid solution in the (Cu,Ag) sites (Fig. 4.2). The plot suggests a maximum of 6 Ag atoms per unit formula and shows an extensive compositional field. Within the tetrahedral

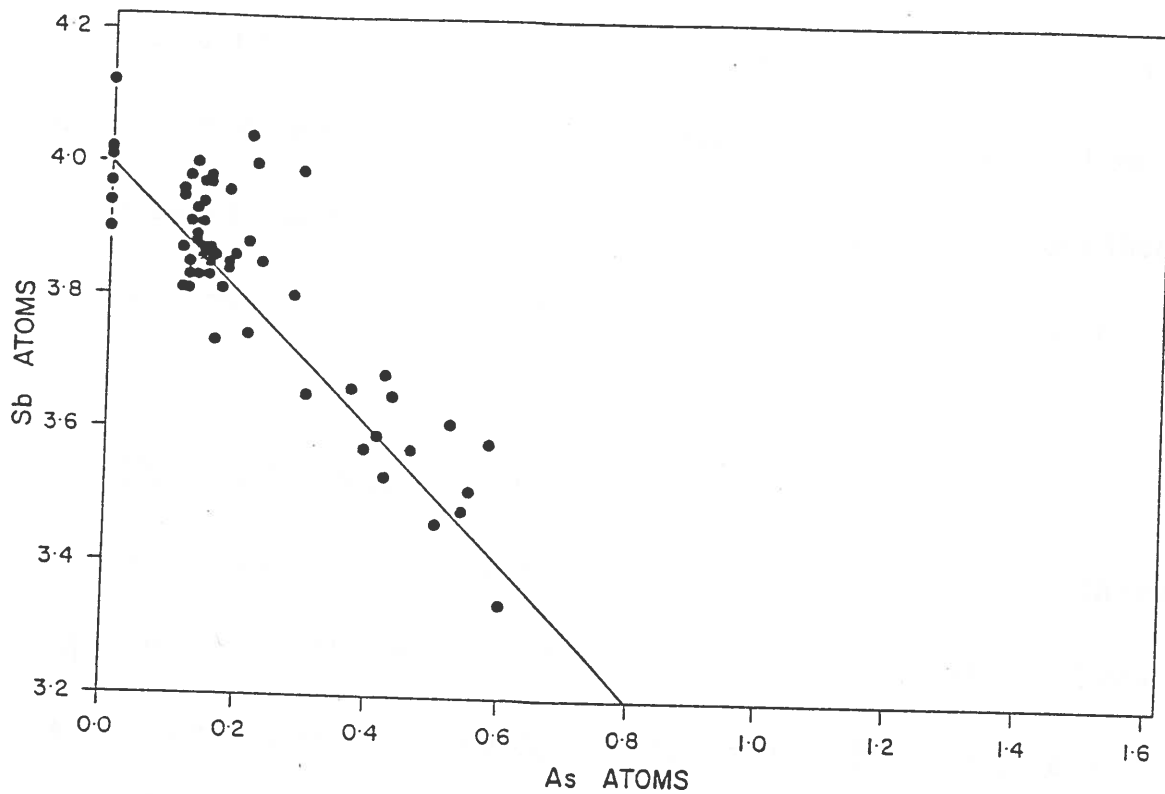




**Fig. 4.2 Linkage of the polyhedra formed by metal atoms coordinated about the sulfur atoms in tetrahedrite. Antimony sites are indicated by the small circles. All other vertices of the polyhedra represent copper sites, where substitution for silver takes place. (After Wuensch, 1963)**

series, the samples with high Ag values ( $Ag > 20$  wt %) according to the limits of Riley (1974) are termed freibergite (Grain 9, 13, 49, Appendix I). The majority of the compositions examined in the study contain 10 atoms of Cu per unit formula. A significant percentage have fewer than 10, to a minimum of 9.1 (Appendix II). This is consistent with experimental findings of Craig et al. (1986), Sack et al. (1985) and Lynch (1989). The plot also shows that the atom for atom substitution of Ag for Cu is continuous.

The analytical data (Fig. 4.3) support the long held premise of complete solid solution between Sb and As end-members. Sb content rises monotonically as As content decreases, demonstrating the diadochy of these two elements. Miller and Craig (1983) proposed that the positive correlation between Ag and Sb is not necessary but permissive or coupled. The plot also shows that there is relatively even distribution of compositions, which indicates that the geochemical conditions necessary for the formation of all members of solid solution probably existed.



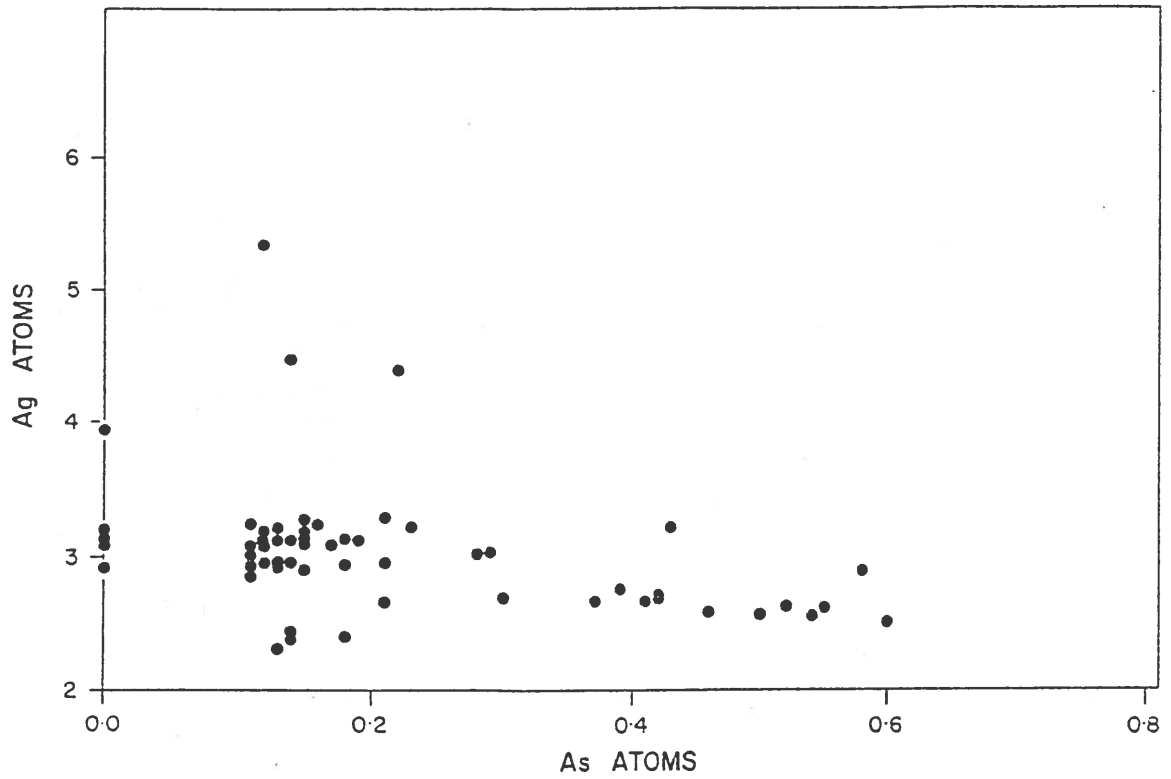
**Fig. 4.3** The number of Sb atoms versus the number of As atoms for tetrahedrite from Mattabi deposit. The solid line is the ideal solid-solution, assuming  $Sb+As = 4$  atoms (based on 29 atoms per unit cell).

The results in Fig. 4.4 show that Ag and As have little tolerance for each other in the tetrahedrite structure. The presence of only one atom of As decreases the maximum number of Ag atoms from 6 to 3. This means that As-rich tetrahedrites will not incorporate Ag even if readily available.

### 4.3 The Brillouin zone model

The Brillouin zone for a compound consists of the volume closer to the origin than to any other point of the compound's reciprocal lattice. Since the lattice of tetrahedrite is body-centred, the first Brillouin zone is bounded by the dodecahedron  $\langle 110 \rangle$  Jones (1975). This zone is filled by four electrons counting spin multiplicity. Johnson and Jeanloz, (1983) proposed that the stability of tetrahedrites is governed by the number of valence electrons available for each composition. A Brillouin zone for tetrahedrite in which 204-208 electrons are accommodated in the 51st Brillouin zone is verified in the analytical data. However, when three or more Ag atoms per unit formula are present, the number of valence electrons increases from 204-208 as Ag atoms increase from 3 to 6 (Fig. 4.5). As composition varies from the classical formula  $C_{12}Sb_4S_{13}$  (Pauling and Newmann, 1934) to the formula  $(Cu, Ag)_{10}(Fe, Zn)_2(As, Sb)_4S_{13}$  the number of valence electrons per unit cell increases from 204 to 208. At a value of 208, the 52<sup>nd</sup>





**Fig. 4.4** The number of Ag atoms versus the number of As atoms for samples of tetrahedrite from Mattabi deposit (based on 29 atoms per unit cell).



Brillouin zone is completely filled. The presence of (Fe+Zn) in excess of two atoms per unit formula appears to stabilize the 52nd Brillouin zone, with >208 valence electrons per unit cell. Such varying compositions with additional valence electrons available require a large increase in energy because electrons must be promoted across the energy gap before the next Brillouin zone can be filled.

## CHAPTER V

### Sphalerite Geobarometry

#### 5.1 Introduction

Sphalerite geobarometry enjoys wide support among petrologists and economic geologists at large (e.g, Essene, 1982; Torium, 1977; Hutchison and Scott, 1981; Scott and Kissin, 1973; Mathieson and Clark, 1984; Shiba, 1988 ) as a reliable tool that gives pressure values consistent with the pressure obtained by silicate equilibria. It was first proposed by Barton and Toulmin (1966) and later refined by Scott and Barnes (1971), Scott (1973) and Lusk and Ford (1978).

The following discussion aims at examining the iron content of sphalerite that has equilibrated with the iron sulfides so that conditions of deposition and subsequent metamorphism of the sulfide bearing ores may be deciphered. The sphalerite geobarometry is based on the continuously decreasing iron content of sphalerite as a function of pressure at any given temperature and in equilibrium with a suitable buffer for the FeS activity ( $a_{\text{FeS}}$ ). At any given temperature and pressure,  $a_{\text{FeS}}$

is buffered by the coexisting pyrite and pyrrhotite through the following reaction :



Electron microprobe analyses were obtained from sphalerite grains in the following different textural relations:

- 1) Sphalerite forming triple junction with pyrite and pyrrhotite.
- 2) Sphalerite encapsulated within pyrite.
- 3) Sphalerite in contact with pyrite
- 4) Sphalerite in contact with pyrrhotite.

The values, quoted as mole % FeS in sphalerite for these various assemblages, are shown in Appendix IV. Mn and Cd were less than 0.1 wt% in all sphalerite samples.

## 5.2 Equilibrium Model

A portion of the system Fe-Zn-S that includes pyrite, pyrrhotite and sphalerite is considered. In this barometer, it is assumed that no other solid solution series is significant for the minerals concerned. The availability of experimental data on pyrrhotite-pyrite and sphalerite-pyrrhotite in equilibrium with pyrite at 1 bar (Scott and Barnes, 1971) enabled the calculation of equilibrium compositions of

pyrrhotite and sphalerite solid solutions as functions of pressure and temperature. Further more, the equilibrium compositions of the three phase equilibrium can actually be reproduced by synthetic experiments (Scott and Barnes, 1971; Scott, 1973; Hutchison and Scott, 1980).

Hutchison and Scott (1980) refined thermodynamic calculation and on the basis of the temperature independence of their 10 kbar isobar, concluded that the discrepancy is insignificant because the thermal expansion and compressibility of the relevant phases are not adequately known. Sphalerite was observed as homogeneous as evidenced by the lack of colour zoning. The microprobe analysis of six samples of sphalerite occurring with pyrite and pyrrhotite show a well defined mode between 11 and 14 mole % FeS (Fig. 5.1a), a mean of  $12.11 \pm 0.79$  mole % FeS. The FeS content of sphalerite indicate a pressure of metamorphism of 7.53 kbar, described by the equation

$$P = 42.30 - 32.10 \log \text{ mole \% FeS}$$

using the sphalerite geobarometer (Hutchison and Scott, 1980). This pressure is approximately 2 - 3.77 kbar too high in comparison with the pressures suggested by the silicate systems in the Mattabi ores (Franklin et al. 1977) that indicate a pressure of < 4 kbar.

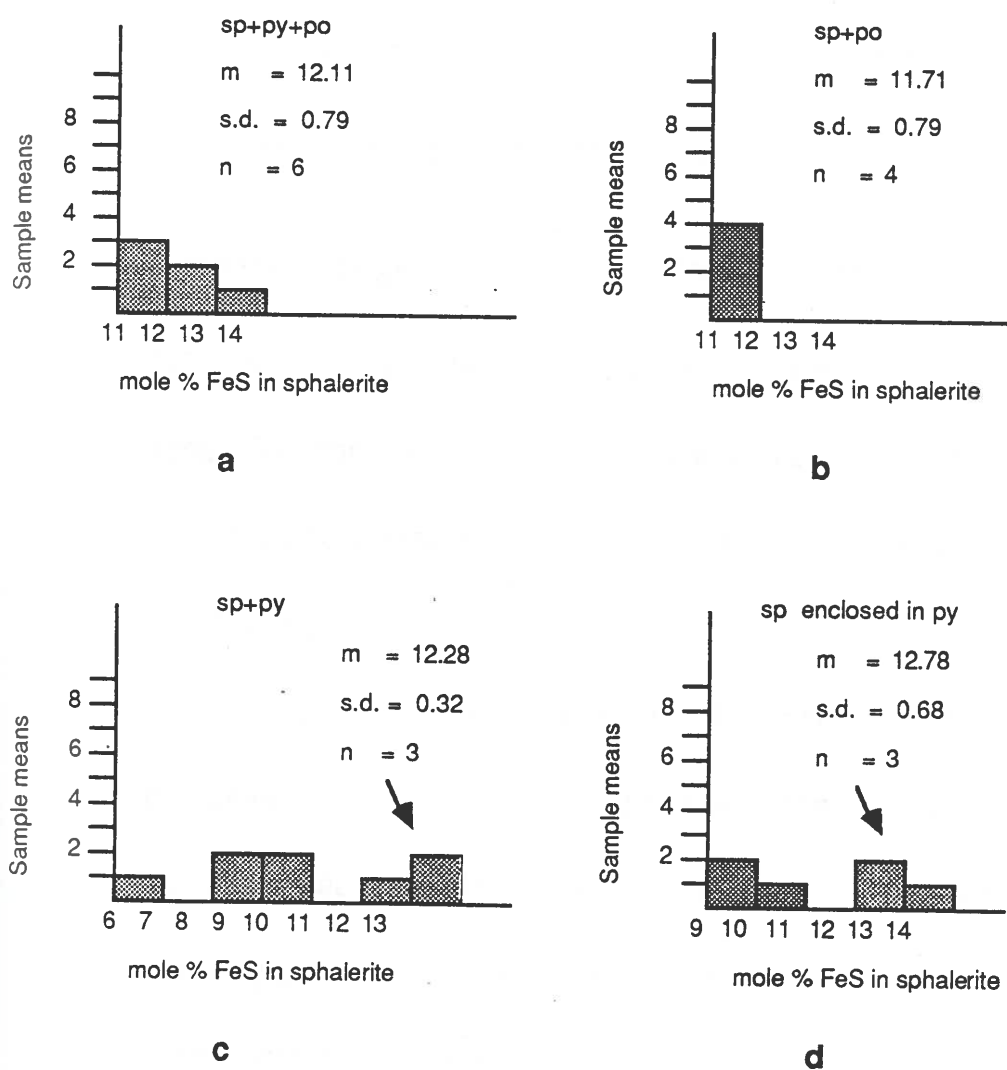


Fig. 5.1 FeS contents and observed iron sulfide assemblages of sphalerites associated with Mattabi massive sulfide deposit, Northwestern Ontario. The arrows point to highest mean value of mode.

A possible explanation is that sphalerite-pyrite-pyrrhotite equilibrated at peak pressure, whereas silicate assemblages indicate conditions of peak temperature in the P-T-t history of metamorphism of the deposit (Fig. 5.2). T-max and sulfur activity both increased resulting in a reduced  $a_{\text{FeS}}$ . The decrease in  $a_{\text{FeS}}$  with increasing temperature conspired to minimize the FeS content of sphalerite. Retrograde alteration variably affected the sphalerite composition producing some scatter in data, as well, as evidenced by variable occurrence of late-stage monoclinic pyrrhotite (Fig. 5.3, 5.4, 5.5).

Compositions of sphalerite totally enclosed within metablastic pyrites represent high P-T equilibria that have been isolated from further reaction during subsequent retrograde conditions by the inert encapsulating pyrite and may provide more reliable estimates of pressure. The histogram (Fig. 5.1d) indicates bimodality between 9-11 and 12-14. The latter mode shows a calculated mean of 12.78 mole % FeS with a standard deviation of 0.68. This assemblage has a higher FeS content compared to the other assemblages, which, on textural grounds is judged to have been extremely recrystallized.

The high FeS-content is observed to be even higher than the texturally



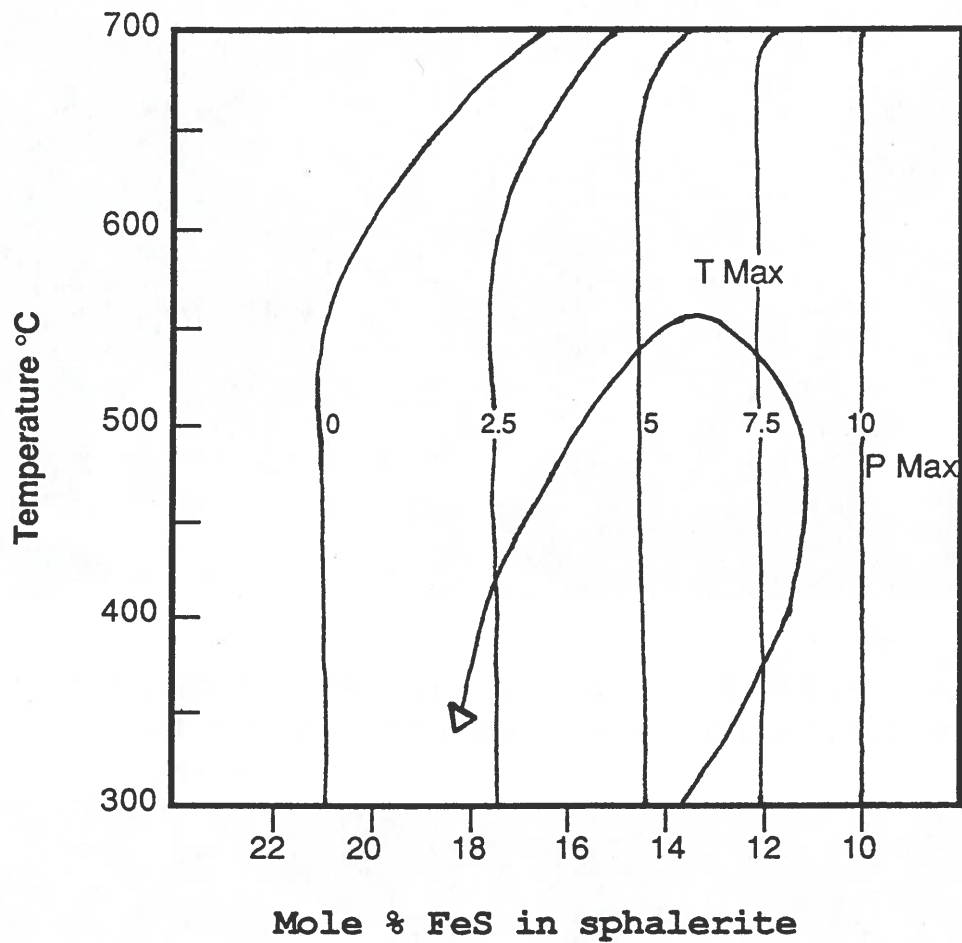


Fig.5.2 A schematic P-T-t path experienced by an assemblage of sphalerite-pyrrhotite-pyrite during regional metamorphism. (After Bryndzia, 1989)

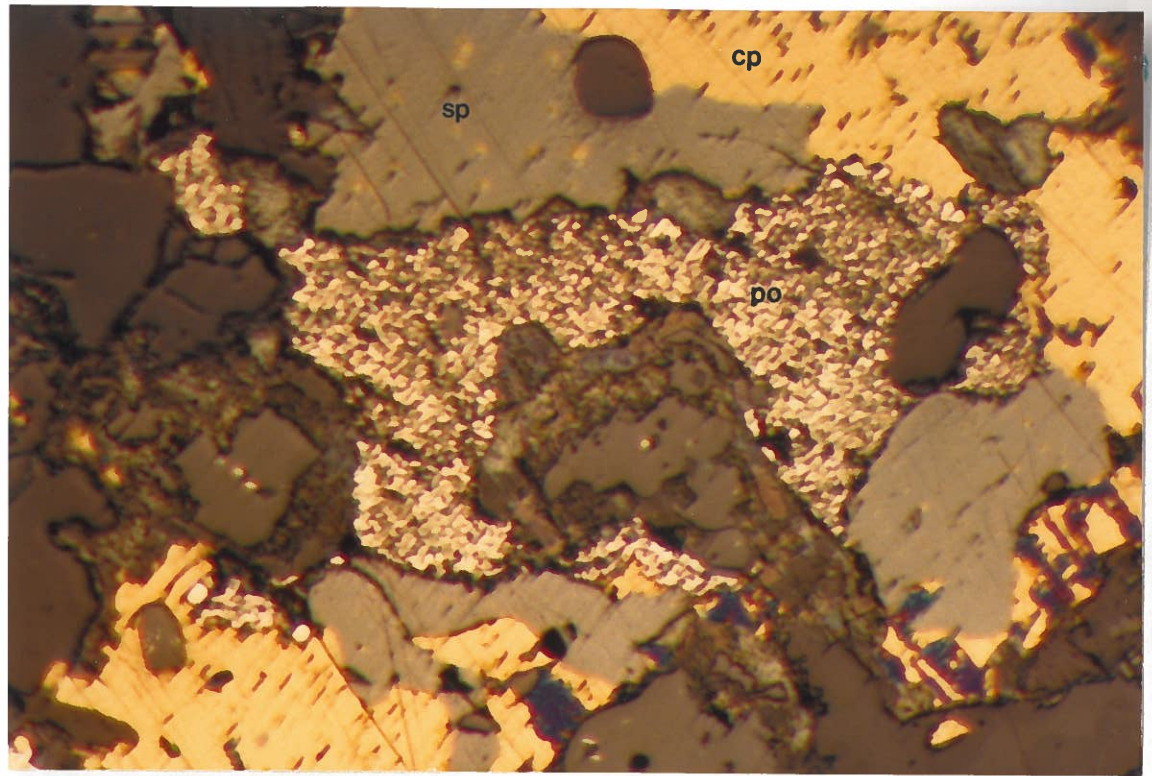


Fig. 5.3 Etched pyrrhotite from sample 49-190 displaying alteration to secondary monoclinic pyrrhotite (white). 0.4mm

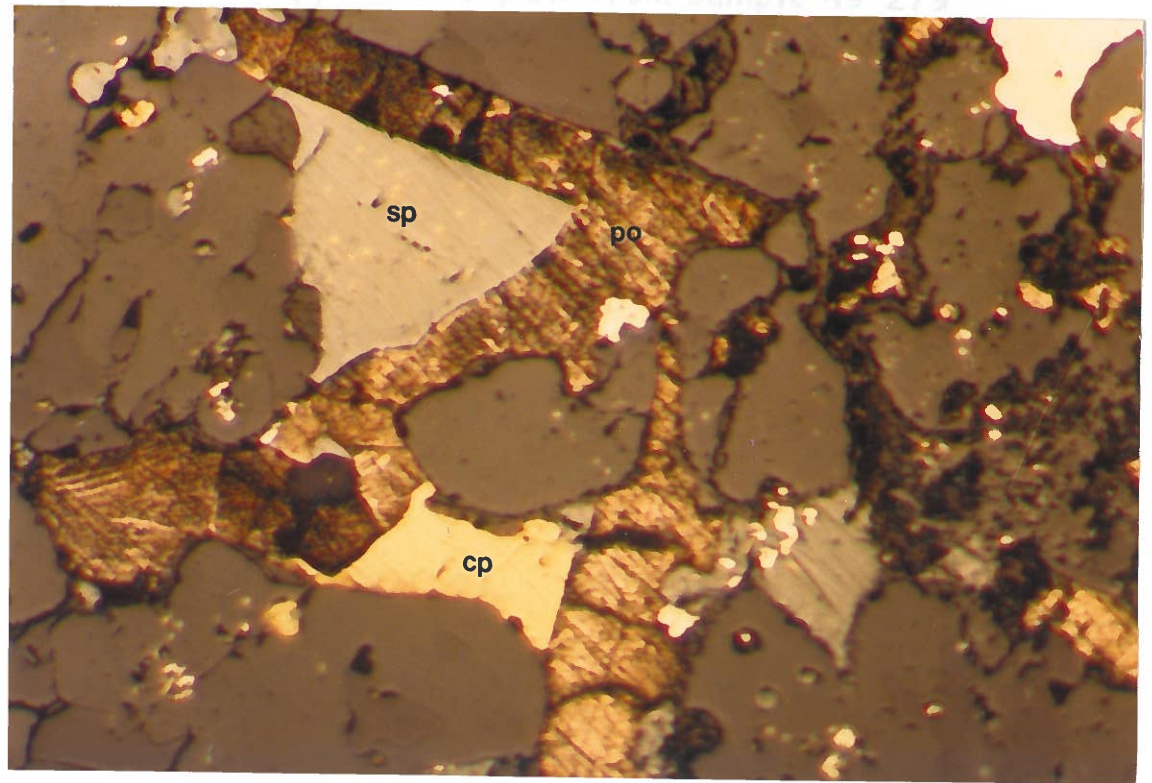


Fig. 5.4 An etched pyrrhotite grain from sample 3-219 exhibiting nearly complete conversion to monoclinic pyrrhotite (white) with finely scattered lamellae (dark) of remnant hexagonal pyrrhotite. 0.4mm

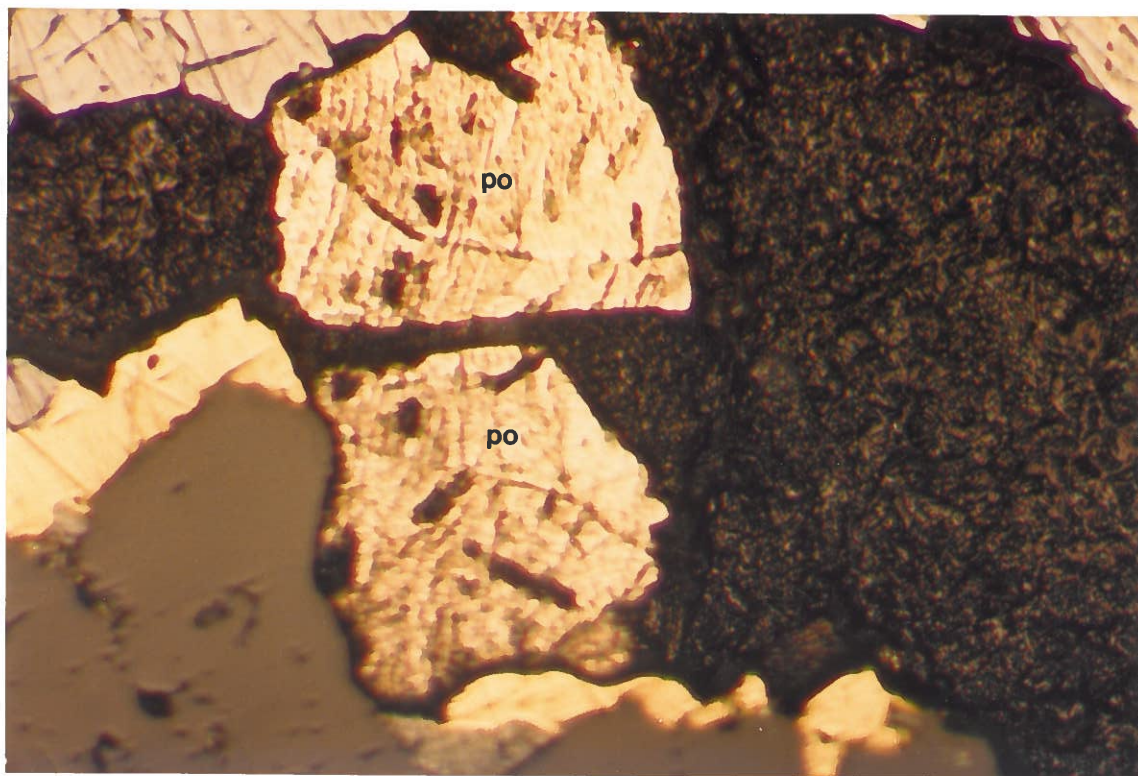


Fig. 5.5 Etched pyrrhotite grain from sample 49-279 displaying unetched secondary monoclinic pyrrhotite (white) surrounded by remnant hexagonal pyrrhotite (dark).

similar sphalerites from kuroko deposit (Kalogeropoulos and Scott, 1983), suggesting that the Mattabi deposit reflects the effects of prograde metamorphism. Hutchison and Scott (1981) have proposed that encapsulation of sphalerite by pyrite, a relatively nonreactive phase, inhibits compositional change during low-grade retrograde events and may render the sphalerite suitable for estimating prograde pressures. This agrees with the findings of Bryndzia (1989) that bimodal sphalerite compositions typically preserved by sphalerite from regional metamorphic terrains are believed to represent pressures at both  $P_{max}$  and  $T_{max}$  and are not attributable to retrograde re-equilibration of sphalerite. Some of these sphalerite grains are indeed iron-rich, consistent with the low pressure of the order of 2 - 3.76 kbar, but the overall range of compositions is so wide as to render such estimates unreliable.

In the sphalerite -pyrrhotite assemblage, the sphalerites do not display a wide range in composition (Fig. 5.1b), the mean being at 11.71 mole % FeS and the mode between 11-12 with a standard deviation of 0.79. In view of the low FeS in sphalerite, equilibrium must have occurred at low (Fig. 5.3) temperature prior to the onset of retrograde alteration of pyrrhotites.

In practice, pyrrhotites do suffer compositional changes on cooling (Kissin and Scott, 1973). But, when  $a_{\text{FeS}}$  is buffered by divariant assemblages in the Fe-S system, retrograde variation in pyrrhotite is not important (Scott, 1976).

Sphalerite in contact only with pyrite shows a wide range of compositions. The histogram (Fig. 5.1c) is bimodal between 8-10 and 11-13 mole % FeS. The latter shows a mean of 12.28 mole % FeS and a standard deviation of 0.32. The low FeS-content indicate that pyrite and sphalerite did not preserve their equilibrium compositions attained during metamorphism. Instead, they readily re-equilibrated during retrograde cooling, so are of little or no use as geobarometers (Barton, 1970).

### **5.3 Pressure and Metamorphism**

A large number of massive sulfide deposits occur in volcanic and sedimentary rocks that have been involved in an orogeny. The Mattabi deposit in particular, is probably associated with Kenoran orogeny (Franklin et al. 1977). Textural studies indicate that regional metamorphism and deformation are well imprinted on the pyritic, sphaleritic and pyrrhotitic ores of Mattabi, suggesting that metamorphism was probably related to

orogenic disturbance. Fig. 5.6 shows that  $T_{\max}$  is  $505^{\circ}\text{C}$  if the  $P \leq 3.77$  kbar because of the aluminosilicate triple point and the kyanite stability field shown by the shaded area. However,  $P$  could have been higher, but  $T$  would be less than  $505^{\circ}\text{C}$  if there is a shift into the andalusite field on reaching  $T_{\max}$  (as shown by trend of arrow). The lower temperature limit is demonstrated by the garnet isograd. The pressure could be in error as little as 2 kbar depending on where the arrow starts. Chloritoid is assumed stable in the entire region of concern.

The FeS content of sphalerite in the sphalerite-pyrite-pyrrhotite assemblage had a mean of 12.11 mole % FeS, reflecting effects of retrograde metamorphism. Any retrograde temperature-pressure path for an original equilibrium three-phase assemblage, will result in re-equilibration toward higher FeS content at temperatures above  $300^{\circ}\text{C}$  (Fig. 5.2). Below  $300^{\circ}\text{C}$ , the sphalerite-pyrite-pyrrhotite isobars all swing to very low FeS content (Scott and Kissin, 1973), suggesting that if re-equilibration occurs at these temperatures, the resulting FeS-content will be low, if equilibrium is maintained. The final result is then a complex function of the P-T conditions of peak metamorphism, the degree of re-equilibration during the retrograde event, the final P-T conditions where re-equilibration stops and



the final FeS-content is frozen into sphalerite.

With the temperature of sphalerite equilibration indicated by the metamorphic grade of the rocks associated with the ores and FeS-content of sphalerite known, the equation from Hutchison and Scott (1980) allowed the estimation of pressures existing at the time of sphalerite equilibration.

A clue as to the metamorphic pressures is provided by aluminium silicate polymorphs reported by Franklin et al.(1977), as opposed to the pressures determined by the sphalerite geobarometry. The highest grade of metamorphism attained by the country rocks surrounding these ores correspond to the chloritoid-kyanite-andalusite subfacies of the amphibolite facies. The maximum temperature of formation of the ores, the aluminosilicate triple point (505°C) agrees with the highest temperature generally accepted for the kyanite-andalusite-chloritoid subfacies. However, a rather low geothermal gradient of 22°C/km has been estimated from the pressure determined by the sphalerite geobarometry.



## CHAPTER VI

### **Comparative study, Summary, Conclusions and Recommendations**

A preliminary study of ore mineralization of Mattabi deposit south of Sturgeon Lake area has been reported by Franklin et al. (1977), and the characteristics of the Mattabi Mine have been described by Franklin et al. (1975). Mineralogical data from Mattabi indicate that pyrite, sphalerite, galena, chalcopyrite and arsenopyrite account for more than 95% of the sulfide minerals. Tetrahedrite, freibergite, boulangierite and freieslebenite are common minor sulfosalt minerals. The Mattabi deposit has two stacked ore lenses, each of which has a central, transgressive pyrite-galena-sphalerite zone accompanied by tetrahedrite and arsenopyrite. The zinc ore is well banded and contains colloform textured pyrite. It appears that at Mattabi, primary textures were destroyed by the later growth of the lower copper-rich zone, indicative of the post depositional alteration of the sulfide mass.

### 6.1 Comparison to related Canadian ore deposits

The Noranda type deposits are Archean and are termed primitive (Hutchinson, 1980), since these deposits are hosted by fully differentiated suites, basaltic to rhyolitic lavas and pyroclastics. Hutchinson (1973) noted that the relationship between frequency of occurrence of massive sulfide deposits in Canada and age is very irregular. He related this irregularity to variations in frequency of major orogenic activity. The characteristics of the Mattabi Mine are different from those of Noranda and Mattagami areas in that it is relatively rich in lead. The Ordovician Bathurst district of New Brunswick with 109.2 metric tons of ore (Franklin and Morton, 1987) differ from Mattabi in containing native Bi. No bismuth minerals have been recorded at Mattabi.

The distribution of Ag and Au in most Precambrian massive sulfide deposits is poorly understood. The Archean Mattabi deposit with higher Ag content (19 wt %) have relatively high lead contents (0.77-1.00% Pb), but silver does not correlate specifically with lead, in contrast to Phanerozoic deposits (Franklin and Morton, 1987). For example, in the relatively lead-rich Mattabi deposit, silver occurs primarily in argentian tetrahedrite or freibergite in the upper portion of the massive ore. The Winston Lake

deposit, 32 km north of Schreiber, Ontario, averages 0.880z/ton Ag, 0.03% Au, 1% Cu and 16% Zn. The Mobern deposit, 30 km north of Rouyn-Noranda, Quebec, averages 43.5g/ton Ag, 1.71g/ton Au, 0.71% Cu and 5.84% Zn in 6 million tons of ore. Like Mattabi, the Proterozoic Snow Lake deposits in northern Manitoba are relatively lead-rich, but the Mandy deposit, although deficient in lead, has an exceptionally high base metal content ( 9% Zn, 7.3% Cu). The Cu/Zn ratio is 10:1 as compared to 6:1 of Mattabi deposit (Franklin and Morton, 1987).

Whereas the Mattabi deposit has been found to be deficient in gold content, the Mobern, Horne, Quemont, Pick Lake, Winston Lake and Mandy deposits bear 5.5g/metric ton of gold, almost ten times the normal Au content of massive sulfide deposits.

The low gold content, high lead-content, diversity of sulfosalt species and abundance of Ag in argentian tetrahedrite or freibergite are features more similar to those of kuroko-type deposits of the Phanerozoic than to Noranda or primitive-type massive sulfide deposits characteristic of the Archean (Hutchinson, 1980). The Archean Mattabi bears superficial resemblance to the Phanerozoic kuroko deposits (Hutchinson, 1980) in being strata-bound, stratiform bodies that occur in probable island arc suites and also show similarity in mineral zonation. The kuroko mineralogy consists of

pyrite, pyrrhotite, sphalerite, galena, chalcopyrite, tetrahedrite group, quartz and barite as gangue. Alteration pipes are not vertically extensive, although they are mineralogically well-defined. The zonation is characterized by sericite-quartz core surrounded by a magnesium-enriched chlorite halo. Hanging wall alteration zones, defined primarily on mineralogical basis, are only evident in kuroko deposits. In cases where overlying deposits do not exist, the hanging wall alteration is more subtle, with little chemical change and is thus more difficult to detect. Like Mattabi, studies of the black ores in kuroko deposits of Japan suggest that As-rich tetrahedrite crystallized earlier from the ascending hydrothermal solutions and hence is concentrated in the lower ore zones, whereas the argentian tetrahedrite is concentrated in the upper ore zone (Ohmoto et al. 1984).

Similarity of metamorphic features and minerals of the kuroko and Mattabi deposits suggests a similarity in metamorphism. The marked difference in mineralogy is that kuroko contains a high concentration of barite, gypsum and anhydrite (Sato, 1974). Iron formations are associated with both deposits. The association however, is not ubiquitous, and its genetic relationship to volcanogenic massive sulfide deposits may be somewhat incidental (Franklin et al. 1981). The siliceous ores of kuroko

deposits occur in intensely altered rocks. A broad range of microscopic ore textures are preserved in addition to the megascopic ones. Colloform and earlier framboidal textures in pyrite are very common in black ores, whereas the yellow and siliceous ores commonly contain submicroscopic, euhedral to subhedral pyrite aggregates (Watanabe, 1974). The euhedral nature of some of the pyrite may indicate that some parts of the kuroko deposit may be recrystallized in spite of a very low regional metamorphic grade. Barton (1978) noted that much of the sphalerite suffers from chalcopyrite disease. He suggested that the sulfide mass underwent considerable repeated recrystallization on the sea floor and that after initial sulfide deposition, the ore underwent diagenetic recrystallization and reaction with intrastretal fluid, which changed the ore composition.

## 6.2 Summary

The ore mineralogy of Mattabi Mine is typical of massive and minor vein occurrences of combined base metal and precious metal ores. The mineralogy is varied and complex. Among the varied species, is argentic tetrahedrite with elemental variations characterized by substitution between silver and copper, antimony and arsenic, as well as silver and arsenic. Recent studies have shown that substitutions in tetrahedrite

Involving arsenic-antimony, iron-zinc and copper-iron may be considered ideal (Sack and Loucks, 1985) but that between copper-silver is non-ideal (Johnson et al. 1987). Contents of the minor elements arsenic, antimony and tin in the deposit are considered normal, and unusual sulfide minerals, e.g. veenite and freieslebenite, have been identified.

The presence of silver-bearing minerals, such as freibergite, stephanite, pyrargyrite and freieslebenite, demonstrate the argentiferous character of the Mattabi ores. The generally intimate association of these mineral phases with galena is intriguing. This probably suggests that lead, antimony and silver in particular, may have been partially remobilized during a post depositional episode of metamorphism or deformation. The extent to which such remobilization takes place during metamorphism is not documented. However, in a detailed mineralogical investigation of the Izok Lake massive sulfide deposit, Northwest Territories, lead, silver, antimony, and copper were found to be dispersed into the footwall and hanging wall rocks for as much as 3 metres from the massive ore apparently during regional metamorphism (Harris et al. 1984).

Textural studies of the ores, and the suggested correlation with regional deformational events, indicate that the mineralization at Mattabi may have resulted from a complex, multistage process of deposition, diagenesis and

regional metamorphism. During the subsequent episodes of regional metamorphism, the orebodies were deformed and recrystallized. The last mineralizing stage was probably the development of the vug associations.

Sphalerite-pyrite, sphalerite-pyrrhotite, sphalerite-pyrite-pyrrhotite, sphalerite enclosed in pyrite, are the four sulfide assemblages that were investigated for FeS content in sphalerite. Sphalerite in the sphalerite-pyrite-pyrrhotite assemblage presumably achieved a mean of 12.11 mol % FeS content at maximum pressure considerably before peak temperature of metamorphism. A possible explanation would be that T-max and sulfur activity both increased resulting in a reduced  $a_{\text{FeS}}$ . The decrease in  $a_{\text{FeS}}$  with increasing temperature minimized the FeS-content of sphalerite. The low FeS-content of sphalerite could further be attributed to retrograde alteration, which affected the sphalerite composition, as evidenced by variable occurrence of late-stage monoclinic pyrrhotite. Overall, hexagonal pyrrhotite is the dominant iron monosulfide polymorph in the sphalerite-pyrite-pyrrhotite assemblage. The presence of hexagonal pyrrhotite only in many of these samples suggests that equilibration was above the pyrrhotite inversion temperature (Scott and Barnes, 1971; Scott, 1973).

### 6.3 Conclusions

The research project has resulted in the following conclusions:

1) Mineral zoning in the orebody is pronounced. Sphalerite, tetrahedrite, galena and sulfosalts all occur in the upper portion of the orebody, whereas pyrrhotite and chalcopyrite are concentrated in the lower portion. The oxide minerals except for jacobsite, occur in the ore zone as well as in the footwall alteration zone.

2) Most of the silver in the deposit is present in argentian tetrahedrite or freibergite and averages 19 wt %. The rest of silver is present in stephanite, pyrargyrite and freieslebenite.

3) The calculated formulae based on 13 sulfur atoms in tetrahedrite show an approximate structural formula of the form:



4) When 3 or more silver atoms are present, the number of valence electrons increases from 204 to 208 as silver atoms increase from 3 to 6. The presence of (Fe+Zn) in excess of two atoms per unit formula appears to stabilize the 52nd Brillouin zone with >208 valence electrons per unit cell.

5) The pressure of metamorphism is 7.53 kbars from the sphalerite geobarometry. This pressure is approximately 2 to 3.77 kbar too high in comparison to the pressures suggested by the silicate systems.



6) The low gold content, high lead content, diversity of sulfosalt species and abundance of Ag in tetrahedrite are features more similar to those of kuroko-type deposits of the Phanerozoic than to Noranda or primitive-type massive sulfide deposits characteristic of Archean.

#### **6.4 Recommendations**

A few recommendations are presented for further research on the deposit.

- 1) Why and how high-temperature ( $>215^{\circ}\text{C}$ ) galena solid solutions of different silver and antimony contents exsolve or become intergrown with a variety of observed silver, antimony and lead sulfosalts in the (Pb-Ag-Sb-S) system.
- 2) Additional detailed studies should be conducted to correlate specific mineralizing events and mineral compositions.
- 3) Sulfur isotopic studies and geothermometry may be needed to provide additional evidence of the processes leading to mineralization.

## REFERENCES

- BRYNDZIA, L.T and DAVIS, A.M (1989); Liquidus phase relations on the quasi-binary join  $\text{Cu}_2\text{S}-\text{Sb}_2\text{S}_3$ : Implications for the formation of tetrahedrite and skinnerite: *American Mineralogist*, volume 74, page 236-242.
- BARTON, P. B. (1978); Some ore textures involving sphalerite from the Furutoba mine, Akita Prefecture, Japan: *Mining Geology*, volume 28, page 293 -300.
- BARTON, P. B and TOULMIN, P. (1966); Phase relations involving sphalerite in the Fe-Zn-S system: *Economic Geology*, volume 61, page 815-849.
- BOHLEN, S. R., WALL, V. J. and BOETTCHER, A. L. (1983); Geobarometry in granulites. In S. K. Saxena (ed) *Advances in Physical Geochemistry*, volume 3 page 71-141.
- BARTON, P. B. (1970); *Sulfide Petrology*: Mineralogical Society of America, Special Paper 3, page 187-198.
- BASU, K. (1981); Rare minerals from Rajpura-Dariba, Rajasthan, India III. Plumbian tetrahedrite: *Neues. Jahrb. Mineralogist*, volume 141, page 280-289.
- CLARK, A. (1970); Native zinc and alpha-copper, zinc, from Mina Dulcinea de Llampos, Copiapo, Chile: *American Mineralogist*, volume 55, page 1019-1025.
- ČECH, F. and HAK, J. (1979); Tetrahedrite high in silver, zinc and cadmium from Jihlava, Czechoslovakia: *Casopis Por Mineralogii a Geologii*, volume 24, page 83-87.
- CHARLAT, M. and LEVY, C. (1974); Substitution multiples dan la Serie tennantite-tetrahedrite: *Bulletin de la Societe francaise de mineralogie et de crystallographie*, volume 97, page 241-250.

- CANADIAN MINING PERSPECTIVE, (1983); Mineral Bulletin MR 206: Energy Mines and Resources Canada, 34 pages.
- EVANS, B.W. (1965); Application of a reaction-rate method to the breakdown equilibria of muscovite and muscovite plus quartz: American Journal Science, volume 263, page 647-667.
- ESSENE, E.J. (1982); Geologic thermometry and barometry. Characterization of metamorphism through mineral equilibria. Mineralogical Society of America, page 153-206.
- ELDRIDGE, C.S. (1988); Hydrothermal Inoculation and Incubation of the chalcopyrite disease in sphalerite: Economic Geology, volume 83, page 978-989.
- FRANKLIN, J.M., GIBBS, W., POULSEN, K.H. and SEVERIN, P. (1977); Archean Metallogeny and Stratigraphy of the South Sturgeon Lake area: Mattabi Trip, 23rd Annual Meeting at Institute on Lake Superior Geology, 73 pages.
- FRANKLIN, J.M., LYDON, J.W. and SANGSTER, D.F. (1987); Volcanic-associated massive sulfide deposits: Economic Geology 75th Anniversary volume, page 485-625.
- FRANKLIN, J.M., KASARDA, J. and POULSEN, K.H. (1975); Petrology and chemistry of the alteration zone of the Mattabi massive sulfide deposit: Economic Geology, volume 70, page 63-79.
- FRANKLIN, J.M., GROVE, D.A. and MORTON, R.L. (1987); Physical volcanology of the footwall rocks near the Mattabi massive sulfide deposit, Sturgeon Lake, Ontario: Canadian Journal Earth Science volume 25, page 280-291.
- FRANKLIN, J.M., and MORTON, R.L. (1987); Two-fold classification of Archean volcanic-hosted massive sulfide deposits: Economic Geology, volume 82, page 1057-1064.

- FRANKLIN, J.M., THORPE, R.I. and SANGSTER, D.F. (1981); Evolution of lead in massive sulfide ores of Bathurst District, New Brunswick, Canada: Institute Mining Metallurgy Transcripts, volume 90, section B, page B55-B56.
- GROVES, D. A (1984); Stratigraphy and Alteration of the footwall volcanic rocks beneath the Archean Mattabi massive sulfide deposit, Sturgeon Lake, Ontario: Unpublished M.Sc. thesis, University of Minnesota-Duluth, 115 pages.
- HUTCHISON, M. N. and SCOTT, S.D. (1981); Sphalerite geobarometry in the Cu-Fe-Zn-S system: Economic Geology, volume 76, page 143-153.
- HARRIS, D.C., CABRI, L.J. and NOBILING, R., (1984); Silver-bearing chalcopyrite, a principal source of silver in the Izok Lake massive sulfide deposit: confirmation by electron and proton-microprobe analyses: Canadian Mineralogist, volume 22, page 493-498.
- HUTCHISON, I. (1978); Calculation of metamorphic pressure using the sphalerite-pyrrhotite-pyrite equilibrium: American Mineralogist, volume 63, page 87-95.
- HUTCHINSON, R.W. (1973); Volcanogenic sulfide deposits and their metallogenic significance: Economic Geology, volume 68, page 1223-1245.
- HUTCHINSON, R.W. (1980); Massive base metal sulfide deposits as guide to tectonic evolution: The continental crust and its mineral deposits: Geological Association of Canada Special Paper, 20 pages.
- HOLDAWAY, M.J. (1971); Stability of andalusite and the aluminium silicate phase diagram: American Journal of Science, volume 271, page 97-131.
- JOHNSON, N.E, CRAIG, J.R. and RIMSTIDT, J.D. (1986); Compositional trends in Tetrahedrite: Canadian Mineralogist, Volume 24, page 385-397.

- JOHNSON, N.E, CRAIG, J.R. and RIMSTIDT, J.D. (1987); Effect of substitutions on the cell dimension of tetrahedrite: *Canadian Mineralogist*, volume 25, page 245-249.
- JOHNSON, M.L. and JEANLOZ, R. (1983); A Brillouin-zone model for compositional variation in tetrahedrite: *American Mineralogist*, Volume 68, page 220-226.
- JOHNSON, N.E, CRAIG, J.R and RIMSTIDT, J.D (1988); Crystal chemistry of tetrahedrite: *American Mineralogist*, volume 73, page 389-397.
- JONES, H. (1975); The theory of Brillouin zones and electronic states in crystals: North-Holland, London.
- JOHAN, Z. and KVACEK, M. (1971); La hakite un nouveau mineral du groupe de la tetrahedrite: *Bulletin Societe Francaise. Mineral Cristallographica*, volume 94, page 45-48.
- JOHNSON, J.A. and De Wall, S.A. (1981); Chemical heterogeneity of sphalerite in a base metal sulfide deposit: *Economic Geology*, volume 76, page 694-705.
- KASARDA, J. (1973); Wall rock alteration and trace element geochemistry of the footwall rocks of the Mattabi deposit, Sturgeon Lake area, Ontario: Unpublished B.Sc. thesis, Lakehead University, Thunder Bay, Ontario, 74 pages.
- KALOGEROPOULOS, S.I and SCOTT, S.D (1987); Mineralogy and geochemistry of an Archean tuffaceous exhalite: the Main Contact Tuff, Millenbach mine area, Noranda, Quebec: *Canadian Journal Earth Science*, volume 26, page 88-105.
- KALOGEROPOULOS, S.I and SCOTT, S.D (1983); Mineralogy and geochemistry of tuffaceous exhalites of the Fukazawa mine, Hokuroku district, Japan: *Economic Geology Monograph* 5, page 412-432.

- LUSK, J. and FORD, C. E. (1978); Experimental extension of the sphalerite geobarometer to 10 kbar: *American Mineralogist*, volume 63, page 516-519.
- LYNCH, J. V. (1989); Large scale hydrothermal zoning reflected in the tetrahedrite-freibergite solid solution, Keno Hill Ag-Pb-Zn district, Yukon: *Canadian Mineralogist*, volume 27, page 383-400.
- MILLER, J.W. and CRAIG, J.R. (1983); Tetrahedrite-tennantite series compositional variations in the Cofer Deposit, Mineral District, Virginia: *American Mineralogist*, volume 68, page 227-234.
- MATHIESON, G. A. and CLARK, A. H. (1984); The Cantung E zone scheelite skarn orebody, Tungsten, Northwest Territories. A revised genetic model: *Economic Geology*, volume 79, page 883-901.
- McLIMANS, R. K. (1980); Sphalerite stratigraphy of the Upper Mississippi Valley district, southwest Wisconsin: *Economic Geology*, volume 75, page 351-361.
- NILSEN, O. and MULKHERJEE, A.D. (1972); Geology of the Kvikne mine with special reference to the sulfide ore mineralization: *Norsk Geologie Tidsskr*, volume 52, page 151-192.
- OHMOTO, H. and SKINNER, B.J. (1983); The Kuroko and related volcanogenic massive sulfide deposits: Introduction and summary of new findings: *Economic Geology*, Monograph 5, page 1-8.
- PETRUK, W. (1971); Characteristics of the sulfides in the silver-arsenic deposits of the Cobalt Gowganda Region, Ontario: *Canadian Mineralogist*, volume II, page 196-213.
- PETERSEN, U. and WU, I (1977); Geochemistry of tetrahedrite and mineral zoning at Casapalca, Peru: *Economic Geology*, volume 72, page 993-1016.

- PAULING, L. and NEWMAN, E. W. (1934); The crystal structure of binnite and the chemical composition of the tetrahedrite group: *Z. Kristallographica*, volume 88, page 54-62.
- PATTRICK, R.D. and HAL, A.J (1983); Silver substitution into synthetic zinc, cadmium and iron tetrahedrites: *Mineralogical Magazine*, volume 47, page 441-451.
- PATTRICK, R. D. (1978); Microprobe analyses of cadmium-rich tetrahedrites from Tyndrum, Perthshire, Scotland: *Mineral Magazine*, volume 48, page 85-91.
- RILEY, J.F. (1974); The tetrahedrite-Freibergite series with reference to the Mount Isa Pb-Zn-Ag orebody: *Mineral Deposita*, volume 9, page 117-124.
- ROSCOE, S. M. (1965); Geochemical and isotope studies, Noranda and Matagami areas: *Canadian Institute Mining Metallurgy Transcripts* 68, page 279-285.
- RICHARDSON, S. W. (1968); Kyanite-sillimanite equilibrium between 700°C and 1500°C: *American Journal of Science*, volume 226, page 513-541.
- SANGSTER, D.F. (1972); Precambrian volcanogenic massive sulfide deposits in Canada: A review: *G.S.C. Paper* 72-22, 44 pages.
- SKINNER, B.J., LUCE, F.D. and MAKOVICKY, E. (1972); Studies of the sulfo-salts of the copper III. Phase and phase relations in the system Cu-Sb-S: *Economic Geology*, volume 67, page 924-938.
- SEVERIN, P.W.A. (1982); Geology of the Sturgeon Lake Cu-Zn-Pb-Ag-Au deposits: *Canadian Institute Mining Metallurgy Bulletin*, volume 75, page 107-123.
- SCOTT, S.D. (1976); Application of the sphalerite geobarometer to regionally metamorphosed terrains: *American Mineralogist*, volume 61 page 661-670.

- SCOTT, S.D and KISSIN, S.A (1973); Sphalerite composition in the Zn-Fe-S system below 300°C: *Economic Geology*, volume 68, page 475-479.
- SCOTT, S.D (1973); Experimental calibration of the sphalerite geobarometer: *Economic Geology*, volume 68, page 466-474.
- SCOTT, S.D and BARNES, H.L. (1971); Sphalerite geothermometry and geobarometry: *Economic Geology*, volume 66, page 653-669.
- SHIBA, M. (1988); Metamorphic evolution of the southern part of the Hidaka belt, Hokkaido, Japan: *Journal Metamorphic Geology*, volume 6, page 273-296.
- SATO, J. (1974); Ores and ore minerals from the Shakanai mine, Akita, Prefecture, Japan: *Society of Mining Geologists Spacial Issue 6*, page 323-336.
- SPRINGER, G. (1969); Elecroprobe analyses of tetrahedrite: *Neues Jahrb. Mineralogie Monatsh*, volume 110, page 24-32.
- SACK, R.O. (1985); Thermodynamic properties of tetrahedrite-tennantites: Constraints on the interdependence of the Ag=Cu, Fe=Zn, Cu=Fe and As=Sb exchange reactions. *American Mineralogist*, volume 70, page 1270-1289.
- SACK, R. O. (1987); Tennahedrite thermochemistry and metal zoning. In *chemical transport in metasomatic processes*: Reidel Dordrecht, Holland. page 701-731.
- STOCKWELL, C. H. (1972); *Geology of the Canadian Shield: Geology and Economic Minerals of Canada*, chapter IV, page 45-145.
- SANDECKI, J. and AMCOFF, O. (1981); On the occurrence of silver rich tetrahedrite at Garpenberg Norra, central Sweden: *Neues Jahrb. mineralogie*, volume 141, page 324-340.



- SANGSTER, D. F. and SCOTT, S. D. (1976); Precambrian stratabound, massive Cu-Pb-Zn sulfide ores in North America. In handbook of stratiform and stratbound ore deposits: Elsevier Scientific Publishing Company, Amsterdam, volume 6, page 129-214.
- TROWELL, N.F. (1983); Geology of the Sturgeon Lake area: O.G.S. Report 221.
- TATSUKA, K. and MORIMOTO N. (1973); Composition variation and polymorphism of tetrahedrite in the Cu-Sb-S system below 400°C: American Mineralogist, Volume 58, page 425-434.
- TROWELL, N.F. (1970); Geology of the Bell Lake- Sturgeon Lake area, districts of Kenora and Thunder Bay: Ontario Department Mines Open File Report 5051, 30 pages.
- TROWELL, N. F. (1980); Geology of Sturgeon Lake area, Districts of Thunder Bay and Kenora: Ontario Geological Survey Open File Rpt. 5291.
- TROWELL, N. F. (1978); Geology of Sturgeon Lake-Chevrier Township area, District of Thunder Bay, Ontario Division of Mines, Open File Report 5250, 97 pages.
- TROWELL, N. F. (1974); Geology of the Bell Lake-Sturgeon Lake area, Districts of Kenora and Thunder Bay, Ontario Division of Mines, Geological Report 114, 67 pages.
- TORIUM, M. (1977); Metamorphism of the Southern Kanto mountains its pressure conditions. In the Sambagawa Belt: Hiroshima University Press, page 217-221.
- TANIMURA, S. (1974); Geology of Kosaka mine, Akita, Prefecture: Society of Mining Geologists Special Issue 6, page 89-100.
- WATANABE, M. (1974); On the textures of ores from the Daikoku ore deposits, Ainai, mine, Akita Prefecture, with special reference to the fluid inclusion study on the ore forming minerals: Unpublished M.S thesis, University of Tokyo, 72 pages.

WUENSCH, B. J. (1963); On the superstructure and twinning in pyrrhotite:  
Mineralogical Society of America Paper 1, page 157-163.

YUI, S. (1983); Some textures of the ores from the Ezuri kuroko deposits,  
Akita Prefecture, Japan: Economic Geology Monograph 5, page 224-230.

# APPENDIX I

## TETRAHEDRITE ANALYSES

Values are quoted in number of atoms ( atomic proportions ) relative to 29 atoms.

Elements	Cu	Ag	Fe	Zn	Sb	As	S	Total	Pt. Count
Wt %	24.95	17.73	5.60	1.20	26.71	0.66	23.16	100.01	1
	25.41	18.04	5.49	1.14	26.71	-	23.67	100.46	2
	24.84	18.40	5.80	1.06	26.19	-	23.22	99.50	3
	24.95	17.78	5.66	0.92	26.17	-	23.33	98.81	4
At. Prop.	24.29	17.00	6.14	1.06	26.32	1.07	22.79	98.67	5
	7.00	2.93	1.79	0.33	3.91	0.16	12.88	29.00	
	7.07	2.96	1.74	0.31	3.88	-	13.05	29.01	
	6.99	3.05	1.86	0.29	3.85	-	12.96	29.00	GRAIN
	7.05	2.96	1.83	0.25	3.86	-	13.06	29.01	1
	6.90	2.84	1.98	0.29	3.89	0.26	12.83	28.99	

Elements	Cu	Ag	Fe	Zn	Sb	As	S	Total	Pt. Count
Wt %	24.82	18.15	5.68	1.00	26.08	0.91	23.63	100.28	1
	24.78	17.61	5.63	1.43	27.04	0.46	23.81	100.76	2
	24.71	17.85	5.73	1.42	25.93	0.94	23.07	99.66	3
	23.95	18.01	5.72	1.27	26.57	-	23.05	98.58	4
At. Prop.	25.52	17.40	5.32	1.02	25.66	0.89	23.09	98.89	5
	6.91	2.97	1.79	0.27	3.79	0.21	13.04	28.98	
	6.89	2.87	1.77	0.38	3.91	0.10	13.08	29.00	
	6.94	2.95	1.83	0.39	3.80	0.22	12.85	28.98	GRAIN
	6.82	3.02	1.85	0.35	3.95	-	13.01	29.00	2
	7.20	2.89	1.71	0.28	3.78	0.20	12.93	28.99	

Elements	Cu	Ag	Fe	Zn	Sb	As	S	Total	Pt. Count
Wt %	25.75	17.39	5.60	1.42	26.19	-	23.78	100.13	1
	25.03	18.65	5.84	0.72	26.76	-	23.67	100.67	2
	24.92	17.96	5.81	0.89	27.41	0.45	23.29	100.72	3
	24.92	17.57	5.62	1.23	26.85	-	23.37	99.57	4
At. Prop.	25.37	17.42	5.71	0.78	25.66	-	23.64	98.59	5
	7.14	2.84	1.77	0.38	3.79	-	13.07	28.99	
	6.96	3.05	1.85	0.19	3.88	-	13.05	28.98	
	6.96	2.95	1.84	0.24	4.00	0.11	12.89	28.99	GRAIN
	7.00	2.91	1.80	0.34	3.94	-	13.02	29.01	3
	7.13	2.88	1.83	0.21	3.76	-	13.18	28.99	

Elements	Cu	Ag	Fe	Zn	Sb	As	S	Total	Pt. Count
Wt %	23.28	18.57	5.58	1.47	27.19	-	22.61	98.70	1
	24.46	18.20	5.67	0.97	26.86	-	22.93	99.09	2
	24.42	18.61	5.57	1.10	26.64	-	22.57	98.90	3
	24.30	18.46	5.77	1.25	26.47	0.60	22.65	99.50	4
At. Prop.	24.37	18.57	6.01	1.38	26.72	0.61	22.39	100.05	5
	6.68	3.14	1.82	0.41	4.08	-	12.87	29.00	
	6.95	3.05	1.83	0.27	3.98	-	12.92	29.00	
	6.98	3.13	1.81	0.30	3.97	-	12.80	28.99	GRAIN
	6.90	3.09	1.86	0.34	3.92	0.14	12.74	28.99	4
	6.91	3.10	1.94	0.38	3.95	0.15	12.58	29.01	

Elements	Cu	Ag	Fe	Zn	Sb	As	S	Total	Pt. Count
Wt %	24.43	18.73	5.96	0.71	26.76	-	22.82	99.41	1
	24.42	18.96	5.65	1.02	27.38	0.46	22.75	100.65	2
	24.43	18.69	5.38	0.92	27.02	-	22.37	98.82	3
	24.82	18.40	5.49	0.85	26.71	-	22.44	98.72	4
	24.42	18.49	5.72	1.03	26.93	0.58	23.05	100.22	5
At. Prop.	6.94	3.13	1.93	0.20	3.96	-	12.84	29.00	
	6.89	3.15	1.81	0.28	4.03	0.11	12.72	28.99	
	7.02	3.16	1.75	0.26	4.05	-	12.74	28.98	GRAIN
	7.12	3.11	1.79	0.24	4.00	-	12.75	29.01	5
	6.87	3.07	1.83	0.28	3.96	0.14	12.86	29.01	

Elements	Cu	Ag	Fe	Zn	Sb	As	S	Total	Pt. Count
Wt %	24.61	18.22	6.17	1.79	26.40	-	22.16	99.35	1
	24.35	19.02	5.71	1.16	27.40	-	22.67	100.32	2
	24.70	19.18	5.76	1.14	26.60	-	22.95	100.32	3
	24.00	19.73	5.68	1.20	27.25	-	22.90	100.76	4
	24.85	18.28	6.19	1.03	27.01	-	23.01	100.36	5
At. Prop.	7.01	3.06	2.00	0.50	3.93	-	12.51	29.01	
	6.90	3.17	1.84	0.32	4.05	-	12.72	29.00	
	6.96	3.18	1.82	0.31	3.91	-	12.81	28.99	GRAIN
	6.77	3.28	1.82	0.33	4.01	-	12.80	29.01	6
	6.97	3.02	1.98	0.28	3.96	-	12.79	29.00	

Elements	Cu	Ag	Fe	Zn	Sb	As	S	Total	Pt. Count
Wt %	24.77	18.49	5.79	0.87	27.36	-	23.38	100.66	1
	24.94	18.68	5.99	1.07	26.45	-	22.76	99.90	2
	24.75	19.12	5.74	0.92	26.80	-	23.54	100.87	3
	24.02	18.37	5.52	1.45	26.73	-	22.69	98.78	4
	23.06	21.37	5.67	0.72	26.31	-	22.49	99.63	5
At. Prop.	6.92	3.05	1.84	0.24	3.99	-	12.94	28.98	
	7.04	3.11	1.92	0.29	3.90	-	12.74	29.00	
	6.89	3.14	1.82	0.25	3.89	-	13.00	28.99	GRAIN
	6.86	3.09	1.79	0.40	3.98	-	12.86	28.98	7
	6.61	3.61	1.85	0.20	3.94	-	12.79	29.00	

Elements	Cu	Ag	Fe	Zn	Sb	As	S	Total	Pt. Count
Wt %	23.79	19.10	5.63	1.12	26.76	0.81	23.53	100.75	1
	24.26	18.60	5.90	1.08	26.31	-	22.71	98.87	2
	23.86	18.81	5.93	0.96	27.24	0.60	22.89	100.28	3
	23.09	18.24	5.84	0.97	27.40	0.71	22.83	99.08	4
	23.59	19.07	5.93	0.69	26.12	0.97	22.65	99.02	5
At. Prop.	6.64	3.14	1.79	0.30	3.90	0.19	13.03	28.99	
	6.92	3.12	1.91	0.29	3.91	-	12.84	28.99	
	6.74	3.13	1.90	0.26	4.01	0.14	12.81	28.99	GRAIN
	6.59	3.07	1.89	0.27	4.08	0.17	12.93	29.00	8
	6.73	3.21	1.92	0.19	3.89	0.23	12.82	28.99	

Elements	Cu	Ag	Fe	Zn	Sb	As	S	Total	Pt. Count
Wt %	16.49	27.62	5.50	1.52	24.93	0.54	22.14	98.74	1
	15.79	28.85	5.81	2.04	25.32	-	21.62	99.43	2
	18.30	27.05	5.49	1.78	25.66	-	21.65	99.93	3
	19.33	22.91	8.52	1.78	25.13	-	23.27	100.95	4
	19.86	23.35	6.81	1.74	25.99	-	22.14	99.89	5
At. Prop.	4.89	4.82	1.85	0.44	3.86	0.14	13.01	29.01	
	4.70	5.06	1.97	0.59	3.93	-	12.75	29.00	
	5.37	4.69	1.84	0.51	3.94	-	12.63	28.98	GRAIN
	5.42	3.78	2.72	0.48	3.68	-	12.93	29.01	9
	5.73	3.97	2.23	0.49	3.91	-	12.66	28.99	

Elements	Cu	Ag	Fe	Zn	Sb	As	S	Total	Pt. Count
Wt %	23.37	20.55	5.58	1.82	25.67	-	22.97	99.97	1
	23.58	20.53	5.89	2.47	24.64	-	22.80	99.92	2
	23.96	19.56	5.36	1.90	25.00	-	23.08	98.87	3
	24.67	18.94	5.14	1.36	26.17	-	24.47	100.76	4
	24.65	18.08	5.22	1.95	25.48	0.69	22.96	99.03	5
At. Prop.	6.61	3.42	1.79	0.50	3.79	-	12.88	28.99	
	6.65	3.41	1.89	0.68	3.63	-	12.75	29.01	
	6.80	3.27	1.73	0.52	3.70	-	12.98	29.00	GRAIN
	6.82	3.08	1.61	0.36	3.77	-	13.36	29.00	10
	6.97	3.01	1.68	0.54	3.76	0.16	12.87	28.99	

Elements	Cu	Ag	Fe	Zn	Sb	As	S	Total	Pt. Count
Wt %	26.84	15.33	5.38	1.21	27.26	-	24.09	100.11	1
	27.09	14.81	5.59	2.21	26.59	-	23.92	100.20	2
	26.86	15.28	5.23	2.20	27.04	-	24.13	100.73	3
	26.87	14.98	5.43	1.80	26.63	0.59	23.88	100.19	4
	26.87	15.04	5.45	1.65	27.33	-	24.07	100.42	5
At. Prop.	7.40	2.49	1.69	0.32	3.92	-	13.17	28.99	
	7.44	2.39	1.74	0.59	3.81	-	13.02	28.99	
	7.36	2.46	1.63	0.58	3.86	-	13.10	28.99	GRAIN
	7.41	2.43	1.70	0.48	3.83	0.14	13.03	29.01	11
	7.39	2.44	1.71	0.44	3.88	-	13.13	28.99	

Elements	Cu	Ag	Fe	Zn	Sb	As	S	Total	Pt. Count
Wt %	27.14	15.38	5.40	1.62	26.79	0.42	24.11	100.87	1
	26.74	14.39	5.18	1.75	26.55	0.69	23.91	99.21	2
	27.02	14.55	4.78	1.69	27.24	0.74	24.28	100.29	3
	27.60	14.70	5.28	1.28	26.81	0.78	24.05	100.50	4
	26.21	14.89	5.40	1.49	26.42	0.50	25.24	100.15	5
At. Prop.	7.42	2.47	1.67	0.47	3.82	0.09	13.07	29.01	
	7.41	2.35	1.63	0.48	3.84	0.16	13.13	29.00	
	7.29	2.31	1.47	0.44	4.33	0.17	12.99	29.00	GRAIN
	7.56	2.37	1.65	0.34	3.83	0.18	13.06	28.99	12
	7.12	2.38	1.67	0.39	3.74	0.11	13.58	28.99	

Elements	Cu	Ag	Fe	Zn	Sb	As	S	Total	Pt. Count
Wt %	15.47	31.22	6.32	0.81	24.68	0.50	21.62	100.62	1
	14.98	31.51	5.69	0.85	25.42	-	21.56	100.00	2
	15.64	31.32	6.13	0.82	24.93	-	21.63	100.47	3
	15.24	31.30	5.86	1.28	24.75	-	21.82	100.25	4
	16.58	28.07	7.42	0.72	23.76	-	22.85	99.40	5
At. Prop.	4.58	5.44	2.13	0.23	3.81	0.12	12.68	28.98	
	4.49	5.56	1.94	0.25	3.97	-	12.80	29.01	
	4.64	5.47	2.07	0.24	3.86	-	12.72	29.00	GRAIN
	4.52	5.46	1.98	0.37	3.83	-	12.83	28.99	13
	4.81	4.80	2.45	0.20	3.60	-	13.14	29.00	

Elements	Cu	Ag	Fe	Zn	Sb	As	S	Total	Pt. Count
Wt %	25.48	16.36	4.92	2.51	25.72	0.53	23.58	99.10	1
	26.36	16.26	4.92	2.75	26.19	0.97	23.40	100.86	2
	25.77	16.71	4.65	2.73	26.14	1.07	24.01	101.08	3
	25.94	15.84	5.04	2.02	25.42	0.99	23.58	98.83	4
	26.11	16.18	4.70	2.70	25.92	0.93	23.48	100.02	5
At. Prop.	7.12	2.69	1.56	0.68	3.75	0.12	13.06	28.98	
	7.27	2.64	1.54	0.74	3.77	0.23	12.80	28.99	
	7.07	2.70	1.45	0.72	3.74	0.25	13.06	28.99	GRAIN
	7.25	2.60	1.60	0.55	3.70	0.24	13.06	29.00	14
	7.24	2.65	1.48	0.73	3.76	0.22	12.92	29.00	

Elements	Cu	Ag	Fe	Zn	Sb	As	S	Total	Pt. Count
Wt %	26.86	17.02	4.69	2.21	24.33	2.26	23.91	101.27	1
	27.17	16.15	5.12	2.18	24.86	1.21	24.12	100.80	2
	27.17	15.19	4.62	2.18	23.28	2.56	23.65	98.65	3
	25.54	17.17	4.67	2.38	26.39	0.91	22.68	99.74	4
	25.93	16.25	4.70	2.84	25.58	1.74	23.57	100.61	5
At. Prop.	7.32	2.73	1.45	0.59	3.46	0.52	12.92	28.99	
	7.40	2.59	1.59	0.58	3.53	0.28	13.03	29.00	
	7.52	2.48	1.46	0.58	3.37	0.60	12.98	28.99	GRAIN
	7.21	2.85	1.50	0.65	3.89	0.22	12.68	29.00	15
	7.15	2.64	1.47	0.76	3.68	0.41	12.88	28.99	

Elements	Cu	Ag	Fe	Zn	Sb	As	S	Total	Pt. Count
Wt %	26.45	16.35	4.59	2.41	25.79	1.14	23.70	100.42	1
	26.68	16.38	4.88	2.55	24.90	1.36	22.93	99.68	2
	26.83	16.05	4.95	2.10	25.20	1.48	23.95	100.55	3
	26.21	17.31	4.65	2.10	25.78	1.45	23.97	101.46	4
	27.03	16.81	4.88	2.29	25.67	1.15	23.94	101.76	5
At. Prop.	7.30	2.66	1.44	0.64	3.72	0.27	12.97	29.00	
	7.44	2.69	1.55	0.69	3.62	0.32	12.68	28.99	
	7.35	2.59	1.54	0.56	3.60	0.34	13.01	28.99	GRAIN
	7.18	2.79	1.45	0.56	3.68	0.33	13.00	28.99	16
	7.36	2.70	1.51	0.60	3.65	0.26	12.92	29.00	

Elements	Cu	Ag	Fe	Zn	Sb	As	S	Total	Pt. Count
Wt %	26.25	16.35	4.60	2.72	25.19	1.94	22.72	99.78	1
	26.05	16.36	4.78	2.59	24.90	1.25	23.54	99.47	2
	26.06	15.90	5.07	2.33	25.00	1.62	22.60	98.59	3
	26.59	16.03	5.11	2.73	25.07	1.60	23.47	100.59	4
	25.88	16.19	4.55	2.85	25.70	1.33	22.93	99.41	5
At. Prop.	7.35	2.69	1.46	0.74	3.68	0.46	12.61	28.99	
	7.24	2.68	1.51	0.70	3.61	0.29	12.97	29.00	
	7.36	2.65	1.63	0.64	3.67	0.39	12.65	28.99	GRAIN
	7.31	2.60	1.60	0.73	3.60	0.37	12.79	29.00	17
	7.26	2.67	1.45	0.78	3.76	0.32	12.75	28.99	

Elements	Cu	Ag	Fe	Zn	Sb	As	S	Total	Pt. Count
Wt %	25.91	16.11	5.09	3.12	24.79	2.43	24.06	101.49	1
	26.99	15.75	4.91	3.26	24.70	2.51	23.61	101.73	2
	26.24	16.22	5.20	2.92	25.17	1.66	23.85	101.26	3
	26.07	15.95	5.02	2.49	24.86	2.39	23.13	99.91	4
	25.76	17.48	4.98	2.31	27.04	-	24.29	101.86	5
At. Prop.	7.03	2.57	1.57	0.82	3.51	0.56	12.93	28.99	
	7.33	2.52	1.52	0.86	3.50	0.58	12.70	29.01	
	7.15	2.60	1.61	0.77	3.58	0.38	12.89	28.98	GRAIN
	7.24	2.61	1.58	0.67	3.60	0.55	12.73	28.98	18
	7.03	2.81	1.55	0.61	3.85	-	13.14	28.99	

Elements	Cu	Ag	Fe	Zn	Sb	As	S	Total	Pt. Count
Wt %	26.99	16.31	5.16	2.32	25.31	0.92	23.92	100.93	1
	27.57	15.43	4.78	2.42	23.44	2.53	23.91	100.07	2
	27.12	15.26	4.90	2.49	23.04	3.03	23.88	99.73	3
	26.83	16.01	4.75	2.34	24.16	2.94	23.56	100.58	4
	26.21	15.98	4.50	2.61	24.64	1.35	23.08	98.37	5
At. Prop.	7.38	2.63	1.60	0.61	3.61	0.21	12.96	29.00	
	7.53	2.48	1.48	0.64	3.34	0.58	12.94	28.99	
	7.42	2.46	1.52	0.66	3.29	0.70	12.95	29.00	GRAIN
	7.36	2.59	1.47	0.62	3.46	0.68	12.81	28.99	19
	7.37	2.65	1.44	0.71	3.62	0.32	12.88	28.99	

Elements	Cu	Ag	Fe	Zn	Sb	As	S	Total	Pt. Count
Wt %	26.72	15.88	4.77	2.82	23.82	1.16	23.49	98.66	1
	28.00	15.67	4.48	2.60	22.67	3.05	23.94	100.40	2
	27.46	15.23	4.76	2.73	23.39	3.60	23.94	101.11	3
	27.25	15.37	4.54	2.30	23.85	3.06	24.06	100.44	4
	26.81	15.42	5.13	2.04	23.10	1.99	23.70	98.21	5
At. Prop.	7.43	2.60	1.51	0.76	3.47	0.27	12.95	28.99	
	7.61	2.51	1.38	0.68	3.21	0.70	12.90	28.99	
	7.43	2.42	1.46	0.72	3.30	0.83	12.83	28.99	GRAIN
	7.43	2.47	1.41	0.61	3.39	0.71	12.99	29.01	20
	7.44	2.52	1.62	0.55	3.35	0.47	13.05	29.00	



Elements	Cu	Ag	Fe	Zn	Sb	As	S	Total	Pt. Count
Wt %	27.48	15.44	4.40	2.33	22.71	2.88	23.86	99.10	1
	26.21	16.99	4.44	2.33	25.11	2.17	23.62	100.86	2
	26.39	15.74	4.46	2.50	23.63	2.00	23.36	98.09	3
	26.96	15.76	4.14	2.39	24.39	2.45	23.93	100.02	4
	26.66	16.53	4.40	1.88	25.21	2.31	24.21	101.20	5
At. Prop.	7.55	2.50	1.38	0.62	3.26	0.67	13.01	28.99	
	7.22	2.76	1.39	0.62	3.61	0.51	12.89	29.00	
	7.39	2.60	1.42	0.68	3.46	0.47	12.98	29.00	GRAIN
	7.38	2.55	1.29	0.63	3.57	0.57	13.02	29.01	2 1
	7.27	2.65	1.38	0.50	3.63	0.53	13.03	28.99	

Elements	Cu	Ag	Fe	Zn	Sb	As	S	Total	Pt. Count
Wt %	26.64	15.50	4.63	2.10	23.81	2.10	23.44	98.22	1
	26.73	15.93	4.24	1.84	25.33	2.08	23.86	100.01	2
	26.98	15.75	4.36	2.47	25.87	1.51	23.96	100.60	3
	26.90	16.45	4.43	2.30	24.98	1.55	24.16	100.77	4
	26.56	15.59	4.37	2.46	24.91	2.75	24.53	101.17	5
At. Prop.	7.45	2.55	1.47	0.57	3.47	0.49	12.99	28.99	
	7.38	2.59	1.33	0.49	3.65	0.48	13.07	28.99	
	7.40	2.57	1.36	0.66	3.66	0.35	13.00	29.00	GRAIN
	7.35	2.65	1.38	0.61	3.56	0.36	13.10	29.01	2 2
	7.19	2.56	1.35	0.65	3.52	0.63	13.11	29.01	

Elements	Cu	Ag	Fe	Zn	Sb	As	S	Total	Pt. Count
Wt %	26.35	15.55	4.13	2.63	23.99	1.94	24.21	98.80	1
	24.21	19.80	4.23	2.48	25.25	0.97	23.17	100.12	2
	26.22	16.46	4.28	2.57	25.69	0.66	23.75	99.62	3
	27.38	15.72	4.34	1.79	25.47	2.44	24.77	101.91	4
	26.33	16.88	4.28	1.85	24.89	2.35	23.78	100.35	5
At. Prop.	7.28	2.53	1.30	0.71	3.46	0.45	13.26	28.99	
	6.81	3.28	1.35	0.68	3.71	0.23	12.93	28.99	
	7.24	2.69	1.37	0.69	3.73	0.16	13.12	29.00	GRAIN
	7.37	2.49	1.38	0.47	3.48	0.56	13.27	29.02	2 3
	7.26	2.74	1.37	0.49	3.47	0.54	13.11	28.98	

Elements	Cu	Ag	Fe	Zn	Sb	As	S	Total	Pt. Count
Wt %	27.39	14.91	4.42	2.14	23.11	3.00	24.00	98.98	1
	26.41	16.28	4.44	2.55	25.01	1.28	23.61	99.57	2
	27.00	16.22	4.43	2.16	25.01	2.47	24.43	101.73	3
	26.71	15.82	4.34	2.24	24.61	2.50	24.30	100.52	4
	26.89	16.16	4.47	2.27	24.37	2.56	24.32	101.05	5
At. Prop.	7.53	2.41	1.38	0.57	3.32	0.69	13.08	28.98	
	7.33	2.66	1.40	0.67	3.62	0.30	13.01	28.99	
	7.30	2.58	1.36	0.57	3.53	0.56	13.09	28.99	GRAIN
	7.29	2.54	1.35	0.59	3.50	0.58	13.14	28.99	2 4
	7.31	2.58	1.38	0.60	3.45	0.59	13.09	29.00	

Elements	Cu	Ag	Fe	Zn	Sb	As	S	Total	Pt. Count
Wt %	26.35	15.21	4.20	2.70	25.29	2.45	23.92	100.11	1
	24.81	18.51	4.39	2.12	25.30	2.05	23.50	100.69	2
	26.63	16.44	4.41	2.19	25.58	1.39	23.59	100.23	3
	27.05	16.26	4.51	2.21	25.95	0.96	24.12	101.07	4
	25.19	16.03	4.76	2.39	25.30	2.18	23.51	99.36	5
At. Prop.	7.25	2.46	1.31	0.72	3.63	0.57	13.04	28.98	
	6.90	3.03	1.39	0.57	3.67	0.48	12.95	28.99	
	7.37	2.68	1.40	0.59	3.70	0.32	12.97	29.03	GRAIN
	7.40	2.61	1.41	0.60	3.71	0.22	13.06	29.01	2 5
	7.02	2.63	1.51	0.65	3.68	0.51	12.99	28.99	

Elements	Cu	Ag	Fe	Zn	Sb	As	S	Total	Pt. Count
Wt %	24.31	17.25	4.98	2.00	27.24	0.85	24.15	100.79	1
	21.83	19.42	4.47	1.88	26.56	0.96	23.66	98.80	2
	24.84	16.16	4.35	2.46	24.72	1.83	23.85	98.21	3
	24.55	16.87	4.34	2.18	25.96	1.78	24.81	100.49	4
	19.57	22.23	4.11	2.14	26.65	0.46	23.25	98.41	5
At. Prop.	6.31	2.64	1.47	0.59	3.69	0.20	12.43	29.00	
	6.22	3.26	1.45	0.52	3.95	0.23	13.36	28.99	
	6.96	2.67	1.39	0.67	3.62	0.43	13.26	29.00	GRAIN
	6.73	2.72	1.35	0.58	3.71	0.41	13.50	29.00	2 6
	5.69	3.80	1.36	0.60	4.04	0.11	13.39	28.99	

Elements	Cu	Ag	Fe	Zn	Sb	As	S	Total	Pt. Count
Wt %	26.17	16.24	4.67	2.11	24.18	2.08	24.18	99.63	1
	23.45	20.01	4.38	2.42	25.28	1.67	23.64	100.84	2
	19.80	24.34	4.12	2.79	25.47	1.56	22.60	100.68	3
	21.97	21.76	4.19	2.40	27.15	0.73	23.20	101.40	4
	27.34	15.00	4.53	2.17	23.51	3.28	24.98	100.81	5
At. Prop.	7.20	2.63	1.46	0.56	3.47	0.48	13.19	28.99	
	6.54	3.29	1.39	0.65	3.68	0.39	13.06	29.00	
	5.69	4.12	1.35	0.78	3.82	0.38	12.87	29.01	GRAIN
	6.21	3.62	1.34	0.66	4.00	0.17	12.99	28.99	2 7
	7.34	2.37	1.38	0.56	3.29	0.75	13.29	28.98	

Elements	Cu	Ag	Fe	Zn	Sb	As	S	Total	Pt. Count
Wt %	26.05	16.05	4.63	2.83	25.60	1.18	24.52	100.86	1
	27.63	15.27	4.50	1.86	23.41	2.73	23.91	99.29	2
	25.86	16.31	4.53	1.53	23.96	2.76	24.61	99.55	3
	26.59	16.18	4.58	2.46	25.21	1.32	24.17	100.51	4
	24.34	19.14	4.77	2.01	24.80	1.09	23.39	99.55	5
At. Prop.	7.10	2.57	1.43	0.75	3.64	0.27	13.24	29.00	
	7.60	2.47	1.40	0.49	3.36	0.65	13.03	29.00	
	7.09	2.63	1.41	0.41	3.43	0.64	13.38	28.99	GRAIN
	7.28	2.61	1.43	0.65	3.60	0.30	13.12	28.99	2 8
	6.84	3.17	1.52	0.55	3.63	0.26	13.03	29.00	

Elements	Cu	Ag	Fe	Zn	Sb	As	S	Total	Pt. Count
Wt %	27.08	14.98	4.63	2.94	23.82	2.60	23.85	99.89	1
	18.30	26.25	3.67	2.77	26.66	-	21.51	99.17	2
	26.96	15.11	4.33	2.04	23.58	2.62	23.59	98.24	3
	26.76	15.60	4.53	2.67	23.74	2.70	23.98	99.98	4
	26.64	15.09	4.84	2.66	24.49	2.09	23.84	99.66	5
At. Prop.	7.41	2.41	1.44	0.78	3.40	0.60	12.94	28.98	
	5.46	4.61	1.25	0.80	4.15	-	12.72	28.99	
	7.51	2.48	1.37	0.55	3.43	0.62	13.03	28.99	GRAIN
	7.33	2.52	1.41	0.71	3.39	0.63	13.01	29.00	2 9
	7.32	2.44	1.51	0.70	3.51	0.47	13.05	29.00	

Elements	Cu	Ag	Fe	Zn	Sb	As	S	Total	Pt. Count
Wt %	24.55	19.04	5.14	1.11	25.59	-	23.40	98.82	1
	24.66	18.94	5.19	1.71	26.53	0.63	23.32	100.97	2
	25.04	18.01	5.30	1.37	26.64	-	23.13	99.49	3
	24.80	18.45	5.21	1.56	25.89	0.39	23.18	99.48	4
	24.89	18.20	5.41	1.35	26.08	-	22.86	98.78	5
At. Prop.	6.95	3.17	1.65	0.30	3.78	-	13.13	28.98	
	6.88	3.11	1.66	0.46	3.86	0.15	12.89	29.01	
	7.07	2.99	1.70	0.37	3.92	-	12.94	28.99	GRAIN
	6.99	3.06	1.67	0.43	3.81	0.09	12.95	29.00	3 0
	7.08	3.05	1.75	0.36	3.87	-	12.88	28.99	

Elements	Cu	Ag	Fe	Zn	Sb	As	S	Total	Pt. Count
Wt %	24.50	18.38	5.30	1.22	26.21	-	23.83	99.44	1
	25.31	18.52	5.21	1.62	26.54	0.48	23.43	101.10	2
	24.03	18.96	5.56	1.09	25.91	-	23.33	98.88	3
	24.59	19.49	5.12	1.41	26.33	0.63	24.03	101.61	4
	24.28	18.71	5.69	1.56	26.12	0.43	22.95	99.74	5
At. Prop.	6.87	3.03	1.69	0.33	3.83	-	13.24	28.99	
	7.03	3.02	1.64	0.44	3.85	0.11	12.90	28.99	
	6.81	3.16	1.79	0.28	3.83	-	13.10	28.97	GRAIN
	6.78	3.17	1.60	0.38	3.79	0.15	13.13	29.00	3 1
	6.85	3.11	1.83	0.43	3.84	0.10	12.84	29.00	

Elements	Cu	Ag	Fe	Zn	Sb	As	S	Total	Pt. Count
Wt %	24.55	17.72	5.95	1.25	26.83	-	23.29	99.59	1
	23.75	18.40	5.50	1.44	26.56	0.72	23.26	99.63	2
	24.50	18.69	5.50	1.55	26.13	0.50	23.89	100.77	3
	24.93	18.47	5.65	0.83	26.25	-	24.07	100.21	4
	23.91	18.26	6.09	1.42	25.55	0.72	23.40	99.35	5
At. Prop.	6.90	2.93	1.90	0.34	3.94	-	12.98	28.99	
	6.70	3.06	1.76	0.39	3.91	0.17	13.00	28.99	
	6.79	3.05	1.73	0.42	3.78	0.12	13.12	29.01	GRAIN
	6.92	3.02	1.78	0.22	3.80	-	13.25	28.99	3 2
	6.71	3.01	1.95	0.38	3.74	0.17	13.02	28.98	

Elements	Cu	Ag	Fe	Zn	Sb	As	S	Total	Pt. Count
Wt %	24.98	18.93	5.48	1.19	26.40	1.06	23.64	101.69	1
	25.32	17.99	5.30	1.42	26.01	0.63	23.46	100.12	2
	23.94	19.12	5.38	1.10	26.51	-	23.31	99.36	3
	24.55	18.84	5.26	1.14	26.41	0.78	23.59	100.58	4
	23.83	19.81	5.48	1.34	26.93	-	23.60	100.99	5
At. Prop.	6.89	3.08	1.72	0.32	3.80	0.25	12.93	28.99	
	7.08	2.96	1.69	0.33	3.79	0.15	13.00	29.00	
	6.78	3.19	1.73	0.30	3.92	-	13.08	29.00	GRAIN
	6.85	3.10	1.67	0.31	3.85	0.18	13.05	29.01	3 3
	6.65	3.26	1.74	0.36	3.93	-	13.06	29.00	

Elements	Cu	Ag	Fe	Zn	Sb	As	S	Total	Pt. Count
Wt %	24.37	18.80	5.21	1.45	26.46	-	23.89	100.17	1
	24.17	18.75	5.28	1.01	26.42	0.75	23.80	100.18	2
	24.45	19.33	5.20	1.21	26.73	-	23.66	100.58	3
	24.36	19.03	5.18	1.70	26.75	0.38	23.92	101.31	4
	23.89	18.94	5.37	1.30	26.21	-	23.70	99.40	5
At. Prop.	6.80	3.09	1.65	0.39	3.85	-	13.21	28.99	
	6.75	3.08	1.68	0.27	3.84	0.18	13.18	28.98	
	6.83	3.18	1.65	0.33	3.90	-	13.10	28.99	GRAIN
	6.74	3.10	1.63	0.46	3.86	0.09	13.12	29.00	3 4
	6.72	3.14	1.72	0.35	3.84	-	13.22	28.99	

Elements	Cu	Ag	Fe	Zn	Sb	As	S	Total	Pt. Count
Wt %	24.39	18.59	5.41	1.53	26.15	0.64	23.86	100.56	1
	24.75	18.92	5.26	1.32	26.13	0.66	23.73	100.76	2
	24.32	19.22	5.04	0.93	26.71	1.00	24.26	101.49	3
	24.78	18.98	5.20	1.20	26.09	-	23.75	100.00	4
	24.31	17.95	5.11	1.50	25.75	0.62	23.24	98.49	5
At. Prop.	6.77	3.04	1.71	0.41	3.79	0.15	13.13	29.00	
	6.88	3.09	1.66	0.35	3.78	0.16	13.07	28.99	
	6.71	3.12	1.58	0.25	3.84	0.23	13.26	28.99	GRAIN
	6.93	3.13	1.65	0.32	3.81	-	13.16	29.00	3 5
	6.90	3.00	1.64	0.41	3.82	0.14	13.08	28.99	

Elements	Cu	Ag	Fe	Zn	Sb	As	S	Total	Pt. Count
Wt %	24.43	18.40	5.25	0.77	27.09	0.67	23.90	100.51	1
	24.08	19.15	5.46	1.27	26.37	0.63	23.70	100.67	2
	23.93	19.49	5.49	1.59	26.97	-	24.26	101.73	3
	24.73	18.34	5.22	1.21	26.56	-	23.77	99.83	4
	24.12	19.98	5.05	1.44	26.61	0.50	23.88	101.59	5
At. Prop.	6.81	3.01	1.67	0.20	3.94	0.16	13.20	28.99	
	6.71	3.14	1.73	0.34	3.83	0.15	13.09	28.99	
	6.59	3.16	1.72	0.42	3.87	-	13.24	29.00	GRAIN
	6.92	3.02	1.66	0.33	3.88	-	13.18	28.99	3 6
	6.68	3.26	1.59	0.39	3.85	0.12	13.11	29.00	

Elements	Cu	Ag	Fe	Zn	Sb	As	S	Total	Pt. Count
Wt %	23.86	18.17	5.49	1.49	26.37	0.66	23.25	99.30	1
	23.98	19.74	5.32	1.53	27.03	0.57	23.77	101.95	2
	23.74	19.72	5.37	1.31	25.77	-	23.31	99.22	3
	23.94	18.81	5.18	1.68	26.26	-	23.62	99.49	4
	23.89	17.84	5.26	1.45	26.30	-	23.76	98.50	5
At. Prop.	6.74	3.02	1.76	0.40	3.89	0.16	13.02	28.99	
	6.63	3.22	1.67	0.41	3.90	0.13	13.03	28.99	
	6.72	3.29	1.73	0.36	3.81	-	13.09	29.00	GRAIN
	6.73	3.12	1.66	0.46	3.85	-	13.17	28.99	3 7
	6.75	2.97	1.69	0.39	3.88	-	13.31	28.99	

Elements	Cu	Ag	Fe	Zn	Sb	As	S	Total	Pt. Count
Wt %	23.91	19.85	4.84	1.44	25.97	0.68	23.28	99.98	1
	24.92	19.98	5.06	1.40	26.48	-	23.38	101.21	2
	24.57	19.18	4.92	1.46	26.86	0.76	23.91	101.65	3
	23.79	19.82	5.09	1.57	26.47	0.80	23.75	101.30	4
	23.69	19.03	4.93	1.34	26.56	1.58	23.31	100.44	5
At. Prop.	6.75	3.30	1.55	0.39	3.82	0.16	13.02	28.99	
	6.95	3.28	1.61	0.38	3.85	-	12.92	28.99	
	6.79	3.12	1.54	0.39	3.87	0.18	13.10	28.99	GRAIN
	6.61	3.24	1.62	0.42	3.84	0.19	13.08	29.00	3 8
	6.66	3.15	1.57	0.36	3.89	0.37	12.98	28.98	

Elements	Cu	Ag	Fe	Zn	Sb	As	S	Total	Pt. Count
Wt %	24.73	17.64	5.60	0.98	26.57	-	23.69	99.21	1
	24.15	18.18	5.52	1.41	26.27	0.46	23.60	99.59	2
	24.80	17.63	5.26	1.45	26.48	0.50	23.56	99.68	3
	23.61	17.72	5.49	1.67	27.61	0.55	24.28	100.94	4
	23.65	18.43	5.34	1.13	27.40	-	24.15	100.09	5
At. Prop.	6.94	2.92	1.79	0.27	3.89	-	13.19	29.00	
	6.77	3.00	1.76	0.38	3.84	0.11	13.20	28.98	
	6.95	2.91	1.67	0.39	3.87	0.12	13.08	28.99	GRAIN
	6.53	2.88	1.73	0.45	3.98	0.13	13.30	29.00	3 9
	6.60	3.03	1.70	0.30	3.99	-	13.37	28.99	

Elements	Cu	Ag	Fe	Zn	Sb	As	S	Total	Pt. Count
Wt %	24.13	17.51	5.67	1.42	27.33	-	24.49	100.55	1
	24.90	17.35	5.48	0.52	27.37	0.62	24.21	100.46	2
	25.20	17.78	5.43	1.26	27.41	-	24.11	101.18	3
	24.70	17.49	5.56	1.14	26.70	-	23.63	99.21	4
	22.73	20.27	5.26	1.16	26.61	0.52	23.61	100.16	5
At. Prop.	6.66	2.85	1.78	0.38	3.93	-	13.40	29.00	
	6.90	2.83	1.73	0.14	3.96	0.14	13.30	29.00	
	6.95	2.89	1.70	0.34	3.94	-	13.18	29.00	GRAIN
	6.94	2.88	1.77	0.31	3.92	-	13.16	28.98	4 0
	6.40	3.36	1.68	0.32	3.91	0.12	13.19	28.98	

Elements	Cu	Ag	Fe	Zn	Sb	As	S	Total	Pt. Count
Wt %	24.68	18.51	4.92	1.32	26.81	0.60	25.09	101.91	1
	24.00	18.27	4.77	1.34	27.16	-	24.40	99.94	2
	23.92	17.86	5.36	1.74	26.43	-	24.19	99.50	3
	25.09	17.25	5.16	1.32	26.80	0.57	24.29	100.48	4
	24.26	17.64	5.33	1.11	27.20	-	24.07	99.61	5
At. Prop.	6.74	2.97	1.52	0.34	3.82	0.13	13.58	29.10	
	6.69	3.00	1.51	0.36	3.95	-	13.48	28.99	
	6.67	2.93	1.70	0.47	3.85	-	13.37	28.99	GRAIN
	6.93	2.80	1.62	0.35	3.86	0.12	13.30	28.98	4 1
	6.78	2.91	1.69	0.30	3.97	-	13.34	28.99	

Elements	Cu	Ag	Fe	Zn	Sb	As	S	Total	Pt. Count
Wt %	23.62	18.12	5.57	1.12	26.92	-	24.31	99.67	1
	24.11	17.18	5.38	1.17	26.66	0.60	23.45	98.55	2
	23.40	18.04	5.38	1.46	26.45	-	23.60	98.34	3
	24.23	17.96	5.63	1.55	26.30	0.49	23.45	99.61	4
	24.74	18.69	5.52	1.10	26.10	-	23.88	100.03	5
At. Prop.	6.59	2.98	1.77	0.30	3.92	-	13.44	29.00	
	6.83	2.87	1.73	0.32	3.94	0.14	13.17	29.00	
	6.64	3.02	1.74	0.40	3.91	-	13.28	28.99	GRAIN
	6.80	2.97	1.80	0.42	3.85	0.11	13.04	28.99	4 2
	6.89	3.07	1.75	0.29	3.79	-	13.19	28.98	

Elements	Cu	Ag	Fe	Zn	Sb	As	S	Total	Pt. Count
Wt %	24.07	18.04	4.91	1.41	27.55	0.64	24.34	100.97	1
	24.32	18.24	5.10	1.40	27.12	0.53	24.43	101.14	2
	24.17	18.01	5.11	1.05	27.07	-	24.47	99.89	3
	24.42	18.24	5.25	1.27	27.32	-	24.17	100.67	4
	24.11	18.05	5.11	1.36	27.38	-	24.41	100.42	5
At. Prop.	6.66	2.94	1.54	0.38	3.98	0.15	13.35	29.00	
	6.70	2.96	1.60	0.37	3.90	0.12	13.34	28.99	
	6.72	2.95	1.62	0.28	3.93	-	13.49	28.99	GRAIN
	6.77	2.98	1.66	0.34	3.95	-	13.29	28.99	4 3
	6.69	2.97	1.61	0.36	3.96	-	13.42	29.01	

Elements	Cu	Ag	Fe	Zn	Sb	As	S	Total	Pt. Count
Wt %	24.56	18.08	5.23	1.13	26.38	-	23.98	99.36	1
	24.52	18.11	5.50	1.29	27.51	-	25.05	101.97	2
	24.32	17.65	5.14	1.22	27.12	-	24.22	99.67	3
	24.68	18.13	5.52	1.78	27.18	-	24.05	101.35	4
	24.61	17.20	5.39	1.21	26.45	-	23.95	98.81	5
At. Prop.	6.88	2.98	1.67	0.31	3.85	-	13.31	29.00	
	6.66	2.90	1.70	0.34	3.90	-	13.49	28.99	
	6.79	2.91	1.63	0.33	3.95	-	13.39	29.00	GRAIN
	6.84	2.96	1.74	0.48	3.93	-	13.04	28.99	4 4
	6.91	2.84	1.72	0.33	3.87	-	13.32	28.99	

Elements	Cu	Ag	Fe	Zn	Sb	As	S	Total	Pt. Count
Wt %	24.32	17.52	5.42	1.13	26.33	0.69	23.93	99.34	1
	24.49	17.48	5.34	1.43	27.00	-	24.53	100.27	2
	24.42	17.84	5.34	0.86	26.79	0.61	24.23	100.09	3
	24.41	18.13	5.32	1.17	26.39	-	24.59	100.00	4
	24.29	17.55	5.06	1.27	26.27	-	24.28	98.72	5
At. Prop.	6.80	2.89	1.72	0.31	3.84	0.16	13.27	28.99	
	6.77	2.84	1.68	0.38	3.89	-	13.43	28.99	
	6.78	2.92	1.69	0.23	3.88	0.14	13.34	28.99	GRAIN
	6.76	2.96	1.67	0.27	3.82	-	13.51	28.99	4 5
	6.81	2.90	1.61	0.35	3.83	-	13.49	28.99	

Elements	Cu	Ag	Fe	Zn	Sb	As	S	Total	Pt. Count
Wt %	24.45	17.07	5.64	2.07	26.51	0.44	23.99	100.16	1
	24.47	17.64	5.22	1.81	26.21	0.52	24.09	99.96	2
	24.12	17.36	5.36	2.55	26.61	-	23.60	99.60	3
	24.27	17.45	5.39	1.99	26.62	-	24.11	99.83	4
	25.16	17.60	5.94	2.12	25.67	-	24.34	100.83	5
At. Prop.	6.77	2.78	1.78	0.56	3.83	0.10	13.17	28.99	
	6.79	2.89	1.65	0.49	3.80	0.12	13.26	29.00	
	6.75	2.86	1.71	0.69	3.89	-	13.10	29.00	GRAIN
	6.76	2.87	1.70	0.54	3.86	-	13.29	29.02	4 6
	6.88	2.84	1.85	0.57	3.67	-	13.20	29.01	

Elements	Cu	Ag	Fe	Zn	Sb	As	S	Total	Pt. Count
Wt %	22.84	19.56	4.72	1.05	26.33	0.89	24.07	99.47	1
	23.55	21.31	4.74	0.77	27.55	-	23.97	101.88	2
	23.67	19.58	4.99	0.89	27.65	-	23.59	100.37	3
	23.60	19.48	4.60	0.51	27.31	-	23.03	98.54	4
	23.18	18.85	4.84	1.26	28.30	-	23.47	99.91	5
At. Prop.	6.43	3.24	1.51	0.28	3.87	0.21	13.44	28.99	
	6.56	3.49	1.50	0.21	4.00	-	13.23	28.99	
	6.67	3.25	1.60	0.24	4.06	-	13.17	28.99	GRAIN
	6.79	3.30	1.50	0.14	4.10	-	13.15	28.98	4 7
	6.57	3.15	1.56	0.34	4.18	-	13.19	29.00	

Elements	Cu	Ag	Fe	Zn	Sb	As	S	Total	Pt. Count
Wt %	23.40	20.17	4.99	0.79	26.58	-	23.56	99.49	1
	23.52	19.61	4.65	0.74	27.16	0.76	23.35	99.79	2
	24.56	19.30	4.73	1.23	26.56	-	23.42	99.80	3
	23.32	19.43	4.83	1.22	26.47	-	23.22	98.49	4
	22.82	19.08	4.92	1.30	27.10	0.50	23.14	98.86	5
At. Prop.	6.63	3.37	1.61	0.22	3.93	-	13.24	29.00	
	6.68	3.28	1.50	0.20	4.02	0.18	13.12	28.98	
	6.93	3.21	1.52	0.33	3.91	-	13.10	29.00	GRAIN
	6.67	3.26	1.57	0.34	3.96	-	13.18	28.98	4 8
	6.53	3.21	1.60	0.36	4.05	0.12	13.13	29.00	

Elements	Cu	Ag	Fe	Zn	Sb	As	S	Total	Pt. Count
Wt %	17.61	26.59	4.49	0.94	25.97	-	22.43	98.03	1
	20.10	24.43	4.63	1.16	27.24	1.10	22.62	101.28	2
	20.46	24.39	4.74	0.70	26.25	0.68	22.81	100.03	3
	18.75	25.45	4.94	0.97	27.12	0.51	23.40	101.14	4
	17.31	27.28	4.88	0.76	25.27	1.21	22.92	99.61	5
At. Prop.	5.25	4.67	1.52	0.27	4.04	-	13.25	29.00	
	5.79	4.10	1.51	0.32	4.09	0.28	12.91	29.00	
	5.91	4.15	1.56	0.20	3.96	0.16	13.06	29.00	
	5.37	4.29	1.61	0.26	4.05	0.12	13.28	28.98	GRAIN
	5.05	4.69	1.62	0.21	3.85	0.30	13.27	28.99	4 9

Elements	Cu	Ag	Fe	Zn	Sb	As	S	Total	Pt. Count
Wt %	24.39	19.08	4.92	1.76	26.90	0.46	23.03	100.55	1
	23.40	19.21	4.83	1.25	26.54	-	22.88	98.11	2
	24.08	18.65	4.95	1.34	26.36	-	23.14	98.51	3
	23.35	20.13	4.70	0.69	26.93	-	23.81	99.61	4
	24.16	19.86	4.75	1.28	26.75	-	23.63	100.43	5
At. Prop.	6.87	3.16	1.57	0.48	3.95	0.11	12.85	28.99	
	6.74	3.26	1.58	0.35	3.99	-	13.07	28.99	
	6.87	3.13	1.61	0.37	3.93	-	13.09	29.00	GRAIN
	6.61	3.36	1.51	0.19	3.96	-	13.36	28.99	5 0
	6.78	3.28	1.52	0.34	3.92	-	13.15	28.99	

Elements	Cu	Ag	Fe	Zn	Sb	As	S	Total	Pt. Count
Wt %	22.53	19.63	4.67	0.84	27.36	-	23.31	98.33	1
	23.85	19.91	4.57	0.68	27.66	-	23.65	100.32	2
	17.06	27.57	3.66	2.02	27.17	-	21.75	99.22	3
	16.62	28.31	4.84	1.21	27.30	-	22.56	100.84	4
	23.07	19.77	5.11	0.86	27.09	-	23.68	99.58	5
At. Prop.	6.49	3.33	1.53	0.23	4.11	-	13.30	28.99	
	6.73	3.31	1.47	0.18	4.07	-	13.23	28.99	
	5.11	4.87	1.25	0.59	4.25	-	12.93	29.00	GRAIN
	4.87	4.89	1.61	0.34	4.17	-	13.11	28.99	5 1
	6.53	3.29	1.64	0.24	4.00	-	13.28	28.98	

Elements	Cu	Ag	Fe	Zn	Sb	As	S	Total	Pt. Count
Wt %	23.47	19.85	5.08	0.85	27.34	0.36	23.53	100.47	1
	23.49	19.26	4.55	0.81	26.61	0.53	23.76	99.00	2
	23.56	19.33	4.80	0.92	27.30	-	23.66	99.57	3
	23.42	18.48	5.15	1.01	27.13	0.66	23.74	99.60	4
	23.56	19.17	5.39	1.09	26.63	-	23.68	99.52	5
At. Prop.	6.61	3.29	1.63	0.23	4.02	0.08	13.13	28.99	
	6.66	3.21	1.47	0.22	3.94	0.12	13.36	28.98	
	6.67	3.22	1.54	0.25	4.03	-	13.27	28.98	GRAIN
	6.60	3.07	1.65	0.27	3.99	0.16	13.26	29.00	5 2
	6.64	3.18	1.73	0.30	3.92	-	13.23	29.00	



Elements	Cu	Ag	Fe	Zn	Sb	As	S	Total	Pt. Count
Wt %	23.73	18.99	5.12	0.80	27.24	-	24.06	99.94	1
	23.51	18.88	5.14	1.08	28.16	-	24.39	101.10	2
	23.51	18.23	5.24	0.90	27.19	-	23.49	98.56	3
	24.03	18.49	5.16	0.99	27.11	-	23.75	99.53	4
	24.15	18.78	5.03	1.24	27.30	-	23.99	100.48	5
At. Prop.	6.65	3.13	1.63	0.22	3.99	-	13.37	28.99	
	6.56	3.09	1.63	0.29	4.10	-	13.49	29.16	
	6.69	3.06	1.70	0.25	4.04	-	13.26	29.00	GRAIN
	6.77	3.07	1.65	0.27	3.98	-	13.25	28.99	5 3
	6.74	3.08	1.59	0.33	3.97	-	13.27	28.98	

Elements	Cu	Ag	Fe	Zn	Sb	As	S	Total	Pt. Count
Wt %	23.31	18.57	4.96	1.18	26.52	0.83	23.43	98.81	1
	23.92	17.88	5.80	1.13	26.36	0.44	23.67	99.20	2
	24.38	19.23	5.38	1.05	27.79	-	23.97	101.80	3
	23.25	18.76	5.39	1.28	27.93	-	24.57	101.18	4
	22.98	18.91	5.46	1.12	26.94	-	23.79	99.20	5
At. Prop.	6.63	3.11	1.60	0.32	3.93	0.20	13.20	28.99	
	6.72	2.96	1.85	0.31	3.87	0.10	13.18	28.99	
	6.74	3.13	1.69	0.28	4.01	-	13.14	28.99	GRAIN
	6.42	3.05	1.69	0.34	4.03	-	13.46	28.99	5 4
	6.49	3.15	1.75	0.30	3.97	-	13.32	28.98	

Elements	Cu	Ag	Fe	Zn	Sb	As	S	Total	Pt. Count
Wt %	23.95	18.71	5.05	1.09	27.28	-	24.24	100.32	1
	24.08	17.55	4.99	1.15	27.29	-	23.77	98.84	2
	23.96	18.86	5.30	0.38	27.32	-	24.12	99.94	3
	23.65	19.15	5.23	0.91	26.92	-	24.10	99.97	4
	21.98	20.33	5.12	1.01	27.58	-	23.27	99.28	5
At. Prop.	6.67	3.07	1.59	0.29	3.97	-	13.39	28.98	
	6.81	2.92	1.60	0.31	4.03	-	13.32	28.99	
	6.71	3.11	1.69	0.10	3.99	-	13.39	28.99	GRAIN
	6.62	3.16	1.66	0.25	3.93	-	13.37	28.99	5 5
	6.29	3.43	1.67	0.28	4.12	-	13.21	29.00	

Elements	Cu	Ag	Fe	Zn	Sb	As	S	Total	Pt. Count
Wt %	22.66	18.49	5.14	1.33	28.00	-	23.88	99.50	1
	24.36	18.14	5.23	0.99	26.07	0.92	23.45	99.15	2
	23.75	18.23	5.28	0.97	27.43	-	23.73	99.38	3
	23.88	18.80	5.07	1.63	27.48	-	24.27	101.13	4
	23.79	17.72	5.09	0.89	26.85	-	23.74	98.08	5
At. Prop.	6.40	3.08	1.65	0.36	4.13	-	13.37	28.99	
	6.87	3.01	1.68	0.27	3.84	0.29	13.11	29.07	
	6.70	3.03	1.69	0.26	4.04	-	13.27	28.99	GRAIN
	6.61	3.06	1.59	0.44	3.97	-	13.32	28.99	5 6
	6.77	2.97	1.64	0.24	3.98	-	13.38	28.98	

Elements	Cu	Ag	Fe	Zn	Sb	As	S	Total	Pt. Count
Wt %	23.97	19.05	5.23	1.00	26.74	-	23.66	99.65	1
	19.10	22.05	7.98	1.10	24.65	0.55	24.49	99.93	2
	23.56	18.58	5.32	1.10	27.67	-	24.20	100.43	3
	23.21	18.66	5.28	0.96	27.45	-	23.65	99.19	4
	23.08	18.59	5.41	0.90	27.22	-	23.68	98.88	5
At. Prop.	6.75	3.16	1.67	0.27	3.93	-	13.21	28.99	
	5.32	3.62	2.53	0.30	3.58	0.13	13.52	29.00	
	6.57	3.05	1.69	0.29	4.03	-	13.37	29.00	GRAIN
	6.58	3.11	1.70	0.26	4.06	-	13.28	28.99	57
	6.55	3.10	1.74	0.25	4.03	-	13.32	28.99	

Elements	Cu	Ag	Fe	Zn	Sb	As	S	Total	Pt. Count
Wt %	22.75	19.13	5.24	1.35	27.29	1.08	24.02	100.85	1
	23.03	18.79	5.31	1.08	28.33	0.42	24.50	101.47	2
	23.57	19.42	5.37	1.19	27.03	0.42	23.87	100.87	3
	23.88	18.88	5.28	1.29	27.62	0.54	24.38	101.88	4
	23.48	18.89	4.97	1.36	26.50	-	23.65	98.85	5
At. Prop.	6.34	3.14	1.66	0.36	3.97	0.25	13.27	28.99	
	6.37	3.06	1.67	0.29	4.09	0.10	13.43	29.01	
	6.57	3.19	1.70	0.32	3.93	0.10	13.19	29.00	GRAIN
	6.56	3.06	1.65	0.34	3.96	0.12	13.29	28.98	58
	6.67	3.16	1.60	0.33	3.92	-	13.31	28.99	

Elements	Cu	Ag	Fe	Zn	Sb	As	S	Total	Pt. Count
Wt %	28.28	14.00	5.70	1.43	25.87	-	23.17	98.44	1
	27.79	15.00	5.30	1.29	27.33	-	24.13	100.84	2
	27.64	14.73	5.46	0.93	27.29	0.58	24.04	100.67	3
	27.91	14.82	5.09	1.25	26.61	0.56	23.26	99.51	4
	28.11	15.34	5.36	1.24	26.36	1.23	23.82	101.45	5
At. Prop.	7.91	2.30	1.81	0.34	3.78	-	12.85	28.99	
	7.61	2.42	1.65	0.30	3.91	-	13.10	28.99	
	7.64	2.37	1.70	0.22	3.89	0.13	13.03	28.98	GRAIN
	7.77	2.43	1.61	0.34	3.87	0.13	12.84	28.99	59
	7.66	2.46	1.66	0.33	3.75	0.28	12.86	29.00	

Elements	Cu	Ag	Fe	Zn	Sb	As	S	Total	Pt. Count
Wt %	27.75	13.64	5.38	1.41	26.61	-	23.66	98.44	1
	27.79	13.84	5.19	1.20	27.03	0.65	23.37	99.06	2
	28.75	13.95	5.66	1.92	26.66	0.61	23.94	101.49	3
	28.47	14.50	5.53	1.47	26.15	0.66	23.89	100.67	4
	27.09	15.12	5.64	1.35	26.64	0.41	23.55	99.80	5
At. Prop.	7.73	2.24	1.70	0.38	3.87	-	13.07	28.99	
	7.75	2.27	1.64	0.32	3.93	0.15	12.92	28.98	
	7.78	2.22	1.74	0.50	3.76	0.14	12.84	28.98	GRAIN
	7.77	2.33	1.71	0.39	3.72	0.15	12.92	28.99	60
	7.51	2.47	1.78	0.36	3.85	0.09	12.93	28.98	

## APPENDIX II

### TETRAHEDRITE ANALYSES

Values are quoted in number of atoms ( atomic proportions ) relative to 13 atoms of sulfur.

Cu	Ag	Fe	Zn	Sb	As	S	Total atoms	Cu atom /unit formula	Valence electr./ unit fml
7.06	2.95	1.80	0.33	3.94	0.16	13.00	29.26	10.01	209.10
7.04	2.94	1.73	0.30	3.86	-	13.00	28.89	09.98	207.20
7.01	3.05	1.86	0.29	3.86	-	13.00	29.08	10.06	207.80
7.01	2.94	1.82	0.24	3.84	-	13.00	28.87	09.95	207.10
6.99	2.87	2.00	0.29	3.94	0.26	13.00	29.37	09.86	210.00
6.88	2.96	1.78	0.26	3.77	0.20	13.00	28.88	09.84	207.70
6.84	2.85	1.75	0.37	3.88	0.09	13.00	28.82	09.69	207.70
7.02	2.98	1.85	0.39	3.84	0.22	13.00	29.31	10.00	209.20
6.81	3.01	1.84	0.34	3.94	-	13.00	28.97	09.82	207.90
7.23	2.90	1.71	0.28	3.80	0.20	13.00	29.14	10.13	208.00
7.10	2.82	1.76	0.37	3.76	-	13.00	28.83	09.92	206.80
6.93	3.03	1.84	0.18	3.86	-	13.00	28.86	09.96	207.00
7.01	2.97	1.85	0.24	4.03	0.11	13.00	29.23	09.98	209.00
6.98	2.90	1.79	0.33	3.93	-	13.00	28.96	09.88	207.70
7.03	2.84	1.80	0.20	3.70	-	13.00	28.59	09.87	205.80
6.74	3.17	1.83	0.41	4.12	-	13.00	29.29	09.91	209.30
6.99	3.06	1.84	0.27	4.00	-	13.00	29.17	10.05	209.10
7.08	3.17	1.83	0.30	4.03	-	13.00	29.44	10.25	209.00
7.04	3.15	1.89	0.34	3.99	0.14	13.00	29.58	10.19	209.90
7.14	3.20	2.00	0.39	4.08	0.15	13.00	29.97	10.34	211.50
7.02	3.16	1.95	0.20	4.00	-	13.00	29.35	10.18	208.80
7.04	3.21	1.84	0.28	4.11	0.11	13.00	29.62	10.25	210.10
7.16	3.22	1.78	0.26	4.13	-	13.00	29.57	10.38	209.50
7.25	3.17	1.82	0.24	4.07	-	13.00	29.57	10.42	209.20
6.94	3.10	1.84	0.28	4.00	0.14	13.00	29.32	10.04	209.20
7.28	3.17	2.07	0.51	4.08	-	13.00	30.14	10.45	211.60
7.05	3.23	1.88	0.32	4.13	-	13.00	29.63	10.28	210.00
7.06	3.22	1.84	0.31	3.96	-	13.00	29.41	10.28	208.80
6.87	3.33	1.84	0.33	4.07	-	13.00	29.46	10.20	209.30
7.08	3.06	2.01	0.28	4.02	-	13.00	29.47	10.14	209.40
6.95	3.06	1.84	0.24	4.00	-	13.00	29.11	10.01	208.20
7.18	3.17	1.95	0.29	3.97	-	13.00	29.59	10.35	209.30
6.89	3.14	1.82	0.25	3.89	-	13.00	28.99	10.03	207.60
6.97	3.12	1.80	0.40	4.02	-	13.00	29.33	10.09	208.80
6.71	3.66	1.88	0.20	4.00	-	13.00	29.47	10.37	208.90
6.62	3.13	1.78	0.29	3.89	0.18	13.00	28.92	09.75	208.00
7.00	3.15	1.93	0.29	3.95	-	13.00	29.34	10.15	208.70
6.83	3.17	1.92	0.26	4.06	0.14	13.00	29.41	10.00	209.40
6.62	3.08	1.90	0.27	4.10	0.17	13.00	29.15	09.70	209.50
6.82	3.25	1.94	0.19	3.94	0.23	13.00	29.39	10.07	209.50
4.88	4.81	1.84	0.43	3.85	0.13	13.00	28.98	09.69	208.10
4.79	5.15	2.00	0.60	4.00	-	13.00	29.56	09.94	210.00
5.52	4.82	1.89	0.52	4.05	-	13.00	29.70	10.34	210.50
5.44	3.80	2.73	0.48	3.69	-	13.00	29.16	09.24	209.30
5.88	4.07	2.28	0.50	4.01	-	13.00	29.76	09.95	210.90
6.67	3.45	1.80	0.50	3.82	-	13.00	29.25	10.12	208.20

Cu	Ag	Fe	Zn	Sb	As	S	Total atoms	Cu atom /unit formula	Valence electr./ unit fml
6.78	3.47	1.92	0.69	3.70	-	13.00	29.57	10.25	209.00
6.81	3.27	1.73	0.52	3.70	-	13.00	29.04	10.08	207.20
6.63	2.99	1.56	0.35	3.66	-	13.00	28.21	09.62	204.70
7.04	3.04	1.69	0.54	3.79	0.16	13.00	29.28	10.08	208.60
7.30	2.45	1.66	0.31	3.86	-	13.00	28.61	09.75	206.40
7.42	2.38	1.73	0.58	3.80	-	13.00	28.94	09.80	207.50
7.30	2.44	1.61	0.57	3.83	-	13.00	28.76	09.74	207.00
7.39	2.42	1.69	0.47	3.82	0.13	13.00	28.95	09.81	207.80
7.31	2.41	1.69	0.43	3.84	-	13.00	28.70	09.72	206.80
7.37	2.45	1.66	0.46	3.79	0.08	13.00	28.85	09.82	207.20
7.33	2.32	1.61	0.47	3.80	0.15	13.00	28.71	09.65	207.20
7.29	2.31	1.47	0.44	4.33	0.17	13.00	29.02	09.60	209.70
7.52	2.35	1.64	0.33	3.81	0.17	13.00	28.85	09.87	207.40
6.81	2.27	1.59	0.37	3.57	0.11	13.00	27.75	09.08	204.00
4.69	5.57	2.18	0.23	3.90	0.12	13.00	29.72	10.26	210.00
4.56	5.64	1.97	0.25	4.03	-	13.00	29.46	10.20	209.30
4.74	5.59	2.11	0.24	3.94	-	13.00	29.63	10.33	209.50
4.57	5.53	2.00	0.37	3.88	-	13.00	29.37	10.10	208.80
4.75	4.74	2.42	0.19	3.56	-	13.00	28.68	09.49	206.60
7.08	2.67	1.55	0.67	3.73	0.11	13.00	28.84	09.75	207.30
7.38	2.68	1.56	0.75	3.82	0.23	13.00	29.44	10.06	209.50
7.03	2.68	1.44	0.71	3.72	0.24	13.00	28.85	09.74	207.60
7.21	2.58	1.59	0.54	3.68	0.23	13.00	28.86	09.79	207.40
7.28	2.66	1.48	0.73	3.78	0.22	13.00	29.17	09.94	208.60
7.36	2.74	1.45	0.59	3.48	0.52	13.00	29.15	10.10	208.20
7.38	2.58	1.58	0.57	3.52	0.27	13.00	28.93	09.96	207.10
7.53	2.48	1.46	0.58	3.37	0.60	13.00	29.02	10.01	208.00
7.39	2.92	1.53	0.66	3.98	0.22	13.00	29.73	10.32	210.40
7.21	2.66	1.48	0.76	3.71	0.41	13.00	29.25	09.87	209.30
7.31	2.66	1.44	0.64	3.72	0.27	13.00	29.06	09.97	208.00
7.62	2.75	1.58	0.70	3.71	0.32	13.00	29.72	10.37	209.90
7.34	2.58	1.53	0.55	3.59	0.33	13.00	28.96	09.92	207.50
7.18	2.79	1.45	0.56	3.68	0.33	13.00	28.99	09.97	208.00
7.40	2.71	1.51	0.60	3.67	0.26	13.00	29.17	10.11	208.10
7.57	2.77	1.50	0.76	3.79	0.47	13.00	29.88	10.34	211.10
7.25	2.68	1.51	0.70	3.61	0.29	13.00	29.06	09.93	207.90
7.56	2.72	1.67	0.65	3.77	0.40	13.00	29.78	10.28	210.70
7.42	2.64	1.62	0.74	3.65	0.37	13.00	29.47	10.06	209.50
7.40	2.72	1.47	0.79	3.83	0.32	13.00	29.55	10.12	210.00
7.06	2.58	1.57	0.82	3.52	0.56	13.00	29.14	09.64	209.20
7.50	2.57	1.55	0.88	3.58	0.59	13.00	29.69	10.07	210.70
7.21	2.62	1.62	0.77	3.61	0.38	13.00	29.22	09.83	209.00
7.39	2.66	1.61	0.68	3.67	0.56	13.00	29.59	10.05	210.50
6.95	2.77	1.53	0.60	3.80	-	13.00	28.67	09.72	206.60
7.40	2.63	1.60	0.61	3.62	0.21	13.00	29.08	10.03	207.70
7.56	2.49	1.48	0.64	3.35	0.58	13.00	29.12	10.05	208.00

Cu	Ag	Fe	Zn	Sb	As	S	Total atoms	Cu atom Valence	
								/unit formula	electr./ unit fml
7.44	2.46	1.52	0.66	3.30	0.70	13.00	29.10	09.90	208.00
7.46	2.62	1.49	0.62	3.51	0.69	13.00	29.41	10.08	209.60
7.43	2.67	1.45	0.71	3.65	0.32	13.00	29.25	10.10	208.50
7.45	2.60	1.51	0.76	3.48	0.27	13.00	29.09	10.05	207.50
7.66	2.52	1.39	0.68	3.23	0.70	13.00	29.21	10.18	208.10
7.52	2.45	1.47	0.72	3.34	0.84	13.00	29.37	09.97	209.60
7.43	2.47	1.41	0.61	3.39	0.71	13.00	29.02	09.90	208.30
7.41	2.51	1.61	0.54	3.33	0.46	13.00	28.88	09.92	207.00
7.54	2.49	1.37	0.61	3.25	0.66	13.00	28.96	10.03	207.30
7.28	2.78	1.40	0.62	3.64	0.51	13.00	29.24	10.06	208.90
7.40	2.60	1.42	0.68	3.46	0.47	13.00	29.04	10.00	207.80
7.36	2.54	1.28	0.62	3.56	0.56	13.00	28.96	09.90	208.00
7.25	2.64	1.37	0.49	3.62	0.52	13.00	28.92	09.89	207.90
7.45	2.55	1.47	0.57	3.47	0.49	13.00	29.00	10.00	207.80
7.34	2.57	1.32	0.48	3.63	0.47	13.00	28.83	09.91	207.50
7.40	2.55	1.36	0.66	3.66	0.35	13.00	28.98	09.95	208.00
7.29	2.62	1.36	0.60	3.53	0.35	13.00	28.77	09.91	206.80
7.12	2.53	1.33	0.64	3.49	0.62	13.00	28.76	09.65	207.70
7.13	2.48	1.27	0.69	3.39	0.44	13.00	28.41	09.61	205.90
6.84	3.29	1.35	0.68	3.73	0.23	13.00	29.14	10.13	208.00
7.17	2.66	1.35	0.68	3.69	0.15	13.00	28.73	09.83	206.70
7.21	2.43	1.35	0.46	3.40	0.54	13.00	28.42	09.64	206.00
7.19	2.71	1.35	0.48	3.44	0.53	13.00	28.73	09.90	206.80
7.48	2.39	1.37	0.56	3.29	0.68	13.00	28.80	09.87	207.10
7.32	2.65	1.39	0.66	3.61	0.29	13.00	28.96	09.97	207.40
7.24	2.56	1.35	0.56	3.50	0.55	13.00	28.78	09.80	207.40
7.21	2.51	1.33	0.58	3.46	0.57	13.00	28.67	09.72	207.10
7.25	2.56	1.37	0.59	3.42	0.58	13.00	28.79	09.81	207.30
7.22	2.45	1.30	0.71	3.61	0.56	13.00	28.88	09.67	208.20
6.92	3.04	1.39	0.57	3.68	0.48	13.00	29.09	09.96	208.60
7.38	2.68	1.40	0.59	3.70	0.32	13.00	29.09	10.06	208.00
7.36	2.59	1.40	0.59	3.69	0.21	13.00	28.87	09.95	207.10
7.02	2.63	1.51	0.65	3.68	0.51	13.00	29.00	09.65	208.90
6.59	2.76	1.53	0.61	3.85	0.20	13.00	28.54	09.35	216.00
6.05	3.17	1.41	0.50	3.84	0.22	13.00	28.20	09.22	206.30
6.82	2.61	1.36	0.65	3.54	0.42	13.00	28.42	09.43	206.50
6.48	2.61	1.29	0.55	3.57	0.39	13.00	27.92	09.09	205.10
5.52	3.68	1.32	0.58	3.92	0.10	13.00	28.14	09.20	206.00
7.09	2.59	1.43	0.55	3.41	0.47	13.00	28.56	09.68	206.40
6.50	3.27	1.38	0.64	3.66	0.38	13.00	28.86	09.77	207.70
5.74	4.16	1.36	0.78	3.85	0.38	13.00	29.30	09.90	209.60
6.21	3.62	1.34	0.66	4.00	0.17	13.00	29.01	09.83	208.50
7.17	2.31	1.34	0.54	3.21	0.73	13.00	28.34	09.48	206.00
6.97	2.52	1.40	0.73	3.57	0.26	13.00	28.47	09.49	206.30
7.58	2.46	1.39	0.48	3.35	0.64	13.00	28.93	10.04	207.20
6.88	2.55	1.36	0.39	3.33	0.62	13.00	28.16	09.43	205.40

Cu	Ag	Fe	Zn	Sb	As	S	Total atoms	Cu atom /unit formula	Valence electr./ unit fml
7.21	2.58	1.41	0.64	3.56	0.29	13.00	28.72	09.79	206.70
6.82	3.16	1.51	0.54	3.62	0.25	13.00	28.92	09.98	207.20
7.44	2.42	1.44	0.78	3.41	0.60	13.00	29.11	09.86	208.50
5.58	4.71	1.27	0.81	4.24	-	13.00	29.62	10.29	210.20
7.49	2.47	1.36	0.54	3.42	0.61	13.00	28.92	09.96	207.50
7.32	2.51	1.40	0.70	3.38	0.62	13.00	28.97	09.83	207.90
7.29	2.43	1.50	0.69	3.49	0.46	13.00	28.88	09.72	207.70
6.88	3.13	1.63	0.29	3.74	-	13.00	28.69	10.01	206.00
6.93	3.13	1.67	0.46	3.89	0.15	13.00	29.25	10.06	208.70
7.10	3.00	1.70	0.37	3.93	-	13.00	29.12	10.10	207.90
7.01	3.07	1.67	0.43	3.82	0.09	13.00	29.11	10.08	207.90
7.14	3.07	1.76	0.36	3.90	-	13.00	29.25	10.21	208.10
6.74	2.97	1.65	0.32	3.76	-	13.00	28.46	09.71	205.70
7.08	3.04	1.65	0.44	3.87	0.11	13.00	28.74	10.12	208.20
6.75	3.13	1.77	0.27	3.80	-	13.00	28.71	09.88	206.60
6.71	3.13	1.58	0.37	3.75	0.14	13.00	29.35	09.84	206.70
6.93	3.14	1.85	0.43	3.88	0.10	13.00	29.03	10.07	209.00
6.91	2.93	1.90	0.34	3.94	-	13.00	29.03	09.84	208.10
6.70	3.06	1.76	0.39	3.91	0.17	13.00	28.99	09.76	208.60
6.72	3.02	1.71	0.41	3.74	0.11	13.00	28.74	09.74	206.90
6.78	2.96	1.74	0.21	3.72	-	13.00	28.44	09.74	205.40
6.69	3.00	1.94	0.37	3.73	0.16	13.00	28.93	09.69	207.80
6.92	3.09	1.72	0.32	3.82	0.25	13.00	29.14	10.01	208.40
7.08	2.96	1.69	0.33	3.79	0.15	13.00	29.00	10.04	207.80
6.73	3.17	1.71	0.29	3.89	-	13.00	28.81	09.90	207.00
6.82	3.08	1.66	0.30	3.83	0.17	13.00	28.89	09.90	207.50
6.61	3.24	1.73	0.35	3.91	-	13.00	28.86	09.85	207.30
6.69	3.04	1.62	0.38	3.78	-	13.00	28.52	09.73	206.00
6.65	3.03	1.65	0.26	3.78	0.17	13.00	28.58	09.68	206.50
6.77	3.15	1.63	0.32	3.86	-	13.00	28.76	09.92	206.60
6.67	3.07	1.61	0.45	3.82	0.08	13.00	28.73	09.74	207.00
6.60	3.08	1.69	0.34	3.77	-	13.00	28.50	09.68	206.20
6.70	3.00	1.69	0.40	3.75	0.14	13.00	28.71	09.70	206.90
6.84	3.07	1.65	0.34	3.75	0.15	13.00	28.83	09.91	207.00
6.57	3.05	1.54	0.24	3.76	0.22	13.00	28.41	09.62	206.10
6.84	3.09	1.62	0.31	3.76	-	13.00	28.64	09.93	206.00
6.85	2.98	1.62	0.40	3.79	0.13	13.00	28.81	09.83	207.10
6.70	2.96	1.64	0.19	3.88	0.15	13.00	28.54	09.66	206.70
6.66	3.11	1.71	0.33	3.80	0.14	13.00	28.78	09.77	207.20
6.47	3.10	1.68	0.41	3.79	-	13.00	28.47	09.57	206.10
6.82	2.97	1.63	0.32	3.82	-	13.00	28.59	09.79	206.10
6.62	3.23	1.57	0.38	3.81	0.11	13.00	28.62	09.85	206.90
6.72	3.01	1.75	0.39	3.88	0.15	13.00	28.94	09.71	208.00
6.61	3.21	1.66	0.40	3.89	0.12	13.00	28.92	09.82	207.80
6.67	3.26	1.71	0.35	3.78	-	13.00	28.79	09.93	206.60
6.64	3.07	1.63	0.45	3.79	-	13.00	28.61	09.71	206.30

Cu	Ag	Fe	Zn	Sb	As	S	Total atoms	Cu atom Valence	
								/unit formula	electr./ unit fml
6.59	2.90	1.65	0.38	3.78	-	13.00	28.31	09.49	205.60
6.73	3.29	1.54	0.38	3.81	0.15	13.00	28.94	10.02	207.20
6.99	3.30	1.61	0.38	3.87	-	13.00	29.16	10.20	207.60
6.73	3.00	1.52	0.38	3.84	0.17	13.00	28.76	09.73	207.10
6.56	3.21	1.60	0.41	3.81	0.18	13.00	28.81	09.77	207.40
6.66	3.15	1.57	0.36	3.89	0.37	13.00	29.02	09.81	208.70
6.83	2.87	1.76	0.26	3.83	-	13.00	28.57	09.70	206.30
6.66	2.95	1.73	0.37	3.78	0.10	13.00	28.61	09.61	206.70
6.90	2.89	1.65	0.38	3.84	0.11	13.00	28.81	09.79	207.20
6.38	2.81	1.69	0.43	3.89	0.12	13.00	28.34	09.19	206.80
6.41	2.94	1.65	0.29	3.87	-	13.00	28.18	09.35	205.50
6.46	2.76	1.72	0.36	3.81	-	13.00	28.13	09.22	205.50
6.74	2.76	1.69	0.13	3.87	0.13	13.00	28.34	09.50	206.10
6.85	2.85	1.67	0.33	3.88	-	13.00	28.60	09.70	206.50
6.85	2.84	1.74	0.30	3.87	-	13.00	28.62	09.69	206.60
6.30	3.31	1.65	0.31	3.85	0.11	13.00	28.55	09.61	206.10
6.45	2.84	1.45	0.32	3.65	0.12	13.00	27.85	09.29	204.10
6.45	2.89	1.45	0.34	3.80	-	13.00	27.95	09.34	204.50
6.48	2.84	1.65	0.45	3.74	-	13.00	28.18	09.32	205.30
6.77	2.73	1.58	0.34	3.77	0.11	13.00	28.32	09.50	205.80
6.60	2.83	1.64	0.29	3.86	-	13.00	28.25	09.43	205.60
6.37	2.88	1.71	0.29	3.79	-	13.00	28.04	09.25	205.10
6.74	2.83	1.70	0.31	3.88	0.13	13.00	28.62	09.57	207.10
6.49	2.95	1.70	0.39	3.82	-	13.00	28.37	09.44	206.00
6.77	2.96	1.79	0.41	3.83	0.10	13.00	28.89	09.73	207.70
6.79	3.02	1.72	0.28	3.73	-	13.00	28.23	09.82	205.80
6.48	2.86	1.49	0.37	3.87	0.14	13.00	28.25	09.34	206.00
6.52	2.88	1.55	0.36	3.80	0.11	13.00	28.25	09.40	205.70
6.47	2.84	1.56	0.26	3.78	-	13.00	27.93	09.31	204.40
6.62	2.91	1.62	0.33	3.86	-	13.00	28.35	09.51	205.90
6.48	2.87	1.55	0.34	3.83	-	13.00	28.10	09.35	205.10
6.71	2.91	1.63	0.30	3.76	-	13.00	28.32	09.62	205.40
6.41	2.79	1.63	0.32	3.75	-	13.00	27.93	09.20	204.50
6.59	2.82	1.58	0.32	3.83	-	13.00	28.15	09.41	205.20
6.81	2.95	1.73	0.47	3.91	-	13.00	28.89	09.76	207.60
6.74	2.77	1.67	0.32	3.77	-	13.00	28.29	09.51	205.40
6.66	2.83	1.68	0.30	3.76	0.15	13.00	28.34	09.49	206.20
6.55	2.74	1.62	0.36	3.76	-	13.00	28.05	09.29	204.90
6.60	2.84	1.64	0.22	3.78	0.13	13.00	28.24	09.44	205.60
6.50	2.84	1.60	0.25	3.67	-	13.00	27.89	09.34	204.00
6.56	2.79	1.55	0.33	3.69	-	13.00	27.93	09.35	204.20
6.68	2.74	1.75	0.55	3.78	0.09	13.00	28.61	09.42	207.10
6.65	2.83	1.61	0.48	3.72	0.11	13.00	28.42	09.48	206.10
6.69	2.83	1.69	0.68	3.86	-	13.00	28.77	09.52	207.50
6.61	2.80	1.66	0.52	3.77	-	13.00	28.38	09.41	206.00
6.69	2.79	1.82	0.56	3.61	-	13.00	28.49	09.48	206.00



Cu	Ag	Fe	Zn	Sb	As	S	Total atoms	Cu atom Valence	
								/unit formula	electr./ unit fml
6.21	3.13	1.46	0.27	3.74	0.20	13.00	28.02	09.34	205.00
6.44	3.42	1.47	0.20	3.93	-	13.00	28.48	09.86	205.80
6.58	3.20	1.57	0.23	4.00	-	13.00	28.56	09.78	206.60
6.71	3.26	1.48	0.13	4.05	-	13.00	28.64	09.97	206.50
6.47	3.10	1.53	0.33	4.11	-	13.00	28.56	09.57	207.10
6.50	3.30	1.58	0.21	3.85	-	13.00	28.47	09.80	205.70
6.61	3.24	1.48	0.19	3.98	0.17	13.00	28.71	09.85	207.10
6.87	3.18	1.50	0.32	3.87	-	13.00	28.77	10.05	206.40
6.57	3.21	1.54	0.33	3.90	-	13.00	28.58	09.78	206.30
6.46	3.17	1.58	0.35	4.00	0.11	13.00	28.70	09.63	205.90
5.20	4.62	1.50	0.26	4.00	-	13.00	28.74	09.82	208.20
5.82	4.12	1.52	0.32	4.11	0.28	13.00	29.19	09.94	209.40
5.88	4.13	1.55	0.19	3.94	0.15	13.00	28.86	10.01	207.40
5.25	4.19	1.57	0.25	3.96	0.11	13.00	28.37	09.44	206.40
4.94	4.59	1.58	0.20	3.77	0.29	13.00	28.39	09.53	206.40
6.94	3.19	1.58	0.48	3.99	0.11	13.00	29.32	10.13	208.90
6.70	3.24	1.57	0.34	3.96	-	13.00	28.83	09.94	207.10
6.82	3.10	1.59	0.36	3.90	-	13.00	28.79	09.92	206.90
6.43	3.26	1.46	0.18	3.85	-	13.00	28.20	09.69	204.90
6.70	3.24	1.50	0.33	3.87	-	13.00	28.65	09.94	206.30
6.34	3.25	1.49	0.22	4.01	-	13.00	28.33	09.55	205.90
6.61	3.25	1.44	0.17	3.99	-	13.00	28.48	09.86	205.90
5.13	4.89	1.25	0.59	4.27	-	13.00	29.15	10.02	208.90
4.82	4.84	1.59	0.33	4.13	-	13.00	28.74	09.66	207.60
6.39	3.22	1.60	0.23	3.91	-	13.00	28.36	09.61	205.80
6.54	3.25	1.61	0.22	3.97	0.07	13.00	28.70	09.79	207.00
6.48	3.12	1.43	0.21	3.83	0.11	13.00	28.19	09.60	205.20
6.53	3.15	1.50	0.24	3.94	-	13.00	28.38	09.68	205.80
6.46	3.00	1.61	0.26	3.91	0.15	13.00	28.42	09.46	206.60
6.52	3.12	1.69	0.29	3.85	-	13.00	28.49	09.64	206.10
6.46	3.04	1.58	0.21	3.87	-	13.00	28.18	09.50	205.20
6.32	2.97	1.57	0.27	3.95	-	13.00	28.09	09.29	205.50
6.55	2.99	1.66	0.24	3.96	-	13.00	28.42	09.54	206.30
6.70	3.04	1.63	0.26	3.94	-	13.00	28.73	09.74	208.20
6.60	3.01	1.55	0.32	3.88	-	13.00	28.38	09.61	205.80
6.52	3.06	1.57	0.31	3.87	0.19	13.00	28.54	09.58	206.90
6.62	2.91	1.82	0.30	3.81	0.09	13.00	28.59	09.53	206.80
6.66	3.09	1.67	0.27	3.96	-	13.00	28.67	09.75	206.90
6.20	2.94	1.63	0.32	3.89	-	13.00	27.99	09.14	205.30
6.33	3.07	1.70	0.29	3.87	-	13.00	28.28	09.40	205.80
6.47	2.98	1.54	0.28	3.85	-	13.00	28.13	09.45	205.20
6.64	2.84	1.56	0.30	3.93	-	13.00	28.29	09.48	205.80
6.51	3.01	1.64	0.09	3.87	-	13.00	28.14	09.52	205.00
6.43	3.07	1.61	0.24	3.82	-	13.00	28.18	09.50	205.20
6.18	3.37	1.64	0.27	4.05	-	13.00	28.53	09.55	206.90
6.22	2.99	1.60	0.35	4.01	-	13.00	28.18	09.21	206.10

Cu	Ag	Fe	Zn	Sb	As	S	Total atoms	Cu atom Valence	
								/unit formula	electr./ unit fml
6.81	2.98	1.66	0.26	3.80	0.28	13.00	28.82	09.79	207.60
6.56	2.96	1.65	0.25	3.95	-	13.00	28.39	09.52	206.20
6.45	2.98	1.55	0.42	3.87	-	13.00	28.29	09.43	205.80
6.57	2.88	1.59	0.23	3.86	-	13.00	28.15	09.45	205.20
6.64	3.10	1.64	0.26	3.86	-	13.00	28.52	09.74	206.10
5.11	3.48	2.43	0.28	3.44	0.12	13.00	27.88	08.59	205.20
6.38	2.96	1.64	0.28	3.91	-	13.00	28.19	09.34	205.70
6.44	3.04	1.66	0.25	3.97	-	13.00	28.37	09.48	206.30
6.39	3.02	1.69	0.24	3.93	-	13.00	28.29	09.41	206.00
6.21	3.07	1.62	0.35	3.88	0.24	13.00	28.39	09.28	207.00
6.16	2.96	1.61	0.28	3.95	0.09	13.00	28.07	09.12	205.90
6.47	3.14	1.67	0.31	3.87	0.09	13.00	28.57	09.61	206.70
6.41	2.99	1.61	0.33	3.87	0.11	13.00	28.34	09.40	206.30
6.51	3.08	1.56	0.32	3.82	-	13.00	28.31	09.59	205.50
8.00	2.32	1.83	0.34	3.82	-	13.00	29.32	10.32	208.10
7.55	2.40	1.63	0.29	3.87	-	13.00	28.76	09.95	206.60
7.62	2.36	1.69	0.21	3.88	0.12	13.00	28.90	09.98	207.40
7.86	2.46	1.62	0.34	3.91	0.13	13.00	29.34	10.32	208.60
7.74	2.48	1.67	0.33	3.79	0.28	13.00	29.31	10.22	208.70
7.68	2.22	1.69	0.37	3.84	-	13.00	28.83	09.90	206.90
7.79	2.28	1.65	0.32	3.95	0.15	13.00	29.15	10.07	208.50
7.87	2.24	1.76	0.50	3.80	0.14	13.00	29.33	10.11	208.70
7.81	2.34	1.72	0.39	3.74	0.15	13.00	29.16	10.15	207.90
7.55	2.48	1.78	0.36	3.87	0.09	13.00	29.13	10.03	208.20

## APPENDIX III

### Reflectivities

Quantitative measurement of the reflectance values of selected samples of tetrahedrite.

## Reflectivities of tetrahedrite

Sample No.	L	$10^3/\text{cm}$	I	A
49-274 VERT	400.0	25.000	39.459	0.404
	420.0	23.810	32.218	0.492
	440.0	22.727	32.366	0.490
	460.0	21.739	32.149	0.493
	480.0	20.833	31.245	0.505
	500.0	20.000	31.005	0.509
	520.0	19.231	31.781	0.498
	540.0	18.519	31.512	0.502
	560.0	17.857	30.838	0.511
	580.0	17.241	31.078	0.508
	600.0	16.667	31.073	0.508
	620.0	16.129	30.225	0.520
	640.0	15.625	30.332	0.518
	660.0	15.152	30.713	0.513
680.0	14.706	29.817	0.526	
700.0	14.286	31.027	0.508	
"	400.0	25.000	30.996	0.509
	420.0	23.810	32.897	0.483
	440.0	22.727	32.502	0.488
	460.0	21.739	32.601	0.487
	480.0	20.833	33.128	0.480
	500.0	20.000	32.527	0.488
	520.0	19.231	32.293	0.491
	540.0	18.519	32.236	0.492
	560.0	17.857	31.912	0.496
	580.0	17.241	32.060	0.494
	600.0	16.667	32.470	0.489
	620.0	16.129	31.578	0.501
	640.0	15.625	31.476	0.502
	660.0	15.152	30.582	0.515
680.0	14.706	30.937	0.510	
700.0	14.286	30.579	0.515	
"	400.0	25.000	28.835	0.540
	420.0	23.810	33.258	0.478
	440.0	22.727	31.846	0.497
	460.0	21.739	32.041	0.494
	480.0	20.833	32.045	0.494
	500.0	20.000	31.502	0.502
	520.0	19.231	31.645	0.500
	540.0	18.519	31.635	0.500
	560.0	17.857	31.719	0.499
	580.0	17.241	31.372	0.503
	600.0	16.667	31.029	0.508
	620.0	16.129	31.053	0.508
	640.0	15.625	31.119	0.507
	660.0	15.152	30.201	0.520
680.0	14.706	30.383	0.517	
700.0	14.286	30.475	0.516	

Sample No.	L	10 <sup>3</sup> /cm	I	A
49-274 HORZ	400.0	25.000	28.280	0.549
	420.0	23.810	34.024	0.468
	440.0	22.727	33.022	0.481
	460.0	21.739	31.989	0.495
	480.0	20.833	33.175	0.479
	500.0	20.000	32.020	0.495
	520.0	19.231	32.151	0.493
	540.0	18.519	31.452	0.502
	560.0	17.857	31.222	0.506
	580.0	17.241	31.133	0.507
	600.0	16.667	31.099	0.507
	620.0	16.129	30.139	0.521
	640.0	15.625	30.325	0.518
	660.0	15.152	29.930	0.524
	680.0	14.706	29.300	0.533
	700.0	14.286	29.159	0.535
"	400.0	25.000	26.574	0.576
	420.0	23.810	32.857	0.483
	440.0	22.727	32.237	0.492
	460.0	21.739	34.831	0.458
	480.0	20.833	34.908	0.457
	500.0	20.000	33.621	0.473
	520.0	19.231	33.693	0.472
	540.0	18.519	32.961	0.482
	560.0	17.857	32.654	0.486
	580.0	17.241	31.730	0.499
	600.0	16.667	31.347	0.504
	620.0	16.129	30.565	0.515
	640.0	15.625	29.285	0.533
	660.0	15.152	29.049	0.537
	680.0	14.706	28.332	0.548
	700.0	14.286	27.979	0.553
"	400.0	25.000	26.574	0.576
	420.0	23.810	32.857	0.483
	440.0	22.727	32.237	0.492
	460.0	21.739	34.831	0.458
	480.0	20.833	34.908	0.457
	500.0	20.000	33.621	0.473
	520.0	19.231	33.693	0.472
	540.0	18.519	32.961	0.482
	560.0	17.857	32.654	0.486
	580.0	17.241	31.730	0.499
	600.0	16.667	31.347	0.504
	620.0	16.129	30.565	0.515
	640.0	15.625	29.285	0.533
	660.0	15.152	29.049	0.537
	680.0	14.706	28.332	0.548
	700.0	14.286	27.979	0.553

Sample No.	L	10 <sup>3</sup> /cm	I	A
3-317	400.0	25.000	31.560	0.501
	420.0	23.810	33.508	0.475
	440.0	22.727	31.714	0.499
	460.0	21.739	32.689	0.486
	480.0	20.833	31.680	0.499
	500.0	20.000	31.713	0.499
	520.0	19.231	32.050	0.494
	540.0	18.519	31.510	0.502
	560.0	17.857	31.889	0.496
	580.0	17.241	31.507	0.502
	600.0	16.667	31.709	0.499
	620.0	16.129	31.073	0.508
	640.0	15.625	30.624	0.514
	660.0	15.152	30.780	0.512
	680.0	14.706	30.135	0.521
	700.0	14.286	29.951	0.524
"	400.0	25.000	27.630	0.559
	420.0	23.810	34.817	0.458
	440.0	22.727	31.147	0.507
	460.0	21.739	32.309	0.491
	480.0	20.833	32.153	0.493
	500.0	20.000	31.895	0.496
	520.0	19.231	31.765	0.498
	540.0	18.519	31.343	0.504
	560.0	17.857	31.330	0.504
	580.0	17.241	31.368	0.504
	600.0	16.667	31.203	0.506
	620.0	16.129	30.635	0.514
	640.0	15.625	30.737	0.512
	660.0	15.152	30.298	0.519
	680.0	14.706	29.846	0.525
	700.0	14.286	30.264	0.519
"	400.0	25.000	28.901	0.539
	420.0	23.810	33.110	0.480
	440.0	22.727	31.188	0.506
	460.0	21.739	31.775	0.498
	480.0	20.833	31.192	0.506
	500.0	20.000	31.189	0.506
	520.0	19.231	30.898	0.510
	540.0	18.519	31.148	0.507
	560.0	17.857	31.302	0.504
	580.0	17.241	30.902	0.510
	600.0	16.667	31.155	0.506
	620.0	16.129	30.981	0.509
	640.0	15.625	30.386	0.517
	660.0	15.152	29.745	0.527
	680.0	14.706	29.265	0.534
	700.0	14.286	29.711	0.527

Sample No.	L	$10^3/cm$	I	A
3-317	400.0	25.000	31.233	0.505
	420.0	23.810	35.146	0.454
	440.0	22.727	31.830	0.497
	460.0	21.739	31.284	0.505
	480.0	20.823	32.589	0.487
	500.0	20.000	31.225	0.505
	520.0	19.231	31.755	0.498
	540.0	18.519	31.391	0.503
	560.0	17.857	31.374	0.503
	580.0	17.241	31.679	0.499
	600.0	16.667	31.532	0.501
	620.0	16.129	30.986	0.509
	640.0	15.625	30.836	0.511
	660.0	15.152	30.078	0.522
	680.0	14.706	30.299	0.519
700.0	14.286	29.846	0.525	
49-284	400.0	25.000	27.287	0.564
	420.0	23.810	29.520	0.530
	440.0	22.727	30.346	0.518
	460.0	21.739	30.346	0.518
	480.0	20.823	30.450	0.516
	500.0	20.000	29.523	0.530
	520.0	19.231	30.001	0.523
	540.0	18.519	28.964	0.538
	560.0	17.857	29.279	0.533
	580.0	17.241	29.134	0.536
	600.0	16.667	29.166	0.535
	620.0	16.129	28.962	0.538
	640.0	15.625	28.548	0.544
	660.0	15.152	28.024	0.552
	680.0	14.706	27.829	0.556
700.0	14.286	27.954	0.554	
"	400.0	25.000	26.486	0.577
	420.0	23.810	29.989	0.523
	440.0	22.727	30.010	0.523
	460.0	21.739	30.376	0.517
	480.0	20.823	30.353	0.518
	500.0	20.000	29.746	0.527
	520.0	19.231	30.202	0.520
	540.0	18.519	29.561	0.529
	560.0	17.857	29.889	0.524
	580.0	17.241	29.951	0.524
	600.0	16.667	29.990	0.523
	620.0	16.129	30.073	0.522
	640.0	15.625	30.252	0.519
	660.0	15.152	29.597	0.529
	680.0	14.706	29.708	0.527
700.0	14.286	29.749	0.527	

Sample No.	L	10 <sup>3</sup> /cm	I	A
3-270	400.0	25.000	29.546	0.529
	420.0	23.810	30.645	0.514
	440.0	22.727	30.597	0.514
	460.0	21.739	31.116	0.507
	480.0	20.823	30.149	0.521
	500.0	20.000	30.321	0.518
	520.0	19.231	30.421	0.517
	540.0	18.519	30.037	0.522
	560.0	17.857	30.923	0.510
	580.0	17.241	29.921	0.524
	600.0	16.667	29.790	0.526
	620.0	16.129	30.162	0.521
	640.0	15.625	29.672	0.528
	660.0	15.152	29.109	0.536
	680.0	14.706	29.003	0.538
700.0	14.286	28.786	0.541	
"	400.0	25.000	33.265	0.478
	420.0	23.810	31.251	0.505
	440.0	22.727	31.065	0.508
	460.0	21.739	30.069	0.522
	480.0	20.823	30.335	0.518
	500.0	20.000	30.760	0.512
	520.0	19.231	29.970	0.523
	540.0	18.519	29.824	0.525
	560.0	17.857	30.315	0.518
	580.0	17.241	29.808	0.526
	600.0	16.667	29.817	0.526
	620.0	16.129	29.525	0.530
	640.0	15.625	29.674	0.528
	660.0	15.152	29.352	0.532
	680.0	14.706	29.290	0.533
700.0	14.286	28.435	0.546	
"	400.0	25.000	33.918	0.470
	420.0	23.810	29.494	0.530
	440.0	22.727	30.623	0.514
	460.0	21.739	29.875	0.525
	480.0	20.823	29.119	0.536
	500.0	20.000	29.785	0.526
	520.0	19.231	29.365	0.532
	540.0	18.519	29.438	0.531
	560.0	17.857	29.774	0.526
	580.0	17.241	28.949	0.538
	600.0	16.667	28.934	0.539
	620.0	16.129	29.103	0.536
	640.0	15.625	29.021	0.537
	660.0	15.152	28.165	0.550
	680.0	14.706	28.602	0.544
700.0	14.286	28.070	0.552	



Sample No.	L	10 <sup>3</sup> /cm	I	A
3-270	400.0	25.000	33.161	0.479
	420.0	23.810	30.155	0.521
	440.0	22.727	30.149	0.521
	460.0	21.739	28.816	0.540
	480.0	20.823	29.043	0.537
	500.0	20.000	29.175	0.535
	520.0	19.231	29.325	0.533
	540.0	18.519	29.355	0.532
	560.0	17.857	29.993	0.523
	580.0	17.241	29.244	0.534
	600.0	16.667	29.099	0.536
	620.0	16.129	29.291	0.533
	640.0	15.625	28.886	0.539
	660.0	15.152	28.599	0.544
	680.0	14.706	28.053	0.552
700.0	14.286	27.596	0.559	
3-165	400.0	25.000	33.335	0.477
	420.0	23.810	33.736	0.472
	440.0	22.727	31.965	0.495
	460.0	21.739	31.292	0.505
	480.0	20.823	31.137	0.507
	500.0	20.000	30.943	0.509
	520.0	19.231	31.123	0.507
	540.0	18.519	30.718	0.513
	560.0	17.857	31.310	0.504
	580.0	17.241	30.486	0.516
	600.0	16.667	30.582	0.515
	620.0	16.129	30.297	0.519
	640.0	15.625	30.588	0.514
	660.0	15.152	29.703	0.527
	680.0	14.706	29.800	0.526
700.0	14.286	29.203	0.535	
"	400.0	25.000	34.567	0.461
	420.0	23.810	32.338	0.490
	440.0	22.727	31.399	0.503
	460.0	21.739	31.348	0.504
	480.0	20.823	30.514	0.515
	500.0	20.000	31.164	0.506
	520.0	19.231	30.767	0.512
	540.0	18.519	31.197	0.506
	560.0	17.857	30.931	0.510
	580.0	17.241	30.983	0.509
	600.0	16.667	30.504	0.516
	620.0	16.129	30.419	0.517
	640.0	15.625	30.649	0.514
	660.0	15.152	29.564	0.529
	680.0	14.706	29.381	0.532
700.0	14.286	29.455	0.531	

Sample No.	L	10 <sup>3</sup> /cm	I	A
3-165	400.0	25.000	29.201	0.535
	420.0	23.810	29.662	0.528
	440.0	22.727	29.837	0.525
	460.0	21.739	29.255	0.534
	480.0	20.823	28.918	0.539
	500.0	20.000	28.979	0.538
	520.0	19.231	28.630	0.543
	540.0	18.519	28.535	0.545
	560.0	17.857	28.865	0.540
	580.0	17.241	28.523	0.545
	600.0	16.667	28.676	0.542
	620.0	16.129	28.648	0.543
	640.0	15.625	28.467	0.546
	660.0	15.152	27.963	0.553
	680.0	14.706	27.720	0.557
	700.0	14.286	27.890	0.555
"	400.0	25.000	31.140	0.507
	420.0	23.810	31.244	0.505
	440.0	22.727	31.487	0.502
	460.0	21.739	29.980	0.523
	480.0	20.823	28.782	0.541
	500.0	20.000	29.202	0.535
	520.0	19.231	28.806	0.541
	540.0	18.519	29.155	0.535
	560.0	17.857	29.272	0.534
	580.0	17.241	28.584	0.544
	600.0	16.667	28.553	0.544
	620.0	16.129	28.756	0.541
	640.0	15.625	29.089	0.536
	660.0	15.152	28.532	0.545
	680.0	14.706	27.886	0.555
	700.0	14.286	27.309	0.564
3-222.5	400.0	25.000	31.545	0.501
	420.0	23.810	31.220	0.506
	440.0	22.727	30.278	0.519
	460.0	21.739	30.516	0.515
	480.0	20.823	30.112	0.521
	500.0	20.000	30.352	0.518
	520.0	19.231	30.524	0.515
	540.0	18.519	30.201	0.520
	560.0	17.857	30.586	0.514
	580.0	17.241	29.470	0.531
	600.0	16.667	30.139	0.521
	620.0	16.129	29.472	0.531
	640.0	15.625	29.524	0.530
	660.0	15.152	29.148	0.535
	680.0	14.706	29.165	0.535
	700.0	14.286	28.674	0.543

Sample No.	L	10 <sup>3</sup> /cm	I	A
3-222.5	400.0	25.000	30.715	0.513
	420.0	23.810	28.736	0.542
	440.0	22.727	30.295	0.519
	460.0	21.739	30.123	0.521
	480.0	20.823	30.721	0.513
	500.0	20.000	30.855	0.511
	520.0	19.231	30.091	0.522
	540.0	18.519	30.319	0.518
	560.0	17.857	30.523	0.515
	580.0	17.241	29.683	0.527
	600.0	16.667	29.670	0.528
	620.0	16.129	29.786	0.526
	640.0	15.625	29.494	0.530
	660.0	15.152	29.066	0.537
	680.0	14.706	28.675	0.542
	700.0	14.286	28.348	0.547
"	400.0	25.000	32.296	0.491
	420.0	23.810	32.458	0.489
	440.0	22.727	32.546	0.488
	460.0	21.739	31.672	0.499
	480.0	20.823	30.818	0.511
	500.0	20.000	30.860	0.511
	520.0	19.231	31.097	0.507
	540.0	18.519	30.331	0.518
	560.0	17.857	31.308	0.504
	580.0	17.241	30.404	0.517
	600.0	16.667	30.525	0.515
	620.0	16.129	30.585	0.514
	640.0	15.625	30.288	0.519
	660.0	15.152	30.111	0.521
	680.0	14.706	29.879	0.525
	700.0	14.286	29.632	0.528
"	400.0	25.000	33.233	0.478
	420.0	23.810	32.530	0.488
	440.0	22.727	32.190	0.492
	460.0	21.739	31.035	0.508
	480.0	20.823	31.050	0.508
	500.0	20.000	30.761	0.512
	520.0	19.231	31.087	0.507
	540.0	18.519	31.215	0.506
	560.0	17.857	31.452	0.502
	580.0	17.241	30.597	0.514
	600.0	16.667	30.573	0.515
	620.0	16.129	30.319	0.518
	640.0	15.625	30.531	0.515
	660.0	15.152	30.077	0.522
	680.0	14.706	29.471	0.531
	700.0	14.286	29.152	0.535

Sample No.	L	10 <sup>3</sup> /cm	I	A
3-222.5	400.0	25.000	28.730	0.542
	420.0	23.810	27.232	0.565
	440.0	22.727	29.026	0.537
	460.0	21.739	27.469	0.561
	480.0	20.823	28.094	0.551
	500.0	20.000	27.956	0.554
	520.0	19.231	28.068	0.552
	540.0	18.519	27.760	0.557
	560.0	17.857	28.267	0.549
	580.0	17.241	27.917	0.554
	600.0	16.667	27.533	0.560
	620.0	16.129	27.969	0.553
	640.0	15.625	27.054	0.568
	660.0	15.152	26.734	0.573
	680.0	14.706	26.639	0.574
	700.0	14.286	27.018	0.568
"	400.0	25.000	28.815	0.540
	420.0	23.810	27.748	0.557
	440.0	22.727	28.366	0.547
	460.0	21.739	28.522	0.545
	480.0	20.823	28.159	0.550
	500.0	20.000	28.383	0.547
	520.0	19.231	28.130	0.551
	540.0	18.519	28.362	0.547
	560.0	17.857	28.745	0.541
	580.0	17.241	28.427	0.546
	600.0	16.667	28.060	0.552
	620.0	16.129	28.115	0.551
	640.0	15.625	27.452	0.561
	660.0	15.152	27.038	0.568
	680.0	14.706	26.932	0.570
	700.0	14.286	25.744	0.589
"	400.0	25.000	33.252	0.478
	420.0	23.810	31.872	0.497
	440.0	22.727	30.187	0.520
	460.0	21.739	30.308	0.518
	480.0	20.823	29.824	0.525
	500.0	20.000	29.827	0.525
	520.0	19.231	30.264	0.519
	540.0	18.519	30.336	0.518
	560.0	17.857	30.847	0.511
	580.0	17.241	30.175	0.520
	600.0	16.667	30.012	0.523
	620.0	16.129	30.327	0.518
	640.0	15.625	30.449	0.516
	660.0	15.152	29.995	0.523
	680.0	14.706	30.076	0.522
	700.0	14.286	29.496	0.530

Sample No.	L	10 <sup>4</sup> /cm	I	A
3-222.5	400.0	25.000	31.819	0.497
	420.0	23.810	30.021	0.523
	440.0	22.727	32.189	0.492
	460.0	21.739	30.983	0.509
	480.0	20.823	31.131	0.507
	500.0	20.000	30.616	0.514
	520.0	19.231	30.083	0.522
	540.0	18.519	30.236	0.519
	560.0	17.857	30.333	0.518
	580.0	17.241	30.291	0.519
	600.0	16.667	30.300	0.519
	620.0	16.129	30.333	0.518
	640.0	15.625	30.168	0.520
	660.0	15.152	29.402	0.532
	680.0	14.706	29.572	0.529
	700.0	14.286	29.215	0.534
49-240	400.0	25.000	31.554	0.501
	420.0	23.810	31.302	0.504
	440.0	22.727	31.891	0.496
	460.0	21.739	29.727	0.527
	480.0	20.823	29.986	0.523
	500.0	20.000	30.111	0.521
	520.0	19.231	30.351	0.518
	540.0	18.519	29.727	0.527
	560.0	17.857	30.169	0.520
	580.0	17.241	30.031	0.522
	600.0	16.667	29.911	0.524
	620.0	16.129	29.759	0.526
	640.0	15.625	29.874	0.525
	660.0	15.152	28.752	0.541
	680.0	14.706	28.629	0.543
	700.0	14.286	28.335	0.548
"	400.0	25.000	31.491	0.502
	420.0	23.810	31.647	0.500
	440.0	22.727	29.937	0.524
	460.0	21.739	29.951	0.524
	480.0	20.823	29.518	0.530
	500.0	20.000	30.118	0.521
	520.0	19.231	29.253	0.534
	540.0	18.519	29.323	0.533
	560.0	17.857	29.561	0.529
	580.0	17.241	29.406	0.532
	600.0	16.667	29.193	0.535
	620.0	16.129	29.439	0.531
	640.0	15.625	29.290	0.533
	660.0	15.152	28.307	0.548
	680.0	14.706	28.384	0.547
	700.0	14.286	27.829	0.555

Sample No.	L	$10^3/\text{cm}$	I	A
49-137	400.0	25.000	25.538	0.593
	420.0	23.810	25.396	0.595
	440.0	22.727	27.440	0.562
	460.0	21.739	28.438	0.546
	480.0	20.823	28.510	0.545
	500.0	20.000	29.002	0.538
	520.0	19.231	28.351	0.547
	540.0	18.519	28.406	0.547
	560.0	17.857	28.758	0.541
	580.0	17.241	27.923	0.554
	600.0	16.667	27.196	0.565
	620.0	16.129	26.796	0.572
	640.0	15.625	26.186	0.582
	660.0	15.152	25.377	0.596
	680.0	14.706	25.347	0.596
	700.0	14.286	24.686	0.608
"	400.0	25.000	24.909	0.604
	420.0	23.810	26.759	0.573
	440.0	22.727	28.117	0.551
	460.0	21.739	27.588	0.559
	480.0	20.823	27.531	0.560
	500.0	20.000	27.724	0.557
	520.0	19.231	27.613	0.559
	540.0	18.519	27.702	0.557
	560.0	17.857	27.190	0.566
	580.0	17.241	27.423	0.562
	600.0	16.667	26.864	0.571
	620.0	16.129	26.693	0.574
	640.0	15.625	26.084	0.584
	660.0	15.152	25.196	0.599
	680.0	14.706	24.800	0.606
	700.0	14.286	23.422	0.630

## APPENDIX IV

### SPHALERITE ANALYSES

Values are quoted in mole % FeS in sphalerite.

## Sphalerite Analyses

Sample no.	Sulfide assemblage	Sphalerite comp. mole % FeS	Pyrrhotite phases
3-219	sp,po	11.94	mpo
		11.41	
		11.75	
		13.64	
		11.30	
3-285	sp,po	10.56	hpo
		11.35	
		13.56	
		12.23	
		11.66	
49-240	sp,po	11.84	hpo
		11.86	
		11.50	
		11.85	
		11.79	
49-190	sp,po	11.03	mpo
		10.28	
		11.42	
		11.39	
		11.83	
49-279	sp,po,py	11.67	mpo
		12.14	
		12.04	
		10.96	
		12.18	



Sample no.	Sulfide assemblage	Sphalerite comp. mole % FeS	Pyrrhotite phases
49-387	sp,po,py	12.02	hpo
		12.44	
		11.98	
		11.28	
		11.73	
49-431	sp,po,py	12.32	hpo
		12.74	
		13.26	
		11.97	
		12.55	
3-243	sp,po,py	13.33	hpo
		13.60	
		13.20	
		13.07	
		12.15	
3-360	sp,po,py	12.48	hpo
		12.01	
		12.35	
		12.14	
		12.57	

Sample no.	Sulfide assemblage	Sphalerite comp. mole % FeS	Pyrrhotite phases
49-392	sp,po,py	10.62	hpo
		10.17	
		11.18	
		11.66	
		11.56	
49-317	sp,py	12.08	-
		12.27	
		12.72	
		12.63	
		12.51	
49-373	sp,py	12.53	-
		12.62	
		12.53	
		12.41	
		12.28	
3-150	sp,py	12.05	-
		12.23	
		12.07	
		11.62	
		11.77	
3-330	sp,py	8.73	-
		8.95	
		8.68	
		9.09	
		10.05	

Sample no.	Sulfide assemblage	Sphalerite comp. mole % FeS	Pyrrhotite phases
49-142	sp,py	6.67	-
		6.60	
		6.35	
		6.98	
		6.78	
3-270	sp,py	8.81	-
		8.49	
		8.96	
		9.12	
		9.03	
49-166	sp,py	7.98	-
		8.21	
		7.83	
		8.53	
		7.78	
3-198.5	sp,py	9.18	-
		9.17	
		8.84	
		8.99	
		8.96	
49-226	sp.encl. in py	12.75	-
		13.03	
		12.15	
		11.39	
		12.36	

Sample no.	Sulfide assemblage	Sphalerite comp. mole % FeS	Pyrrhotite phases
49-373	sp.encl. in py	12.38	
		13.15	
		12.02	
		12.88	
		12.91	
3-150	sp.encl. in py	13.37	
		13.31	
		13.21	
		12.57	
		14.29	
3-330	sp.encl. in py	10.41	
		10.16	
		9.86	
		9.81	
		10.63	
3-270	sp.encl. in py	9.35	
		9.59	
		9.47	
		9.29	
		9.29	
3-198.5	sp.encl. in py	8.78	
		9.05	
		9.11	
		9.29	
		9.82	

## APPENDIX V

Frequency distribution of Mattabi ore minerals with respect to depth from diamond drill holes 3 and 49.

300	
305	
310	
315	
320	
325	
330	
335	
340	
345	
350	
355	
360	
365	
370	
375	
380	
385	
390	
395	
400	
405	
410	
415	
420	
425	
430	
435	
440	
445	
450	
455	
460	
465	
470	
475	
480	
485	
490	
495	
500	
505	
510	
515	
520	
525	
530	
535	
540	
545	
550	
555	
560	
565	
570	
575	
580	
585	
590	
595	
600	
605	
610	
615	
620	
625	
630	
635	
640	
645	
650	
655	
660	
665	
670	
675	
680	
685	
690	
695	
700	
705	
710	
715	
720	
725	
730	
735	
740	
745	
750	
755	
760	
765	
770	
775	
780	
785	
790	
795	
800	
805	
810	
815	
820	
825	
830	
835	
840	
845	
850	
855	
860	
865	
870	
875	
880	
885	
890	
895	
900	
905	
910	
915	
920	
925	
930	
935	
940	
945	
950	
955	
960	
965	
970	
975	
980	
985	
990	
995	
1000	

DDH 3: Frequency distribution of Mattabl ore minerals with respect to depth

Depth (m)	py	sp	cp	gn	po	apy	mk	tet	mt	hm	ll	rt	bn	cc	ld
125	X	X	X												
130	X	X				X									
135	X	X	X												
140	X	X	X	X											
150	X	X	X	X											
155	X	X	X	X					X						
159	X	X	X	X					X						
165	X	X	X	X		X									
170	X	X	X	X	X				X						
174	X		X	X	X				X						
179	X	X	X												
184	X	X	X												
189		X	X												
194	X														
198.5	X		X	X					X						
204	X	X	X			X									
209	X		X												
214	X	X	X	X		X									
219	X	X	X	X	X				X						
222.5	X	X		X	X			X							
228	X	X	X	X	X				X						
233	X	X		X											
238	X	X		X	X				X						
243	X	X	X		X										
254	X	X	X		X				X						
259	X	X	X		X	X									
264	X	X	X	X			X				X				
270	X		X	X			X	X							
275	X	X	X	X					X						
285	X	X	X	X	X	X		X	X						
290	X	X	X									X			
295	X	X	X									X			
299.5	X	X		X			X								
305	X	X		X			X	X							
309.5	X	X								X					
314	X	X	X						X						
317	X	X	X	X		X		X	X						
319	X	X	X	X				X	X						
325	X		X	X			X								X
330	X	X	X				X		X						X
335	X	X													
340	X	X													
345	X	X	X			X	X								X
350	X	X	X	X			X						X		
355	X		X		X	X	X		X						









## APPENDIX VI

### SAMPLE PREPARATION

The polished microprobe sections were prepared as follows:

- 1) Sectioning was performed with a diamond cut-off wheel to reduce the parent sample to a workable and representative piece.
- 2) Rough grinding was performed on a rotating lap with a fixed or loose abrasive to produce a flat, smooth surface free from deformation.
- 3) Cementing the "chip" to the glass slide was performed on a No. 30-8010 AB slide warmer by petropoxy or araldite epoxy to hold the chip to the slide.
- 4) Resectioning was performed on an Ingram cut-off saw to remove excess material prior to coarse-finish grinding on an Ingram thin grinder with a diamond impregnated wheel, to approximately 50 microns. Fine finishing was accomplished by hand on a glass plate with 600 grit silicon carbide, followed by 5 micron alumina. The edges of the slides were beveled on silicon carbide paper on a cast iron lap to smoothen the edges to improve the transit of the sections on the polishing machine. The sections were then polished on cloth laps with diamond powder and oil. However, these sections had problems with lead adhering to small pits on the surface of the sections. This is not apparent in ordinary microscopy but is obvious on the scanning electron microscope (SEM) when the sections are greatly magnified.

